TEMPERATURE FRACTIONATION OF MERCURY IN THE CEMENT PRODUCTION PROCESS

Sabina Berisha

Doctoral Dissertation
Jožef Stefan International Postgraduate School
Ljubljana, Slovenia

Supervisor: Prof. Dr. Milena Horvat, Jožef Stefan Institute, Ljubljana, Slovenia
Industry Co-Supervisor: Dr. Tanja Ljubič Mlakar, Salonit Anhovo, d.d., Deskle, Slovenia

Evaluation Board:

Asst. Prof. Jože Kotnik, Chair, IPS and Jožef Stefan Institute, Ljubljana, Slovenia
Prof. Aleksandra Lobnik, Member, IPS, Ljubljana and Faculty of Mechanical Engineering, University of Maribor, Slovenia
Prof. Lesley Sloss, Member, International Centre for Sustainable Carbon, Gloucester, UK

MEDNARODNA PODIPLOMSKA ŠOLA JOŽEFA STEFANA
JOŽEF STEFAN INTERNATIONAL POSTGRADUATE SCHOOL

Sabina Berisha

TEMPERATURE FRACTIONATION OF MERCURY IN THE CEMENT PRODUCTION PROCESS

Doctoral Dissertation

TEMPERATURNA FRAKCIONACIJA ŽIVEGA SREBRA V PROCESU PROIZVODNJE CEMENTA

Doktorska disertacija

Supervisor: Prof. Dr. Milena Horvat

Industry Co-Supervisor: Dr. Tanja Ljubič Mlakar

Ljubljana, Slovenia, December 2023

Acknowledgments

This doctoral dissertation was conducted in cooperation with the company Salonit Anhovo, Joint-Stock Co., and Jožef Stefan International Postgraduate School (Contract No. 2017/1) and has received additional financial support from the Ministry of Education, Science and Sport (Contract No. P-SOF-DR-ŠT-2016/6) and the Slovenian Research Agency ARRS through the programme P1-0143 and project STRAP, J1-1716 and IsoCont J1-3033.

I am deeply grateful for the opportunity provided to me for the completion of this doctoral dissertation, a journey that has been both intellectually enriching and personally transformative. I would like to extend my sincere gratitude to the individuals and institutions that supported me along the way.

First and foremost, I would like to express my gratitude to my supervisor, Professor Dr. Milena Horvat, for her unwavering guidance, expertise, and constructive feedback. My gratitude goes also to my co-supervisor, Dr. Tanja Ljubič Mlakar, for her help, suggestions, and openness during my studies. Their mentorship has been invaluable in shaping the direction and quality of this research.

I am also thankful for the suggestions of the committee members, Asst. Prof. Jože Kotnik, Prof. Aleksandra Lobnik, and Prof. Lesley Sloss, whose insightful suggestions have greatly improved the depth of this work. I would also like to extend my appreciation to the Jožef Stefan International Postgraduate School collective and the resources provided by the Department of Environmental Sciences within the Jožef Stefan Institute. Gratitude goes also towards collaborators of Salonit Anhovo for their assistance provided during this work.

Completing this dissertation marks a significant milestone in my academic and personal journey. It is a culmination of years of hard work, dedication, and the support of countless individuals. I express my heartfelt gratitude to my coworkers, Dr. Pavlin, Dr. Živković, Dr. Kotnik, Dr. Begu, Dr. Gačnik, my "office-mates" Jasmina Masten Rutar and Staša Hamzić Gregorčič, and many other wonderful people who played a part, big or small, in making this achievement possible. Your contribution has been instrumental, and I am honored to have had you by my side.

The emotional support and encouragement of my family has been a cornerstone of this journey. Their belief in my abilities has been a constant source of motivation, and for that, I am truly grateful to my dear parents, my sisters, and my brother. To Fevzi and my little Gentian, thank you for always being with me.

Abstract

Cement production is one of the main contributors to mercury emissions into the atmosphere. Many national and international legal instruments aim to control and reduce Hg emissions. Hg enters the cement production process as an impurity in fuels and raw materials, with the latter being the main source of Hg. The behavior of Hg in the production process is influenced by various factors, such as: counterflow of materials and flue gases, different temperature gradients, recycling of the filter dust to the high-temperature process, operating regimes of raw mills, etc. Consequently, Hg can exist in elemental, oxidized, and particulate form.

This thesis is centered on methodological approach to study Hg transformation in the cement production process. In relation to this, the thesis consists of both quantitative and qualitative approach to the issue. Having an overview of Hg content in input materials for cement production is useful information in monitoring Hg emissions. Methods that employ direct thermal decomposition coupled to atomic absorption spectrometer (TPD AAS) have shown to be suitable for quantification of Hg in various matrices, especially soils, sediments, gypsum, etc. Acknowledging the advantages that such techniques provide; the first part of this study was dedicated to validating the method for determination of total Hg in solid samples of raw materials used for cement production. In this regard, two calibration approaches were employed: calibration using matrix-matched certified reference materials (CRM), and the so-called "spike calibration" where standard calibrating solution was added to the solid matrix that was free from natural Hg. While both calibration approaches were found to be appropriate for the calibration of the instrument, the uncertainty of the mass fraction and the need for several CRMs are major drawbacks of the matrix-matched CRM calibration. The second approach was found to be suitable and had less associated uncertainty.

The second part of the thesis is dedicated to studying Hg temperature fractionation in solid samples. For this purpose, a quadrupole mass spectrometer (QMS) was utilized based on several advantages that it provides: better sensitivity, the possibility to observe the release of other ions during decomposition process, lack of carrier gas, etc. From the results of fractionation analysis, it was shown that Hg in primary raw materials, such as limestone, is found to be strongly bound to the matrix and exhibited only one fraction. With the addition of other materials needed for cement production, both the Hg content and the desorption profile change. Once the raw meal enters the preheater section where the temperatures are from ~290 °C in the first cyclone to ~900 °C in the fifth cyclone, Hg from the solid phase evaporates and is transformed into the elemental form. Clinker as a final product of pyro-process has a very low Hg content and its thermo-desorption profile does not show any identifiable fraction. Dust from the fabric filter consistently showed the same desorption curve, with the peak maxima at the temperature range of 150–350 °C, indicating the presence of chlorine-containing compounds.

The implemented approach provides better insight into Hg mobility in the cement production and can therefore be of great support in the development of emission control technologies.

Povzetek

Proizvodnja cementa je med pomembnimi povzročitelji emisij živega srebra (Hg) v ozračju. Številni nacionalni in mednarodni pravni instrumenti so namenjeni nadzoru in zmanjšanju emisij Hg. Hg se v procesu proizvodnje cementa vnaša kot nečistota v gorivih in surovinah, pri čemer so slednje glavni vir Hg. Na obnašanje Hg v proizvodnem procesu vplivajo različni dejavniki, kot so: protitočni tok materialov in dimnih plinov, različni temperaturni gradienti, recikliranje filtrirnega prahu nazaj v visokotemperaturni proces, režimi delovanja mlinov surovine itd. Posledično lahko Hg obstaja v elementarni, oksidirani in v partikularni obliki.

Ta disertacija je osredotočena na metodološki pristop k preučevanju pretvorbe Hg v procesu proizvodnje cementa. V zvezi s tem je to delo sestavljeno iz kvantitativnega in kvalitativnega pristopa k problematiki. Pregled nad vsebnostjo Hg v vhodnih materialih za proizvodnjo cementa je koristna informacija pri spremljanju emisij Hg. Metode, ki uporabljajo neposredno termično razgradnjo v povezavi z atomskim absorpcijskim spektrometrom (TPD AAS), so se izkazale za primerne za kvantitativno analizo Hg v različnih matricah, zlasti v zemlji, sedimentih, mavcu itd. Ob priznavanju prednosti, ki jih takšne tehnike zagotavljajo, je bil prvi del te študije namenjen validaciji metode za določanje skupne vsebinosti Hg v trdnih vzorcih surovin, ki se uporabljajo za proizvodnjo cementa. Pri tem sta bila uporabljena dva kalibracijska pristopa: kalibracija z uporabo certificiranih referenčnih materialov (CRM), usklajenih z matriko, in tako imenovana "spike calibration", pri kateri je bila trdni matrici brez naravnega Hg dodana standardna kalibracijska raztopina. Čeprav je bilo ugotovljeno, da sta oba kalibracijska pristopa primerna za kalibracijo instrumenta, sta negotovost masnega deleža in potreba po več CRM glavni pomanjkljivosti pri kalibraciji matrično usklajenih CRM. Drugi pristop se je izkazal za primernega, njegova negotovost pa je bila manjša.

Drugi del disertacije je namenjen preučevanju temperaturne frakcionacije Hg v trdnih vzorcih. V ta namen je bil uporabljen kvadrupolni masni spektrometer (QMS), ki ima več prednosti: boljšo občutljivost, možnost opazovanja sproščanja drugih ionov med procesom razgradnje, odsotnost nosilnega plina itd. Rezultati analize frakcioniranja so pokazali, da je Hg v primarnih surovinah, kot je apnenec, močno vezan na matrico in ima le eno frakcijo. Z dodajanjem drugih materialov, potrebnih za proizvodnjo cementa, se spreminjata tako vsebnost Hg kot profil desorpcije. Ko surova moka vstopi v toplotni izmenjevalnik, kjer so temperature med ~ 290 °C v prvem ciklonu in ~ 900 °C v petem ciklonu, Hg iz trdne faze izhlapi in se pretvori v elementarno obliko. Klinker kot končni proizvod piro-procesa ima zelo nizko vsebnost Hg in njegov termo-desorpcijski profil ne kaže nobene prepoznavne frakcije. Prah iz prašnih filtrov dosledno kaže enako desorpcijsko krivuljo z maksimumom pri temperaturi od 200 do 250 °C, kar kaže na prisotnost kloro vsebujočih spojin.

Izvedeni pristop omogoča boljši vpogled v mobilnost Hg v proizvodnji cementa in je zato lahko v veliko pomoč pri razvoju tehnologij za nadzor emisij.

Contents

List of Figures

List of Tables

Abbreviations

AAS ... Atomic Absorption Spectrometry
AC ... Activated Carbon
ACI ... Activated Carbon Injection
APCD ... Air Pollution Control Devices
ASGM ... Artisanal and Small-Scale Gold Mining
BAT ... Best Available Techniques
CEM ... Continuous Emission Monitoring
CFPP ... Coal-Fired Power Plant
CKD ... Cement Kiln Dust
CRM ... Certified Reference Material
DGM ... Dissolved Gaseous Mercury
DMHg ... Dimethyl Mercury
DTD ... Direct Thermal Decomposition
IED ... Industrial Emissions Directive
IPPC ... Integrated Pollution Prevention and Control
LCPD ... Large Combustion Plant Directive
LRTAP ... Long-Range Transboundary Air Pollution
LOD ... Limit of Detection
LOQ ... Limit of Quantification
TPD ... Temperature Programmed Desorption
TGM ... Total Gaseous Mercury
THg ... Total Mercury
RGM ... Reactive Gaseous Mercury
MeHg ... Methyl Mercury
SCR ... Selective Catalytic Reduction
SRM ... Standard Reference Material
UNECE ... United Nations Economic Commission for Europe
QMS ... Quadrupole Mass Spectrometer
WID ... Waste Incineration Directive

Chapter 1

Introduction

1.1 Mercury: Physicochemical Properties

Mercury (Hg) is a unique element and among the most researched ones due to its impact on the environment and human health. Originally named hydrargyrum in Latin from where its chemical symbol is derived, Hg is the only metallic element liquid at standard conditions for pressure and temperature. Named after the messenger of the gods in Roman mythology, it is known as quicksilver due to its quick water movement despite its heavy mass. Hg is positioned in the subgroup IIB in the periodic table together with zinc (Zn) and cadmium (Cd), which are all known to have a low melting and boiling point. Hg has seven stable isotopes and 40 synthetic and radioactive ones, among which is Hg^{203} that is used as a spiked tracer in studies of Hg methylation in aquatic systems (Gilmour & Riedel, 1995; Meierfrankenfeld, Bury, & Thoennessen, 2011). Apart from its elemental form (Hg^0), it is also found in two ionic forms, Hg_2^{2+} and Hg^{2+} that are predominant in water (Schroeder & Munthe, 1998). Mercurous ion Hg^{1+} is thought to be an intermediate in the oxidation of Hg^0 to Hg^{2+}, but it cannot be detected by conventional methods due to its short life. Hg is relatively inert chemically due to its high ionization potential compared to other electropositive elements (except for hydrogen). The vapor pressure of Hg is larger than that of water; the anomaly attributed to the weak inter-atomic bonds caused by the nucleus having a strong hold on the valence electrons. Another atypical characteristic of Hg is it being the only element apart from noble gases, whose vapor is almost entirely monoatomic, while its noticeable vapor pressure (Table 1.1), in conjunction with its toxicity, makes it necessary to handle it with care. Hg reacts with oxygen, sulfur, and halogens on being heated, and is chemically inert with non-oxidizing acids. However, it dissolves in concentrated nitric acid (HNO_3) and in hot concentrated sulfuric acid (H_2SO_4) forming Hg^{2+} salts along with the oxides of nitrogen and sulfur. Hg has a much greater tendency to covalency and a preference for N-, P- and S- donor ligands, with which Hg^{2+} forms a complex whose stability is rarely exceeded by those of any other divalent cation. It has a very low solubility in water which increases by the factor of 1.3 for every 10 degree rise in temperature (Glew & Hames, 1971), but has a good solubility in lipids. Hg forms amalgams with gold (Au), silver (Ag), copper (Cu), zinc (Zn), although the interaction between Hg and these elements is not very strong (Cremer et al., 2008).

Hg has been used in numerous industrial applications and common goods such as thermometers, barometers, batteries, dental amalgams, fluorescent light bulbs, and thermostats. Its use for precious metal extraction by amalgamation was known for a long time and was widely used by Spain in the sixteenth century when the fleet carried Hg from Almaden to Mexico and returned with silver.

Table 1.1: Mercury chemical and physical properties (Kozin & Hansen, 2013).

Atomic number	80
Atomic mass	200.59
Density	13.55 g cm^{-3}
Atomic volume	14.26 $\cdot 10^{-6}$ m^3 mol^{-1} at 25 °C
Melting point	– 38.83 °C
Boiling point	357.3 °C
Isotopes	202, 200, 199, 201, 198, 204, 196
Oxidation states	0, +1, +2
Vapor pressure	14 mg m^{-3} at 20 °C, 31 mg m^{-3} at 30 °C
Solubility in water	~ 49 µg L^{-1} at 20 °C

Gaseous elemental Hg is regarded as a global pollutant due to its atmospheric residence time of up to a year, which allows it to travel long distances (Ariya et al., 2015). As the range of Hg species that are found within our environment is broad, its chemical form influences the bioavailability, transport, human health impact and persistence in nature. Biogeochemical transformation and mobility of Hg make it a global pollutant that can be transported over thousands of kilometers through the atmosphere. As a result, understanding Hg species transformation and accurate monitoring in the environment are essential for reliable risk assessment (Bank, 2012).

Before it was recognized as a toxic element, Hg was widely used in many activities. The medicinal use of Hg is known from 3000 years, where it was used for treatment of syphilis. It was widely used in cosmetics, in making felt hats where mercuric nitrate was used in treatment of pelts, etc. (Brooks, 2012). Two major events brought attention to the Hg toxicity: the 1971 farming incident in Iraq, where large quantities of wheat seed were treated with alkyl Hg fungicide, where the seeds were ground into flour and consumed. The second major incident is the Minamata disaster, caused by the discharging of the methyl Hg (MeHg) in the industrial wastewater from the chemical factory (Harada, 1995). As Hg has an ability to bioaccumulate and biomagnify along the trophic chain, the local population became exposed to its toxic effect through the consumption of fish.

As Hg can exist in various forms, the level of toxicity and exposure differs between them (Sakamoto et al., 2018). Acute high dose exposure to elemental Hg may give rise to severe pneumonitis (Cortes et al., 2018). A significant part of inhaled elemental Hg (around 80%) is absorbed in the blood via the lungs, and due to its lipo-solubility, easily passes the blood-brain barrier. Eventually, the gaseous elemental Hg in patients' brain is oxidized to inorganic divalent Hg and causes damage to the brain, and also accumulates in the kidneys that leads to the renal damage (Sakamoto et al., 2018). Other inorganic forms of Hg (Hg salts) have a corrosive effect to the skin, eyes, and gastrointestinal tract. Some of the most common neurological effects of Hg poisoning are mental retardation, seizures, delayed development, memory loss, tremors, vision and hearing loss, cognitive and muscular dysfunction, etc. (Eto, 1997).

The most toxic form of Hg are organic Hg compounds. These compounds are the most frequent form of Hg exposure. The most recognized compound is MeHg which is a potent neurotoxin. MeHg has the ability to accumulate in the fatty tissues of many organisms, fish, and seafood among the most important ones. MeHg bioaccumulates and biomagnifies along the trophic chain, thus the population that feeds on seafood is the most exposed to it. As it can cross the blood-placenta barrier accumulating rather in the fetus than in the mother, it affects the development of the fetus which results in serious mental and physical problems in later life (Harada, 1978).

1.2 Mercury Biogeochemical Cycle

1.2.1 Sources of mercury

Hg is a naturally occurring element, with an abundance of about 50 ng g^{-1} in the Earth's crust (Barbalace, 1995). The global reserves of Hg total around 600 000 t, the largest Hg deposits are found in Spain, Russia, Kyrgyzstan, China, Slovenia, etc. (Kozin, Hansen, Zakharchenko, & Gray, 2013). Hg is in a group of chalcophile elements, meaning that in the reducing atmosphere prevailing when the Earth's crust solidified, these elements separated in the sulfide phase, and their most important ores are sulfides. Cinnabar (HgS) is the most important Hg ore which was widely used in the Mediterranean for metal extraction by amalgamation as early as 500 BC. It can be found along the lines of previous volcanic activity. Less abundant minerals are calomel (Hg_2Cl_2), livingstonite ($HgSb_4S_8$), corderoite ($Hg_3S_2Cl_2$) (Bank, 2012; Hazen et al., 2012; Jasinski, 1995; Kim et al., 2000).

Hg is released from both natural and anthropogenic processes. **Natural sources** of Hg include volcanoes, largely recognized as the most significant natural source of mercury in the atmosphere (Bagnato et al., 2015), geothermal vents, degasification from soils and water surfaces, degradation of minerals, and forest firing. Emissions from these sources vary over time and geografically as they depend on a variety of factors such as the presence of volcanic belts or geothermal activity, as well as geological formations with high Hg levels, re-emission of previously deposited Hg from top soils and plants into the atmosphere, etc. (Pirrone et al., 2009). From these natural sources, Hg is released predominantly in the form of Hg^0 vapors, although Hg bound to particulates and aerosols that are released from volcanoes or soil erosion is another possible form. When compared to current-day anthropogenic Hg emissions, the natural flux of Hg into the atmosphere from primary geological sources is modest.

Anthropogenic sources of Hg include industrial activities where Hg emission occurs due to its presence as an impurity in fuels and raw materials, but also due to its intentional use. In the first group of industrial activities where Hg is released unintentionally are stationary combustion of fossil fuels, mining, industrial activities that process ores to produce various metals, and cement production. Intentional use sectors include the use of Hg-added products, such as lamps, batteries, etc., dentistry, and artisanal and small-scale gold mining (ASGM), where Hg is used to extract gold from gold-bearing rocks (UN Environment, 2019). Currently, anthropogenic emissions account for 30% of emitted Hg annually to the atmosphere, while the remaining 60% come from the environmental processes resulting in re-emission of previously deposited Hg to soils and water. The most abundant form of Hg emitted from anthropogenic activities is Hg^0, although they also emit divalent Hg, and Hg associated with particulate matter-Hg_p.

Sector-wise, ASGM dominates Hg emissions (~33.8%) followed by stationary combustion of coal (~22.4%), emissions from non-ferrous metal production (~15.1%) and cement production (~10.8%) (Figure 1.1).

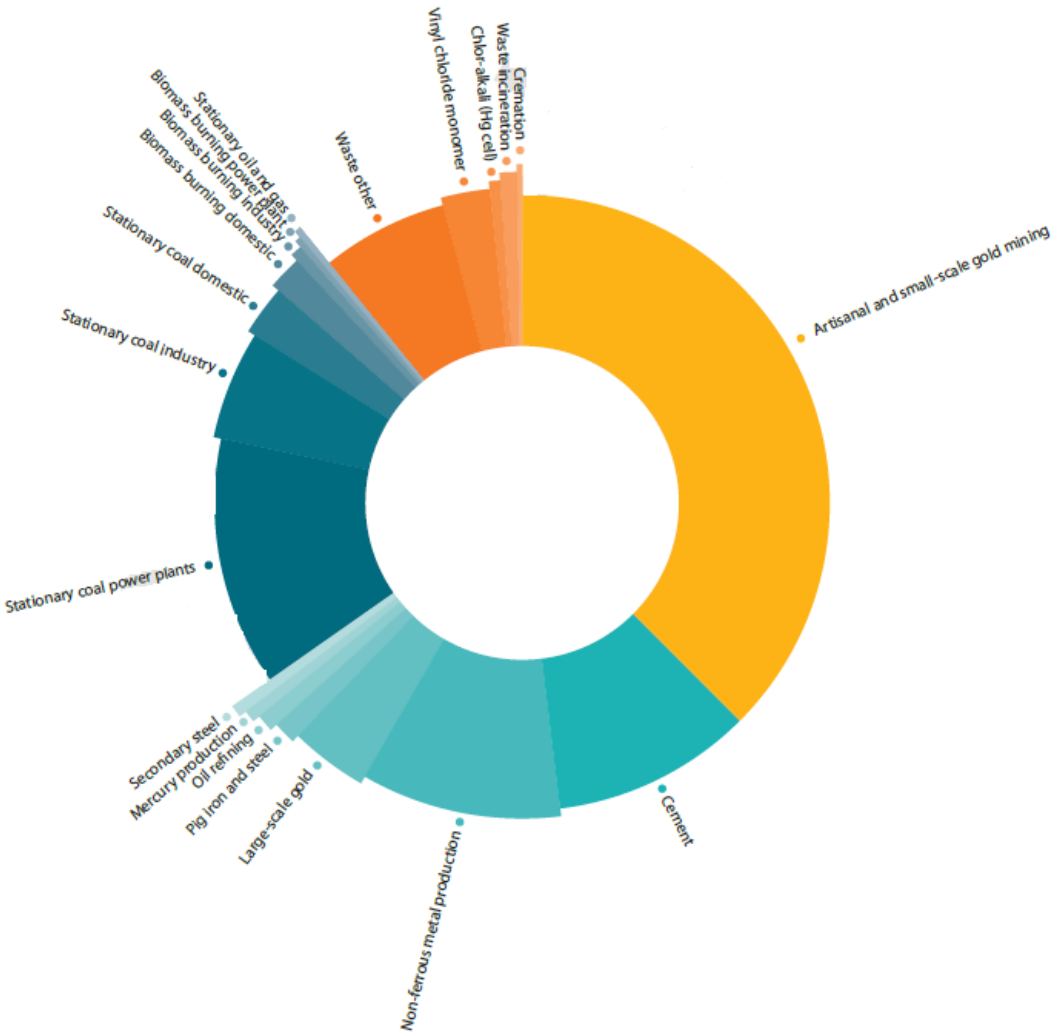

Figure 1: Contributions of different anthropogenic sectors to Hg emissions to air in 2015 (AMAP/UN Environment, 2019).

1.2.2 Mercury cycling in the environment

Once released, Hg is transported across the major environmental compartments – air, soils, and waters (Figure 1.2) until it is removed by burial in ocean and lake sediments and subsurface soils (Amos et al., 2014; Amos, Jacob, Streets, & Sunderland, 2013). Because of its long-range transport, Hg can be found even in areas where there are no atmospheric releases. Hg biogeochemical cycling is a complex process involving various transformations and transportations of its species in the environment.

The most abundant form of Hg in the **atmosphere** is Hg^0, with a global mean concentration of ~1.6 ng m^{-3} (Slemr et al., 2011; Sprovieri et al., 2016), and can be considered as well dispersed due to its atmospheric lifetime of up to 1 year (Lin & Pehkonen, 1999). In contrast, oxidized forms of Hg – Hg^{2+} and Hg_p have shorter lifetime in the atmosphere (days to weeks), are more soluble in water making them the predominant forms of Hg deposited via wet and dry deposition. These oxidized species undergo partition between the gas and aerosol phase, and can be reduced back to Hg^0 from either phase (Amos et al., 2012; Saiz-Lopez et al., 2018). Their surface concentrations are estimated to

range from 1–100 pg m^{-3} (Selin, 2009). The concentration and speciation of Hg species in the atmosphere is conditional on proximity to emission sources, the presence of oxidants, aerosol concentration, meteorology and surface conditions (Jiskra et al., 2018; Malcolm et al., 2009; Obrist et al., 2011). Measurement of total gaseous Hg (TGM) shows higher concentrations to be in the Northern Hemisphere (1.3 to 1.6 ng m^{-3}) compared to the Southern (0.8 to 1.1 ng m^{-3}) (Sprovieri et al., 2016). The main removal path of Hg^0 from the atmosphere is oxidation to Hg^{2+}. The dominant oxidants of Hg were considered to be ozone or OH-radicals (Calvert & Lindberg, 2005), however, most recent analyses have suggested bromine (Br) as the main global Hg oxidant (Saiz-Lopez et al., 2018). The oxidation by Br is assumed to take place in a two-step mechanism, in which gaseous Hg^0 reacts with photolytically produced Br to produce unstable HgBr which either dissociates to Hg^0 or reacts with other species to form inorganic Hg^{2+} compounds (Dibble, Zelie, & Mao, 2012; Dibble & Schwid, 2016; Goodsite, Plane, & Skov, 2004; Holmes et al., 2010; Horowitz et al., 2017; Jiao & Dibble, 2017). Other potential oxidants are thought to be Cl, H_2O_2 and NO_3.

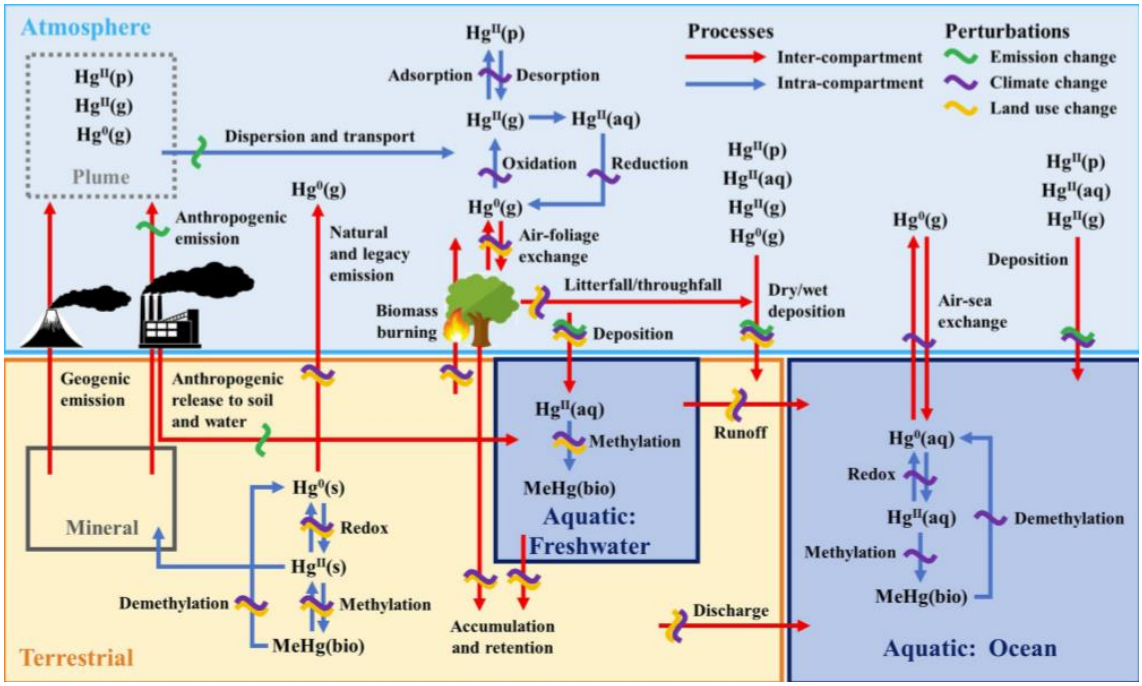

Figure 2: Mercury biogeochemical cycle (Obrist et al., 2018).

Measurements of Hg^{2+} in the atmosphere can assist in reducing uncertainties with redox reactions. Such measurements are performed by collecting Hg^{2+} on potassium chloride (KCl)-coated denuders to be reduced to Hg^0, a species known as reactive gaseous Hg (RGM). Oxidation of Hg^0 to Hg^{2+} is assumed to be controlled by photochemistry, consequently the production of Hg^{2+} is expected to peak at midday. Direct emissions of Hg^{2+} and Hg_p from anthropogenic sources are expected to be deposited on a regional scale since these species are soluble and with a shorter lifetime in the atmosphere than Hg^0. Hg^0 emissions have a longer lifetime, and large-scale oxidation and reduction patterns will govern conversion to Hg^{2+} and subsequent deposition.

Hg^{2+} from the atmosphere is deposited to the **terrestrial surface** through dry and wet deposition. Upon deposition, a portion of Hg will re-volatilize to the atmosphere in a phenomenon that is known as prompt recycling (Selin et al., 2008), while the remaining

Hg will be incorporated into soil. These processes can depend on Hg species, surface chemistry and environmental conditions.

It is estimated that more than 80% of annual atmospheric Hg deposition to terrestrial watershed is retained in the soil, thus protecting the aquatic ecosystems from netting the entire Hg anthropogenic deposition (Aastrup et al., 1991; Hintelmann et al., 2002; Y. H. Lee et al., 1998; Shanley & Bishop, 2012). Deposition of Hg per unit area is greater to the land than water because forest canopies and other vegetative surfaces forage Hg from the atmosphere efficiently compared to water surfaces (Miller et al., 2005). Still, this has made soil and vegetation reservoirs of Hg which poses a risk in the future (Harris et al., 2007).

From 5 to 60% of deposited Hg is estimated to be recycled back to the atmosphere, with higher values for water and surface snow (Ferrari et al., 2005; Hintelmann et al., 2002; Lalonde et al., 2002). Most of the Hg in terrestrial system dwells in soil associated with organic matter, where it binds to reduced sulfur groups. The estimated concentration of Hg in this media ranges from 20–70 ng g^{-1} (Frescholtz & Gustin, 2004). With the aid of isotope techniques, it was shown that recently deposited Hg that is not re-volatilized is preferentially associated with vegetation. Such techniques can differentiate between Hg in the aboveground vegetation that comes from the atmosphere, and that from the roots that come from the soil. Hg^{2+} is deposited to the leaves through both dry and wet deposition, and the uptake is assumed to occur at the leaf interior through gas exchange at the stomata. Type of soil, dissolved organic carbon and other species (S-, Cl-) are factors that control the adsorption and desorption of Hg in soil (Gabriel & Williamson, 2004). Terrestrial Hg cycling is important for many reasons (Evers et al., 2007; Miller et al., 2005; Shanley & Bishop, 2012):

- Terrestrial vegetation enhances atmospheric Hg capture.
- Regardless of the high Hg retention in terrestrial systems, Hg leakage from land areas frequently results in it being the dominant source to water bodies.
- A significant proportion of MeHg in freshwater forms in the terrestrial environment, mostly in wetlands but also in upland soils.
- Hg export from watersheds is likely episodic, and these occurrences may either stimulate methylation or comprise a major source of MeHg on their own.
- There is increasing documentation in terrestrial food webs as well as the potential of direct effects on soil microbial communities.

In forests, a small pool of Hg is retained by vegetation and is associated with coarse woody debris (Grigal, 2003). This reservoir is approximately 4 times the annual Hg deposition, indicating a 4-year average residence time of Hg in vegetation. More than half of this amount is stored in tree boles with a much longer residence time, and approximately 15% is stored in foliage with a shorter residence time (Shanley & Bishop, 2012). With increasing adjacency of the plant's habitat to the water table, increased concentrations of total Hg (THg) and MeHg are observed (Moore et al., 1995). The typical content of Hg in soils is about 100 ng g^{-1}, with the approximate concentration of 140 ng g^{-1} found in both natural and agricultural soils (Grigal, 2003). In the mineral soil, it is assumed that Hg is associated with organic matter. The geogenic origin of Hg in deeper levels of mineral soils cannot be excluded.

Through reduction, Hg can be emitted back to the atmosphere from terrestrial surface. This process is mostly abiotic, although some studies have pointed out that Hg speciation and emission from the soil can be partially influenced by biotic processes (Fritsche et al., 2008). Fe^{2+} and humic and fulvic compounds are assumed to be the reductant species,

though this process can be further promoted by temperature, and solar radiation (Gustin et al., 2002; Lindberg et al., 1995). Stream water Hg export is another output of Hg from terrestrial landscape. Although it is considered that only a small fraction of deposited Hg is exported through this route, it has great ecological implications. Another way how Hg can be released back to the atmosphere is through the burning of organic matter (Weisspenzias et al., 2007) where a considerable amount of Hg can be mobilized.

In **freshwater systems**, atmospheric Hg comes from direct deposition to lake surfaces and through runoff from watersheds, predominantly as Hg^{2+}, which can reduce to Hg^0 and volatilize to the atmosphere. A relatively small portion of Hg^{2+} can be converted to MeHg. This process is biologically mediated through strains of sulphate and iron-reducing bacteria (Benoit et al., 2002; Gilmour et al., 1998; Kerin et al., 2006). MeHg is bioconcentrated in fish and can be further biomagnified along the trophic chain as the predators feed on contaminated organisms.

In aquatic sediments, a small fraction of Hg^{2+} is converted to MeHg, which is affected by many factors such as sulfur, sediment structure, organic carbon, etc. These factors influence the amount of bioavailable inorganic Hg and by stimulating microbial activity. MeHg has been measured in the water column in lakes and in anoxic coastal waters (Eckley et al., 2005; Eckley & Hintelmann, 2006).

In **saline waters**, Hg is found as elemental Hg, inorganic Hg^{2+}, MeHg, and dimethyl-Hg (DMHg). The typical levels of Hg in the ocean are in the picomolar to subpicomolar range, creating a challenge in quantifying it. Dissolved gaseous Hg (DGM) is a combination of volatile forms (elemental and DMHg), but due to the low concentration of DMHg, it is usually measured as dissolved elemental Hg. Reactive Hg is an operationally defined fraction of easily reducible Hg under acidic conditions that includes some fraction of inorganic Hg^{2+} and some organomercury (Black et al., 2012). Hg^0 is volatile and is commonly found as a dissolved gas at subpicomolar concentrations. Rarely, it can be present as liquid, in association with marine geothermal metal-bearing fluids (Dekov, 2007; Stoffers et al., 1999) or anthropogenic discharge to the ocean. Inorganic Hg^{2+} can be found as a variety of dissolved complexes in saline aquatic environments. Hg-binding ligands in this environment include chloride, inorganic reduced sulfur species, and dissolved organic matter (Dyrssen & Wedborg, 1991; Han & Gill, 2005; Lamborg et al., 2004). MeHg is only detectable in open ocean waters at very low concentrations, possibly present as a dissolved complex bound to chloride, organic matter, or reduced sulfur species. DMHg is found as a dissolved gas in saline water, and is the predominant methylated form of Hg in the open ocean, with the exception of surface waters, coastal environments and the Mediterranean Sea where concentrations of MeHg are higher than DMHg (Cossa et al., 1994; Cossa et al., 1997; Horvat et al., 2003; Mason & Fitzgerald, 1993; St.Louis et al., 2007).

In coastal and estuarine water, Hg concentrations are higher compared to open ocean, mostly because they are highly influenced by industrial activities (Balcom et al., 2008; Faganeli et al., 2003; Laurier et al., 2003; Leermakers et al., 2001; Rolfhus & Fitzgerald, 2001). These higher concentrations can also be attributed to the terrestrial runoff as a source of Hg to coastal waters relative to the open ocean, and are therefore controlled by sediment transport and resuspension (Black et al., 2012). Within the aquatic systems, Hg is mostly transported by particulate phase, and some 90% of the riverine Hg inputs to the ocean are deposited in the coastal sediments (Sunderland & Mason, 2007). Estuaries serve as a sink for inorganic and particle-bound Hg, but can also be net sources of MeHg (Faganeli et al., 2003; MacLeod, McKone, & Mackay, 2005; Mason et al., 1999).

Hg in the oceans originates from atmospheric deposition, and runoff from coastal and freshwater systems (Lamborg et al., 2002; Mason & Sheu, 2002; Sunderland & Mason, 2007). Hg in the oceans can originate also from natural sources such as hydrothermal vents,

submarine volcanic activity, and weathering of oceanic crust and other structures. Inorganic Hg^{2+} can be reduced to Hg^0 via photochemical reactions and biologically mediated pathways (Lalonde et al., 2004; Mason, Lawson, & Sheu, 2001; Poulain et al., 2007; Rolfhus & Fitzgerald, 2004; Whalin, Kim, & Mason, 2007). The net flux of Hg^0 to the atmosphere is slightly higher in the open ocean than in coastal and estuarine bodies, although it cannot be determined whether this is due to higher rates of Hg reduction or lower rates of its oxidation in the open ocean. This gaseous exchange of Hg^0 represents the largest sink of Hg from the oceans, apart from deposition and burial in sediments which is another significant Hg sink (Lamborg et al., 2002; Mason & Sheu, 2002; Sunderland & Mason, 2007; Žagar et al., 2007).

1.3 Cement Production

The use of cement as a binding material dates back to ancient times, however, the manufacturing process has considerably advanced throughout time. Cement is one of the most important materials in the manufacturing of concrete and mortar in the construction sector. The most used type of cement is Portland cement, although other types are produced for specific applications. The cement production process comprises several production phases and includes the mining of raw materials, crushing, pre-homogenization, grinding, preheating, calcination, cooling, storage, mixing with additives and cement grinding. A simple schematic presentation of cement production process is presented in Figure 1.3.

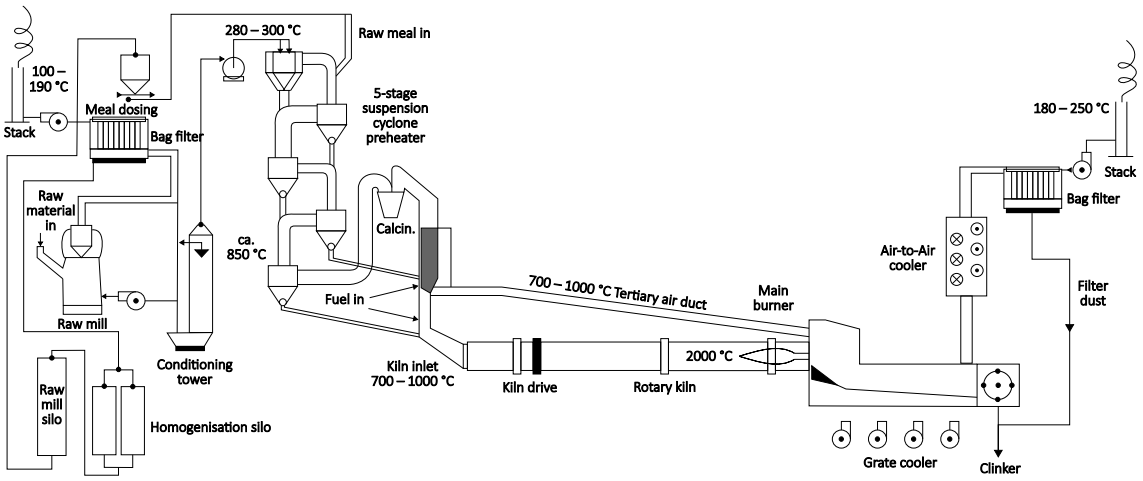

Figure 3: Cement production process (Schoenberger, 2015).

Ground limestone, shale, sand, and clay are common raw materials in Portland cement, containing required elements for clinker formation. Being a resource-intensive process, 1.5 to 1.7 tonnes of raw materials are quarried per tonne of clinker produced. Calcium is mostly obtained from raw materials such as limestone, marl, or chalk, which accounts for 75–80 wt.% of the raw materials. Clay, shale, and other materials supply components such as silica, aluminum, and iron, as well as other elements. Small amounts of additives such as iron ore, bauxite, and shale can be used to ensure more iron oxide (Fe_2O_3), alumina (Al_2O_3), and silica (SiO_2) to modify the raw mix's chemical composition to the process and product needs (Bye, 1999; Lea & Hewlett, 2004). The various raw materials required to achieve the desired cement composition are then ground and blended to create a homogeneous blend

that is processed in the kiln. Lately, the use of selected waste products, such as blast furnace slag and fly ash are utilized in the cement production. Such measures have the additional benefit of decreasing the demands on local landfills. Depending on the way raw materials are prepared, cement manufacturing process can be classified in four categories, i.e., the wet process, the semi-wet process, the semi-dry process, and the dry process, which is the most conventional production process nowadays. The homogenous blend of input raw materials is termed raw meal, and is stored in homogenizing silos in order to minimize the variation in material (Bhatty et al., 2004). After the homogenization step, the raw meal is introduced to the preheater tower, where the chemical transformations of raw meal into the clinker take place. The raw meal is introduced into the cyclone preheater at the top by dispersing it in the hot flue gas. After direct heat exchange between the hot flue gas and the cold raw meal particles, they are further separated in the cyclone and fed into the next stage, until the last cyclone where the raw meal particles are fed to the calciner. In this stage, due to its high temperature (850–900 °C), the limestone decomposes to form CaO (calcium oxide). After the calcination step, the calcinated raw meal is fed to the rotary kiln, where temperatures are maintained at 1450 °C for the sintering reaction to take place. This high temperature is achieved by applying peak combustion temperatures of 2000 °C in the main burner flame. The residence time of the solid materials in the kiln is anywhere from 20 to 60 minutes depending on the length of the kiln. After cooling down by grate or planetary cooler, clinker is milled and together with the addition of selected additives the product constitutes cement.

To maximize energy recovery, the flue gas from the preheater is often routed to the raw mills to dry the incoming solid feed. After passing through raw mills, flue gasses are routed to air pollution control devices (APCD) – usually fabric filters, which are used to capture fine particles from the flue gas. The collected dust in these fabric filters has the same composition as the raw meal and is often recycled back to the production process.

The cement manufacturing process is also energy-intensive. A typical requirement for a tonne of cement produced is 60 to 130 kg of fuel, averaging 40% of manufacturing costs. The main fossil fuels used in cement production are coal, pet coke, heavy fuel oil, and natural gas. Apart from these conventional fuels, the utilization of alternative fuels such as tires, waste oil, plastic waste, and wood waste is continuously increasing due to environmental concerns and the increase of conventional fuels price. When considering the selection of alternative fuels, they should fulfill certain characteristics, such as the heating value, ash content and composition, particle size and moisture content before being used.

The cement production process differs from other combustion plants due to an enhanced formation of materials cycle, derived from the varying volatility of trace elements in the raw materials and fuels. During pyro-processing, the temperature of the flue gases and solid materials has a very wide range from about 2000 °C (kiln burner flame) down to around 120 °C in the APCD. At the same time, the solid feed and flue gas are at the counter-current flow. Based on this feature, two cycles can be identified – internal and external (Figure 1.4). The internal cycle is comprised of the preheater and the rotary kiln. At the temperatures prevailing in the kiln, the volatile compounds enter the gas phase and are transported with the gas flow to the preheater. There, they are adsorbed onto the cold particles of the raw meal and are again reintroduced to the rotary kiln with the incoming kiln feed. The most known compounds of this cycle are chlorine species, sulfur, heavy metals, and alkaline components. The external cycle follows the stream of the flue gas and comprises raw mills, raw meal silo and the APCD – usually fabric filters. Volatile species present in the flue gas might condense at the temperatures present in these parts, especially in the filter dust. Usually, the dust collected by filters is recycled back to the raw meal and is reintroduced to the production process. Species known to condense during external cycle are NH_3 and heavy metals (Kern et al., 2015).

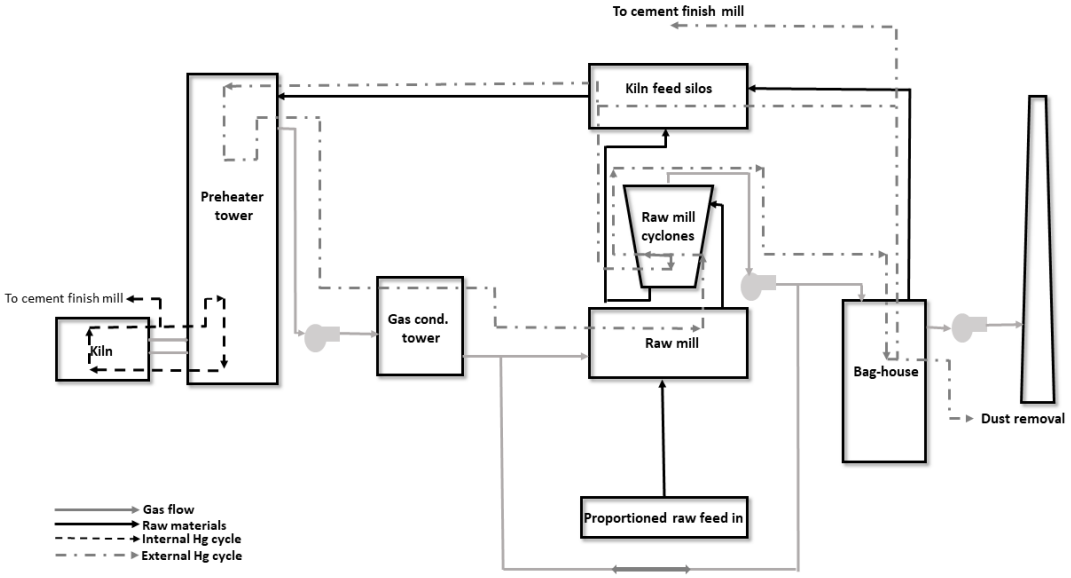

Figure 4: Internal and external Hg cycle (Schreiber et al., 2015).

As these cycles are closely connected to the operation of raw mills, two operation modes are distinguished: compound mode – during which raw mill is operating, and direct mode – during which raw mill is not used. In compound mode, the dust-containing flue gas from the preheater is used to dry the raw meal in the raw mill. As such, there is no need to cool the flue gas. In the direct mode the raw mill is not operating, and the incoming flue gas is cooled down by water injection and de-dusting. These modes of operation influence the material flow and temperatures between the raw mill, kiln system, and fabric filters, but especially the mass flows of volatile elements in the production process. Another fixture of cement production plants is the installation of bypasses. The function of such a fixture is to remove partial flows of certain compounds. One such fixture is hot gas bypass, which is used to remove alkali chlorides and sulfates. With this bypass, part of the kiln gases between the rotary kiln and the lowermost cyclone are extracted, cooled, and often de-dusted.

1.3.1 Mercury in cement production

Hg enters the cement production process as an impurity present in the raw materials and fuels. There is a wide variance of Hg levels in both raw materials and fuels. Generally, raw materials such as limestone, shale, clay, etc., show low levels of Hg, although this can vary even within the same limestone quarry as higher Hg levels can be associated with specific zones, faults, and inclusions in the quarry. The same situation also presents with fuels. It is assumed that Hg in the raw materials is present in the form of mercury sulfate ($HgSO_4$) or mercury sulfide (HgS), while in the fuels in the form of mercuric chloride ($HgCl_2$) or mercuric oxide (HgO) (Schreiber, Kellet, & Joshi, 2005). Apart from Hg, both fuels and raw materials contain other constituents, such as alkalis, sulfur, chlorine, etc. which influence intrinsic kiln chemistry and consequently Hg emissions to the air.

Hg present in raw materials and fuels is volatilized and transformed to elemental form at high temperatures (>500 °C) present in the kiln system. This volatilized form is carried

with the flue gases through the kiln system towards the conditioning tower, raw mill and/or main dust collector. Once Hg is in the kiln system, possible outcomes can be (Schreiber et al., 2005):

- Remain unchanged and exit the kiln as part of the clinker.
- React with raw materials and exit the kiln as part of the clinker.
- Vaporize in the high temperature zone of the kiln/preheater.
- Condense/react with the CKD (cement kiln dust) and be removed by APCD.
- Exit the kiln system in vapor form or be absorbed to dust particles as emitted from the stack.

Hg in the flue gas exists in varying percentages in the form of Hg^0, Hg^{2+}, and Hg_p. Elemental Hg is insoluble in water and highly volatile; it exits the system through the stack in the vapor phase. As the flue gas cools, Hg is subjected to various oxidizing reactions with the compounds present in raw materials and fuels. This oxidation is promoted by a sufficiently high concentration of halogens. The oxidized Hg^{2+} can condense onto CKD particles in colder sections of the cement production process forming Hg_p. Hg contained in the dust is captured by the APCD, and usually returned to the kiln.

The speciation of Hg is controlled by complex thermo-chemical gas-phase reactions. Flue gas contains hydrogen chloride (HCl), which can accelerate Hg oxidation in the kiln through Deacon reaction, forming $HgCl_2$ (Diamantopoulou, Skodras, & Sakellaropoulos, 2010; Li et al., 2009; Murakami et al., 2010). The probable mechanism of Hg oxidation is described to be either a homogeneous or heterogeneous phase reaction (Cao et al., 2008). The first one is thought to occur in the gas phase, whereas heterogeneous oxidation occurs on the interface of solid particles inside the kiln system or APCD.

Hg behavior in cement production is also closely connected with the operating regime of the raw mill. During the raw mill-off operation, the flue gas from the top of the preheater tower is directed to the APCD and has a higher concentration of Hg. In contrast, when the raw mill is operating, flue gas exits the top of the preheater tower and is routed to the raw mills to dry the solid feed. The temperature of the flue gas exiting the preheater tower ranges from 315–400 °C, and the concentration of fine dust particles is typically 100–150 g Nm^{-3} (Schreiber & Kellet, 2009). The temperature of the flue gas is reduced through the heat exchange in the raw mill to the exit temperature of 90–120 °C, making the raw mill act as both a dry scrubber and condenser. The flue gas from the raw mill is then directed towards the APCD where further gas/particulate separation takes place. With the raw mill operating, Hg condensed onto particles is captured by both raw mill and the APCD and is transported to the blend silos where it is re-blended into the raw meal and used as kiln feed, creating a Hg recycle loop. The re-blended raw meal is again reintroduced to the preheater, the captured Hg is again volatilized and returned in the gas stream to the raw mill, where again it is recaptured on the particulates. This repeated cycle between the preheater, raw mill and APCD constitute an enriching Hg loop during the raw mill on operating regiment. However, beside these two known Hg loops, other cycling processes can be identified, which depend on the process-specific technology, such as (Mlakar et al., 2010):

- Filter-kiln cycle – recycling of filter dust in the raw mill, dosage of the raw meal in the kiln, evaporation/desorption of Hg in the preheater and returned Hg flow with the flue gas from the preheater.

- Raw mill-kiln cycle – condensation/adsorption of Hg from the hot flue gas from the preheater on particulates of cold raw meal in the raw mill, dosage of the meal in the preheater, evaporation/desorption of Hg in the preheater and returned Hg flow with the flue gas from the preheater.
- Coal mill-kiln cycle – condensation/adsorption of gaseous Hg from the hot flue gas from the preheater on particles of coal in the coal mill, dosage of coal in the kiln, fuel combustion and returned Hg flow with the flue gas from the kiln and preheater.
- Coal mill-kiln cycle – removal of dust from the gas flow from the preheater to the coal mill and recycling back into the flow of raw meal dispensed in the preheater, evaporation/desorption in the preheater and returned flow to the coal mill.
- Preheater cycling – condensation/adsorption of gaseous Hg from the hot gas from the preheater on particles of cold raw meal dispensed in the preheater and evaporation/desorption of Hg from the raw meal in the heat exchanger passing individual cyclones.

The form of Hg in the production process will depend on the cooling rate, temperatures, and the potential for certain chemical reactions to take place. These conditions in turn are kiln specific, and are controlled by operating and gas conditions, as well as the composition of raw materials. There is limited research on Hg speciation in cement kilns (Johansen & Hawkins, 2003; Mlakar et al., 2010; Zheng et al., 2012). From equilibrium studies in coal-based flue gas, below temperature of 480–590 °C, the dominant oxidizing specie is $HgCl_2$, formation of which among others depends on the chlorine concentration and the quenching of flue gas. With the continuation of the flue gas cooling to the Hg boiling point, some of the Hg will react to form HgO, which could further react with chlorine to form $HgCl_2$. With decreasing temperatures (below 325 °C) Hg can react with sulfur dioxide (SO_2) to form $HgSO_4$, which can react with gaseous HCl and produce volatile Cl_2 that remains in the flue gas, thus limiting the concentration of chlorine and subsequent conversion of Hg^0 to $HgCl_2$ (Abu-Daabes & Pinto, 2005). Due to the high content of silica in the raw feed and the sufficient residence time, the formation of complex silicates in the kiln system cannot be excluded. However, such reactions might be constrained by the presence of chlorine and sulfur.

All Hg forms that are emitted through the stack are thought to be gaseous or condensed on the fine particles. Another Hg output is the clinker, where limited data point to low but detectable levels of Hg (Mlakar et al., 2010; Wang et al., 2016).

Some studies have attempted to model Hg behavior in the cement production process. In a model developed by Schreiber et al., (Schreiber, Kellett, & Streitman, 2009), the prediction of Hg in exhaust gas was done by taking into account the Hg concentrations within kiln inputs, continuous emission monitoring (CEM) data, and partitioning coefficients. This model attempted to address whether the removal of CKD captured in the baghouse was going to be a viable control strategy for Hg reduction. The model showed only a modest reduction of 4.1% of emissions on an annual basis in the event of 100% removal of the dust captured in the baghouse. The main drawback of this approach was that the model is not applicable as a general use tool and does not consider complex internal Hg transport mechanisms. Another model of Hg behavior is presented in the work of Senior et al., (Senior et al., 2010). It reproduces key features of Hg behavior by assuming five modes in which it exists within the production process: (1) adsorbed on raw meal, (2) adsorbed on dust, (3) gas phase, (4) chemically bound on raw meal, (5) chemically bound on dust. The model is an improvement in understanding Hg fate, as it was able to reproduce some of the characteristics of Hg behavior and is a useful tool for planning Hg emission

reduction strategies by increasing the removal of dust from APCD and lowering the temperature of such devices. Because the model is divided into nodes with specific mass flows, it is possible to apply it to other facilities. However, the model does not distinguish between different Hg species.

1.3.2 Mercury reduction techniques

Hg emission reduction has been a topic of interest for quite some time in coal-fired power plants (CFPP). Although Hg transformation in combustion gases has been investigated intensively, cement production process presents unique challenges in mitigating Hg emissions. Cement plants differ from CFPP and waste incinerators with respect to flue gas composition, residence time, temperature, and inherent material circulation. Another difference is the introduction point of raw materials and fuels which in cement production process happens in several points. The application of the following strategies will have varying removal efficiency, mostly because this requires more research to understand the sorption, desorption and the Hg compounds involved in the internal Hg loop (Sikkema et al., 2011).

Hg emission reduction technologies can be divided in three categories:

- Maintaining the existing process while reducing the input of emission precursors into the system,
- Modifying the existing process by primary or integrated reduction measures,
- Using secondary measures through maintaining an existing process while adding a separate gas cleaning unit for the exhaust gas.

With the careful selection and control of all input materials containing Hg, next to the use of effective APCD's, Hg emissions from cement plant could be better controlled. To implement this option, an approximate estimation of the typical Hg content of raw materials and fuels is needed and a careful monitoring program for determining Hg input values. Although, this option can have financial implications, as cement plants are in the vicinity of quarries making raw materials readily available. Alternative materials could substitute natural raw materials to a certain extent, provided that their Hg content is low. The same provisions apply for conventional fuels also.

Among techniques used to limit the build-up of Hg in cement plants is **dust shuttling.** The Hg-enriched kiln dust is extracted from the process in what is known as bleeding mechanism and is primarily used to bleed the system of alkali salts that circulate in a process in a similar pattern as Hg (Schreiber et al., 2015). After the removal, the extracted CKD is incorporated usually in small quantities in the final product (Adaska & Taubert, 2008; Paone, 2010). Dust shuttling can be carried out in both configurations of raw mill operation (UNEP, 2019):

- Raw mill off – because the flue gas containing Hg bypasses the raw mill, the collected dust has higher concentrations of Hg, and its removal is more efficient.
- Raw mill on – since the flue gas passes through the raw mill and is used to dry the raw meal, this mode is less efficient in removing Hg.

The temperature of the dust collection is very important as the adsorption of Hg on the dust surface increases with decreasing temperature. To maximize the efficiency of this technique, the temperature of the gas should be at or below 120 °C. When the raw mill is

off, the temperature is between 140–170 °C, making it necessary to reduce it in a conditioning tower or by air quenching.

Among the technologies widely utilized in control of Hg emissions are activated carbon injection (ACI), wet scrubbing, and selective catalytic reduction (SCR). **Activated carbon (AC)** is extensively used in other industries such as power plants, municipal waste incinerators, etc. Its chemical and physical properties such as large surface area, pore volume and size distribution make it a potential adsorbent also for Hg removal from cement kiln flue gas. However, due to high dust loading of calcium and alkali materials together with the variable concentration of SO_2 and HCl, application of AC is not without its challenges. The percentage removal of Hg using ACI will depend on the temperature and composition of the kiln flue gas and the amount and type of activated carbon used. Utilizing ACI option for Hg removal may require an additional APCD to be installed between the existing APCD and the stack. AC would be injected in the gas stream between the first and the second APCD. The second APCD then captures the Hg-laden AC, removing it from the system. This type of control technology is mostly effective for oxidized Hg. Although bromine is shown to enhance Hg removal by oxidizing it (Pavlish et al., 2003), it may cause operational concerns if it is reintroduced leading to an imbalance in the alkali-halogen ratio in the kiln.

Additionally, using the absorption capacity of the kiln system together with AC could be another strategy to control Hg emissions. AC could be injected into the main baghouse, where Hg will adsorb onto the dust. Part of this dust would be shuttled to the finished mill, and the remainder to the blend silos. But even this option has certain drawbacks as only 1% organic processing additions are allowed in the cement products (ASTM, 2009). Another issue is the temperature, as AC is effective on temperatures below 160 °C, and the temperature of the flue gas when raw mill is not operating can be higher.

Non-carbon-based sorbents are a better option for cement plants, because they can be included in the final cement product or can be separated and regenerated. Of these sorbents, chemically synthesized manganese oxide powder exhibits Hg, NO_x, and SO_2 removal abilities. It can be regenerated by a wet chemical process if the sorbent is injected before the added polishing filter (Wocken, 2004). Mineral oxides including silica gel, zeolites, alumina, montmorillonite have been modified with various functional groups such as thiol, amine, urea, amide, and additives such as sodium sulfide, sodium polysulfide and elemental sulfur, to explore their prospect as Hg sorbents (Lee et al., 2006).

Wet scrubbing is a technique widely used in electrical power generation to control SO_2 emissions. In this technique, SO_x are absorbed by a slurry which contains lime or limestone in a spray tower. It provides the highest removal efficiencies for soluble acid gases with the lowest solid waste production rate. Beside SO_2 emissions, they also reduce HCl, NH_3, dust, and to some extent metals under favorable conditions (UNEP, 2019). This technique has not been extensively used in the cement industry, mainly because the lime in the kiln system already acts as a scrubbing agent. The effectiveness of such an approach depends on the Hg species present in the flue gas, as only gaseous oxidized Hg species are removed. Another issue is the re-emission of the captured Hg, which is a result of Hg reduction chemistry in wet scrubbers, where Hg^{2+} is reduced to Hg^0, and is released from the aqueous phase back into the flue gas. The main factor that affects Hg retention in wet scrubber is the liquid-to-gas ratio, which may limit the mass transfer of pollutants (Schreiber et al., 2015).

Selective catalytic reduction (SCR) is used to reduce NO_x emissions by injecting ammonia or urea into the flue gas at the upstream side of the catalyst bed. This catalyst bed contains oxides of vanadium or titanium, with the main purpose to reduce NO_x compounds to nitrogen and water vapor. In cement plants, SCR is installed before the APCD, because the temperature required for the catalyst to be effective ranges between

288–460 °C. After the APCD is usually a wet scrubber to control SO_2 emissions. SCR provides co-beneficial conversion of elemental Hg to oxidized forms, mainly $HgCl_2$, which can be captured in the wet scrubber. Factors that affect the oxidation of Hg in SCR process are the type of coal combusted, physical and chemical properties of the catalyst and furnace conditions (Lee et al., 2006).

The implementation of SCR technology in cement plants is controlled by site-specific conditions, as it would have to be placed in an area where the temperature of the flue gas is in the appropriate range. Concerns can arise, as the flue gas may contain alkali metals and calcium oxide that can deactivate the catalyst by reacting with active sites.

1.3.3 Legislation and regulations

Cement kilns are among the biggest sources of Hg emissions from human activities. Several countries are implementing measures to address Hg pollution, and many international agreements are aimed at reducing the impact of Hg release. Of paramount importance is the Minamata Convention. The Minamata Convention is a global treaty designed to protect human health and the environment from the detrimental effects of Hg. It was agreed upon at an intergovernmental meeting held in Minamata, Japan in 2013, and entered into force in 2017. The Convention includes provisions to reduce Hg emissions and releases into the environment, phase out the use of Hg in various products and processes, promote the use of alternatives to Hg, and improve Hg waste management. Over 140 countries have signed the Convention and are working to implement its provisions.

The United Nations Economic Commission for Europe (UNECE) has a Convention on Long-Range Transboundary Air Pollution (LRTAP) that intends to address the problem of air pollution. The convention includes several protocols that set specific emissions reduction targets for various types of pollutants, among them also Hg. Despite the fact that the protocol invites the utilization of best available techniques (BAT) at stationary sources, it does not define such arrangements or specify any reduction strategy (Sloss, 2015). Nevertheless, the convention has been credited with significant reductions in sulfur dioxide (SO_2) and nitrogen oxide (NO_x) emissions in Europe, although challenges remain in reducing other pollutants and addressing emerging air pollution issues. There are also other programs and agreements that aim to reduce Hg emissions, such as OSPAR (Oslo and Paris Commission's program on reduction of land-based pollutants transported to the North Sea), MEPOP (European political initiative studying the atmospheric cycling of Hg and persistent organic pollutants), though none of these include guidelines on how such reduction could be achieved.

In the European Union, the Industrial Emissions Directive (IED) is an instrument that aims to prevent and control pollution arising from industrial activities. It has replaced three previous directives, namely the Integrated Pollution Prevention and Control (IPPC) Directive, the Large Combustion Plant Directive (LCPD), and the Waste Incineration Directive (WID). In this document, the standards for emissions of pollutants (Hg included) from certain industrial sectors are set. The Directive establishes a prerequisite for CEM of particulates, SO_2, and NO_x on all plants. For Hg, the average emission limit value over a sampling period of a minimum of 30 minutes and a maximum of 8 hours is 0.05 mg/Nm^3. More stringent emission limits are outlined in the document "*Best Available Techniques (BAT) Reference Document for Large Combustion Plants*" (Lecomte et al., 2017), where limits for large combustion plants that use coal is set as low as <1-3 µg/Nm^3, and lignite <1-5 µg/Nm^3 for plants with thermal input <300 MW_{th} for new plants, and <1-9 µg/Nm^3 and <1-10 µg/Nm^3 for existing plants. For plants with thermal input larger than 300 MW_{th}, the limits are slightly lower, <1-2 µg/Nm^3 for new plants that burn coal, and <1-4 µg/Nm^3 for those that utilize lignite. The existing plants in this thermal input range will have to

lower their Hg emissions up to <1-4 µg/Nm^3 in the existing plants that burn coal, while those that burn lignite the limits are set at <1-7 µg/Nm^3. Clearly, these emission limits can only be achieved by employing specific Hg abatement techniques.

Countries that are members of the EU must adopt EU legislation within a certain period. In this regard, Slovenia has adopted all relevant European legislation into national regulations. However, some countries have adopted more stringent emission limits regarding Hg. In Germany, an emission limit of 30 µg m^{-3} of Hg at all coal-fired plants is set by the Thirteenth Ordinance of the Federal Emission Control Act (13 BImSchV) together with the requirement of installation of CEM (Sloss, 2015).

1.4 Characterization of Hg in Solid Samples

Determination of only total Hg in solid environmental or industrial samples does not provide a comprehensive understanding of Hg behavior because it can exist in various chemical forms and undergo transformations that affect its toxicity and environmental impact. THg provides information about the overall concentration of Hg in the sample, but cannot distinguish between different forms of Hg, as they each have distinct characteristics and effects on human health and environment. To address these limitations, speciation analysis is often used to differentiate between different forms of an element in solid samples. In this respect, depending on the form of the element of interest in the sample that one wants to investigate, a difference between speciation and fractionation should be made (Templeton et al., 2000):

- Speciation is defined as the analytical activity of identifying the quantities of one or more individual chemical species in a sample.
- Fractionation is the process of classification of an analyte or a group of analytes according to physical or chemical properties.

This sort of analysis provides a more accurate picture of the environmental risks associated with Hg contamination and aids in selecting appropriate mitigation and regulatory decisions. Among the approaches used to study Hg speciation/fractionation are sequential extraction procedures, temperature-programmed desorption, X-ray absorption spectroscopy, etc. Each of these methods has its advantages and disadvantages in relation to Hg analysis. Sequential extraction partitions Hg in solid samples into several operationally defined groups based on their solubility (Rubio & Rauret, 1996). This analysis consists of several steps, including extraction, derivatization, purification, and analysis. Some of the drawbacks of sequential extraction methods include the oversimplification of the complexity of interactions between elements and matrix in environmental samples, incomplete extraction, difficulty matching extractions to specific species, possible re-adsorption, poor reproducibility and selectivity, lack of standardization, loss of volatile species, etc. (Issaro et al., 2009).

Alternatively, temperature-programmed desorption (TPD) methods have been shown to be suitable in fractionation studies in specifying and quantifying Hg binding forms in environmental and industrial solid samples. The method is based on the thermal decomposition/desorption of Hg from solid samples at different temperatures and continuous determination of released Hg, which enables the identification of Hg compounds by the difference in temperature and the pattern of release. The advantage of this approach lies in the absence or minimal preparation step and stabilization of the analyte, it is fast and relatively simple to perform. TPD analysis serves as a valuable tool in understanding

temperature stability of Hg in solid substrates, and defining fractions released during controlled heating as proxies for the identification of Hg compounds in solid samples (Pavlin, 2018; Windmöller et al., 1996). It has been widely used to identify Hg compounds in samples such as soils, sediments, gypsum, development of sorbents, etc. (Biester & Scholz, 1997; Lopez-Anton et al., 2010; Rumayor, Diaz-Somoano, et al., 2015; Rumayor, Lopez-Anton, et al., 2015; Sedlar et al., 2014; Shuvaeva et al., 2008). The information provided in Table 1.2 represents decomposition of pure Hg compounds.

Table 1.2: Temperature characteristics of Hg compounds.

Hg compound	Decomposition or sublimation temperature (°C)	Reference
Hg^0	– 39	(Lide, 2009)
	<80	(Watling et al., 1972)
	<150	(Bombach et al., 1994)
Hg_2Cl_2	383 – sublimation	(Lide, 2009)
$HgCl_2$	277 – melting point	
	304 – boiling point	(Schroeder & Munthe, 1998)
HgO (red)	500 – decomposition	(Schroeder & Munthe, 1998)
HgS	344 – transforms to black HgS	(Lide, 2009)
	584 – sublimation	(Schroeder & Munthe, 1998)
$HgSO_4$	450 – decomposition	(Lide, 2009)
	500 – decomposition	(Tariq & Hill, 1981)
Hg_2SO_4	335 – 500 – decomposition	(Tariq & Hill, 1981)

However, there are certain shortcomings in utilizing TPD methods. Among them is the sample matrix, particle size distribution, the type and flow rate of the carrier gas, and each of them can affect the release of Hg by shifting the peak towards lower or higher temperatures (Sedlar et al., 2014). Due to these constraints, there is no standardized method for TPD analysis, making the results obtained difficult to compare. As such, this analysis is considered as qualitative evaluation.

Mostly, TPD studies related to Hg fractionation in solid samples were performed using AAS as a detection method. This approach only detects Hg released from the sample, and the sensitivity often poses an issue. TPD analysis coupled with the quadrupole mass spectrometer (QMS) is an approach that helps overcome some of the shortcoming of the TPD-AAS approach, as it is more sensitive and additionally enables the observation of evaporation of other molecules from the solid sample.

Chapter 2

Aims and Hypothesis

The purpose of the dissertation is the study of Hg transformation within the cement production process by using TPD-QMS approach. Due to the complexity of the process of cement production, Hg undergoes a series of transformations, influenced by temperature and operating conditions among others. Hg fractionation study of solid samples gives us insight into how Hg is transformed from chemically bound in the matrix of raw materials, to more labile fractions in a separate part of the process, and the use of QMS provides the sensitivity needed to study this transformation process.

The goals of the dissertation are:

- To validate a method for determination of total Hg based on combustion coupled to AAS for samples from cement production and to assess the expanded uncertainty of the method.
- To optimize TPD-QMS for Hg in cement production process.
- To study the desorption of Hg in solid samples through TPD-QMS.
- By employing TPD-QMS, to clarify and confirm Hg reactions within the process of cement production.

The following hypotheses were established:

- Combustion coupled to AAS detector is a suitable method for the determination of total Hg in solid samples from the cement production process.
- Temperature desorption method coupled to the QMS offers sensitivity that allows for measurement of Hg released from all solid samples in the cement production.
- QMS allows the identification of other decomposition products released during the heating of solid samples.
- Hg in natural raw materials is strongly bound to the matrix and is thermally stable. Hg decomposes at high temperature in cement kiln and is transported by exhaust gas towards colder parts of the system, such as preheater, raw mill, and baghouse dust.
- At lower temperatures gaseous mercury forms a partition between gaseous and solid phases. Temperature fractionation analysis of the solid phase is a good predictor/indicator of Hg partitioning during these processes.
- Clinker as a final product of cement production has relatively low content of thermally stable Hg compounds.

Chapter 3

Materials and Methods

3.1 Description of the Technological Process

The cement plant is situated in the western part of Slovenia, with a current production capacity of about 1 million tonnes of cementitious materials per year. The cement plant utilizes a dry process to produce clinker. The kiln system consists of a five-stage suspension cyclone preheater, an inline calciner, a rotary kiln, and a grate cooler (Figure 3.1). The introduction of the fuels is carried out via the main burner and with the secondary combustion device (hot disc) located in the preheater, with temperatures of the main burner flame reaching up to 2000 °C, while the gas temperature at the bottom of the preheater reaches up to around 1000 °C. The crushed raw material mixture from the quarry enters the process via two ball mills. The obtained mixture of raw meal is stored in the silos and then dispensed in the preheater, where this solid feed is gradually heated up to 900 °C with flue gas from the kiln. The formation of the clinker takes place in the rotary kiln at a temperature range of 1000–1450 °C, and the clinker is then released through the clinker cooler. Part of the flue gas from the kiln is used to dry the incoming kiln feed in the raw mill. Fabric filters are used as a de-dusting device and are located just before the stack. Mineral raw materials, such as limestone and clay materials, are sourced from the local quarry. Some external additional materials with proper compositions can also be used as additions to mineral raw materials, such as to control the content of iron and some waste materials (e.g., waste concrete materials) from other processes.

3.2 Sampling of Solid Materials

Solid heterogeneous samples were taken as spot samples from the different parts of the production process and were homogenized and ground to the desired consistency. The chosen locations for the sampling of solid materials marked by red dots in Figure 3.1 represent the characteristic points in the production process where the specific performance of Hg could be observed, as well as points where mass flows of Hg are the largest, mainly due to cycling processes (Mlakar et al., 2010). The collection of solid samples included raw materials (limestone), raw meal from selected parts of the production process, cement kiln dust from fabric filters, bypass dust, clinker, and fuels (petrol coke and 2D and 3D refuse-derived fuels). Sampling of solid materials was performed during regular emissions monitoring campaigns.

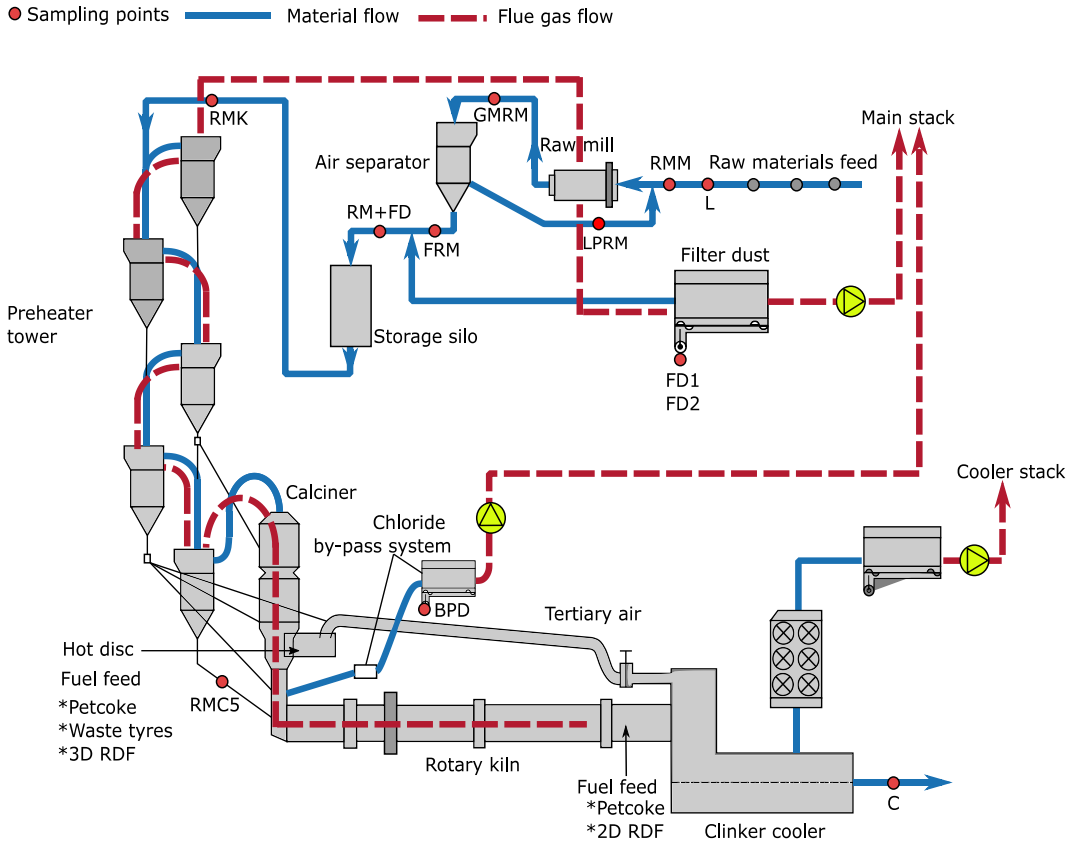

Figure 5: Simplified schematics of the cement production process with red-dot-tagged sampling locations.

3.3 Determination of Total Hg

Total Hg in solid samples was determined with the method of combustion coupled to an atomic absorption spectrometer (AAS), or usually known as direct thermal decomposition (DTD). The mercury analyzer RA-915M with a PYRO-915+ thermal decomposition attachment (Lumex Scientific, St. Petersburg, Russia) is based on differential Zeeman atomic absorption spectrometry using high frequency modulation of light polarization. The instrument is used for the determination of total Hg by the manner of thermal decomposition, in various types of samples (Sholupov et al., 2004).

The working principle of the instrument is based on the thermal evaporation of Hg from the sample. Using a quartz boat, an aliquot of the sample is placed in the dosing unit of the first chamber of the atomizer that operates at temperatures 680–750 °C using a gas flow rate of 0.8–1.2 L min^{-1}. The first chamber decomposes the solid samples, where Hg compounds are evaporated and dissociated to form elemental Hg. Afterwards, the gaseous compounds that are formed are transported into the second chamber of the atomizer, which is constantly heated at 800 °C to avoid Hg recombination with other oxidants, during which the complete combustion of the remaining volatile compounds takes place, where smoke and interference compounds are burnt. The Hg electrodeless discharge lamp (EDL) is placed in the gap between the poles of the magnet and is excited by the high frequency generator. The light successively passes through the polarization modulator to the optical

bridge which automatically switches the light beam direction depending on the selected operation mode. In the external cell, which is used in this work, the radiation passes through the removable optical unit of the external analytical cell, then through the single-path cell compartment and arrives at the photodetector. Downstream from the atomizer, the airflow enters the detector where the absorption of the elemental Hg is detected at a wavelength of 253.7 nm. The photodetector signal reaches the electronic signal-processing unit where it is separated at the modulation frequency and the analytical signal is formed. The whole decomposition procedure and detection of Hg takes place in an enclosed system. The time that was required for the analysis ranged from 60 s to 180 s, depending on the mass of the sample and the Hg content.

The measurement procedure included weighing a portion of the sample (~ 0.1 g, Mettler Toledo AE 240 balance) in a quartz boat, which was afterward subjected to high temperatures in the combustion unit, where Hg was released quantitatively. The total area under the peak of the thermal release profile was considered an analytical signal for Hg quantification. After each measurement, the residue from the combustion is disposed and the quartz boat is "cleaned" by inserting it again in the combustion unit.

Two different approaches were employed to calibrate the output signal of the instrument by introducing known quantities of Hg. The relationship between a known amount of Hg and the output signal was represented by a calibration curve, which was constructed by plotting the absolute amount of Hg (ng) versus the integrated absorbance.

3.3.1 Reagents and certified reference materials (CRM)

For calibration and validation purposes, the CRMs from Table 3.1 were employed in the study.

Table 3.1: Average matrix CRM masses used for calibration and their respective relative standard deviation.

Matrix CRM	Average CRM mass (mg)	RSD %	Average Hg mass (ng)
ERM CC 141	12	8	1
	63.2	1	5.25
	188	2	15.6
	244	2	20.2
BCR 320R	39	0	33.2
	63.5	3	54
BCR 280R	71	3	103
	171	2	250

A solution of 5% HNO_3 (v/v) was prepared prior to dilution of standards and stored at room temperature (21 °C). This acid solution was used for the preparation of all standard dilutions. A new ampoule of Standard Reference Material (SRM) NIST 3133, Mercury (Hg) Standard Solution (Lot No. 061204), was gently shaken for 2 min and opened according to the certificate. The stock standard solution (100 µg mL^{-1} = 97800 ng g^{-1}) was prepared by transferring 937 µL of SRM NIST 3133 solution with the pipette to a 100-mL glass flask containing 70 mL of previously prepared 5% HNO_3 acid solution, stirred, and topped up with the same acid solution to the mark. The flask was then capped, well shaken and left at room temperature for 1 h before preparing further dilutions. The same principle was applied for the preparation of other concentrations (100, 500, 1000, 5000, 10000, 50000 ng mL^{-1}).

All pipettes were calibrated prior to use by weighing the appropriate volumes of Mili-Q water 10 times at 20 °C (density of Mili-Q water was taken from literature). The exact densities of the NIST 3133 solution and its dilutions were determined separately by weighing three aliquots using calibrated pipettes. All volumes described above were weighed on the balance at the same time to calculate exact Hg concentration on mass basis. The prepared solutions were kept at constant temperature (21 °C). The uncertainty of the volumes (pipettes, glass flasks) and expected variations in the temperature (± 4 °C) were included in the uncertainty budget.

3.3.2 Calibration with the matrix CRM

The external calibration of the instrument was conducted by weighing different portions of the matrix CRM (Table 3.1). Under the influence of the high temperature in the pyrolizer, vapors of elemental Hg were transported into the analytical cell, with background absorption being eliminated by the high-frequency Zeeman correction system. The absolute mass of the Hg (ng) was calculated from the relationship between the certified value of the Hg content in the matrix CRM and the mass (mg) that was used for calibration. Each point of the calibration curve consisted of four repeated measurements, although it was practically impossible to accurately weigh the same mass more than once. The plotting of the absolute Hg mass was done by correcting for moisture content.

3.3.3 Spiked calibration

For the second approach to calibration, ~0.1 g of the sample was weighed. The naturally present Hg in this portion was firstly released quantitatively and then measured for blank. When it was assured that all Hg was released, and the material was cooled down to the ambient temperature, it was spiked with the Hg^{2+} calibration solution. Afterward, the portion was again subjected to high temperatures in the pyrolizer, and the instrument's signal was recorded. Calibration solutions were prepared in different concentrations to obtain the proper working range as well as to keep the material's moisture at a minimum. Each calibration point consisted of four repeated measurements.

3.3.4 Validation parameters

The reliability of the measurement depends on the methods, which provide qualitative, reliable, and consistent results, with the final goal being a result that is close enough to the unknown true value of the content of the analyte in the sample. In this context, the parameters that were used for method validation included the following: calibration curve and working range, linearity, the limit of detection (LOD), the limit of quantification (LOQ), recovery, precision (repeatability and intermediate precision), as well as combined and expanded uncertainty of the result. Combined standard uncertainty, which considers all uncertainty components in a complex measurement process, was calculated by combining the relative standard uncertainties of the major contributors during measurement, as presented in Figure 3.2. The expanded uncertainty in the result consists of the combined standard uncertainty (u_c) multiplied by a coverage factor of $k = 2$.

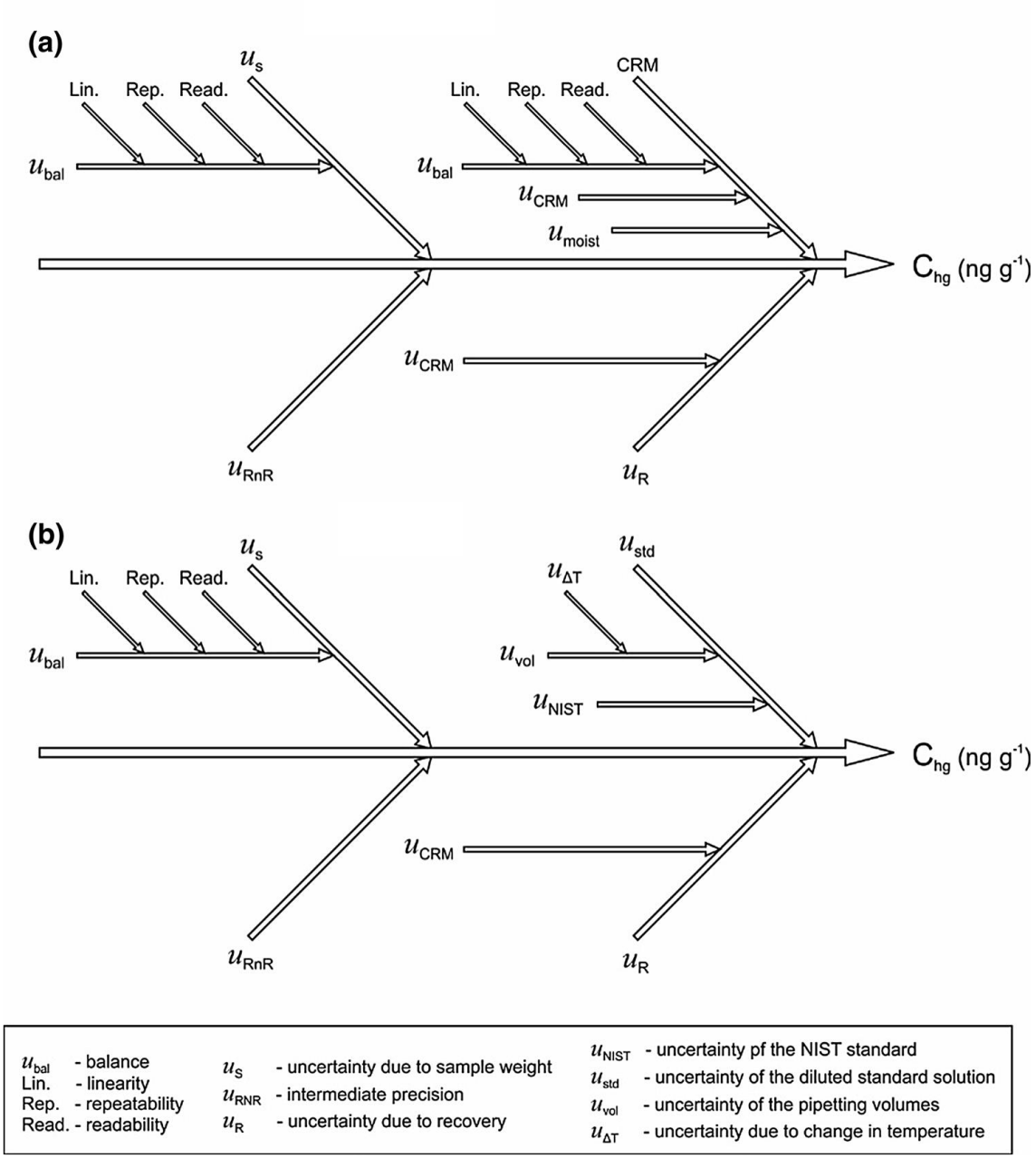

Figure 6: Fishbone diagram of all relevant sources of uncertainty in the determination of Hg content; a) with matrix CRM calibration; b) with spiked calibration.

Validation experiments were performed over an extended period, and the results were used to evaluate different validation parameters. The absolute LOD and LOQ were obtained from the elements of the regression function—the standard error of the intercept and the slope. Correspondingly, the LOD was calculated as three times the standard error of the intercept divided by the value of the slope, and the LOQ was ten times the standard error of the intercept divided by the slope. The repeatability included a contribution from any part of the procedure that varied within a run, including those from gravimetric errors. Five subsamples were measured three times during the day, and repeatability standard deviation was calculated. The evaluation of intermediate precision was carried out by analyzing three samples that corresponded to three different concentration levels on

different days. A recovery analysis was performed by analyzing the matrix CRM BCR 277R Estuarine Sediment and comparing the content recovered with the one certified. To determine whether the recovery significantly differed from 1, a significance test was used, and the obtained value was compared with the two-tailed critical value $t_{crit.}$, for n–1 degrees of freedom at a 95% confidence level. All relevant calculations are summarized in Table 3.2.

Table 3.2: Equations used for calculation on the combined relative standard uncertainties.

Equation	Explanation of parameters
$s_{xy} = \sqrt{\frac{\sum_{i=1}^{n}(y_i - \hat{y}_i)^2}{n-2}}$	s_{xy} – residual standard deviation y_i – observed detector response $\hat{y}_i$ – predicted detector response by the regression line n – number of calibration points
$s_{x_0} = \frac{s_{xy}}{b}\sqrt{\frac{1}{\mathrm{N}} + \frac{1}{\mathrm{n}} + \frac{(\mathrm{y} - \bar{y})^2}{b^2 \cdot \sum_{\mathrm{i}}^{\mathrm{n}}(\mathrm{x}_i - \bar{x})^2}}$	s_{xo} – prediction interval of the Hg mass (x) b – calibration slope N – number of parallel sample measurements x_i – value on the x-axis $\bar{x}$ – the mean of the x values
$u_{cal} = \frac{s_{xo}}{c_s}$	u_{cal} –uncertianty resulting from the calibration of the instrument c_s – concentration of the sample
$\overline{R} = \frac{\bar{x}}{x_{cert.}} \cdot 100$	$\overline{R}$– mean recovery from the results of the replicate analysis of the CRM $x_{cert.}$ –certified value of the CRM used for recovery calculation $\bar{x}$ –mean of the replicates analysis of CRM
$u(\overline{R}) = \overline{R} \cdot \sqrt{\left(\frac{s_{obs}^2}{z \cdot C_{obs}^2}\right) + \left(\frac{u(C_{CRM})}{C_{CRM}}\right)^2}$	$u(\overline{R})$ – uncertainty of the recovery s_{obs} – the standard deviation of the results from the replicate analysis of the CRM z – the number of replicates $u(C_{CRM})$ – the uncertainty of the certified value C_{CRM} – certified Hg content in the CRM C_{obs}^2 – mean value of the replicates of CRM
$t = \frac{\lvert 1 - \overline{R} \rvert}{u(\overline{R})}$	t value for significance test
u_{RnR}	Uncertainty due to intermediate precision
$u_c = \sqrt{u_{CRM}^2 + u_{cal}^2 + u_m^2 + u_{RnR}^2 + u_R^2}$	Relative combined standard uncertainty
$u_i = \frac{u_i^2}{\sum_i^n u_i^2}$	Contribution index for each parameter that was used to calculate the combined standard uncertainty

The relative combined uncertainty was multiplied by the coverage factor $k = 2$ to obtain the expanded relative combined standard uncertainty (U) at the 95% confidence level:

$$U = u_c \cdot k \tag{3.1}$$

3.4 Thermo-Desorption Analysis

Thermo-desorption analysis is a very useful method utilized to observe the desorbed molecules from a surface under the influence of the increased temperature. By recording how many and which molecules desorb as a function of time for a given surface temperature ramp, it is easy to identify the desorption activation energy of a particular molecule. This approach is based on a programmed sample heating, during which the desorbed species flow towards the ion source becoming ionized, and then pass through the quadrupole rods where ions of a specific mass-to-charge ratio (m/z) reach the detector.

In this study, the quadrupole mass spectrometer (QMS) was employed (Pfeiffer QMS 700) (Figure 3.3). Among the benefits of the QMS is the ability to distinguish various molecular species that desorb from the sample upon heating at the same time. The introduction of the sample in the system is performed via a thick wall quartz tube. All desorbed species enter an almost closed ion source, thus increasing the ionization and sensitivity. The QMS consists of two parts: a pre-chamber and the central part of the spectrometer. The pre-chamber serves for sample introduction, while the central part of the instrument contains cross beam ion source, quadrupole mass filter (four parallel rods for ion filtering) and detector (Faraday cup and secondary electron multiplier – SEM). After the introduction, the sample is heated to 800 °C at 10 °C min^{-1} under high vacuum ($<10^{-5}$ mBar) using a EUROTHERM temperature regulator.

Figure 7: QMS used for TPD analysis.

Computer software Quadera was used for interpretation of the data as graphs that show the concentration of the Hg ion in the signal of ion current (A) as a function of time (or in this case the time is converted to temperature since the heating rate is known). Isotope ^{202}Hg and ^{200}Hg concentrations were measured simultaneously. The thermograms are presented as a signal for the continuous measurement of Hg concentration in counts per second (CPS) on the ordinate axis versus the temperature (°C) on the abscissa axis, that enables the observation of Hg release with incremental increases in temperature. For easier comparison between mercury fractions with different intensities, the intensity of the signal is normalized to match the highest release of the peak to 100%.

For comparison purposes, the desorption profiles of pure Hg compounds mixed with $CaSO_4 \bullet 2H_2O$ (Figure 3.4) from the study of Pavlin (Pavlin, 2018) were used to aid in the interpretation of different spectra.

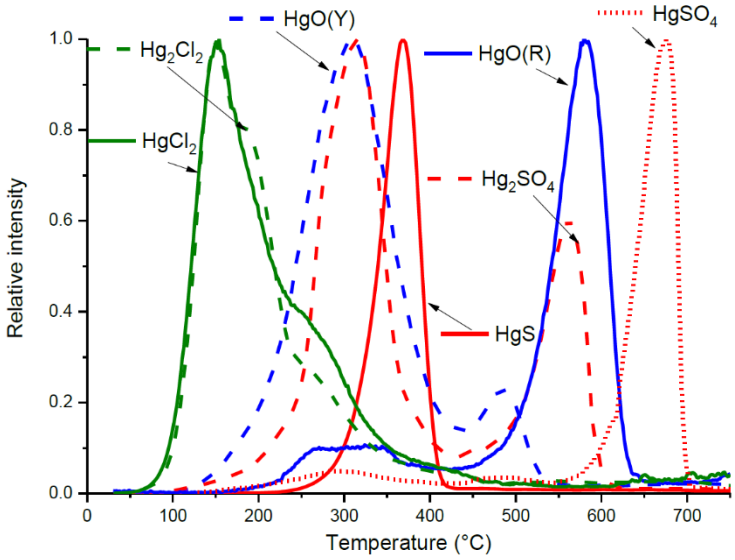

Figure 8: Dry Hg standard used to compare obtained spectra in this study (Pavlin, 2018).

All TPD spectra obtained were prepared using Origin 2018 Software (*OriginPro 2018*, n.d.). Where appropriate, the deconvolution step was used, by using the *Gauss* function of the *Multiple peak fit* analysis.

Chapter 4

Results and Discussion

4.1 Validation of AAS for Determination of Total Hg in Cement Samples

Monitoring Hg input to the cement production process is among the techniques mentioned in the document "*Guidance on the best available techniques and best environmental practices*" (UNEP, 2019). Although, such information cannot be used to predict Hg emissions, as already mentioned, cement plants have an internal control mechanism that captures and recirculates Hg between hot and cold sections of the production process, it is beneficial to have an overview on the Hg content in raw materials and fuels.

Many analytical techniques have been utilized for the determination of total Hg in various samples, such as: inductively coupled plasma mass spectrometry (ICP-MS), inductively coupled plasma atomic emission spectroscopy (ICP-AES), neutron activation analysis, cold vapor atomic fluorescence spectrometry (CV-AFS), CV atomic absorption spectroscopy (CVAAS), etc. All these methods require lengthy procedures of sample preparation, which involve decomposition, Hg reduction, phase separation of Hg vapor and detection. Choosing the appropriate method for measuring Hg depends on the detection limit required, sample matrix, sample size and potential interferences (Lasorsa et al., 2012). Direct thermal decomposition (DTD) coupled to the AAS detector is an analytical technique that can be used to measure total Hg in solid samples. It involves the heating of the sample in a controlled environment to volatilize Hg from the solid matrix. This method is rapid and sensitive and has many advantages over traditional digestion techniques, such as: utilization of few or none of the reagents, minimal requirement for sample preparation, fast analysis, and minimal analyte loss. DTD methods have been used for measurement of total Hg in various environmental samples (Hall & Pelchat, 1997; Kelly et al., 2012; Panichev & Panicheva, 2015; Pontes et al., 2013).

Quantitative analysis in spectrometric techniques produces results whose accuracy depends on the instrument's calibration to ensure comparability over time and among laboratories (Jochum & Enzweiler, 2014). A vital component of comparability is the ability to calibrate instrumentation using traceable reference materials (Kirkup & Mulholland, 2004). Most analytical techniques use calibration standards in aqueous solutions (Furtado Da Silva et al., 2006; Park et al., 2013; Rezende et al., 2018). However, when employing DTD for total Hg quantification where the samples are analyzed in their solid form, calibration using aqueous solutions does not take into consideration the sample's matrix. The difference in the physical form of the calibration standards and the samples leads to the difficult evaluation of metrological parameters (Mandjukov et al., 2015). Owing to these peculiarities, two approaches to calibration of the instrument were employed, which also consider the physical form of the samples under study.

In cases of multi-point external calibration, the relationship between an analytical signal y to the analyte content x that is present in either a matrix CRM or a standard calibration solution is represented by the linear calibration function: $y = a + bx$. After performing the least-squares regression (the default regression function of the instrument) on a set of calibration data, the inverse of the calibration function is used to predict the content x_0 of an unknown sample corresponding to the observed absorbance y_0. In the case of solid sampling analysis, the calibration curve passes through the origin due to the absence of the blank sample. As there is no analyte being introduced in the combustion unit, no response of the instrument is observed, so the linear calibration function in this case can be given by $y = bx$ (Kurfürst, 1998).

Due to the counter-current flow of materials and flue gas in colder parts of the production process (i.e., raw mill and de-dusting devices), oxidized Hg in flue gas becomes attached to particles of incoming feed, which significantly increases the concentration. The Hg content of individual raw materials from the quarry and limestone varies from 7–47 ng g^{-1}. As the raw materials and flue gases flow in opposite directions and through different temperature gradients of the system, the Hg concentration of solid material in certain parts of the process reaches up to 3400 ng g^{-1} (Mlakar et al., 2010). This variable concentration requires a working range that is wide enough to cover all the concentrations that may be encountered during the measurements of real samples. For this purpose, three different CRMs which differed in analyte content were employed for calibration. The certified values of Hg in the matrix CRM are expressed as dry weight and their use in quality control should follow the recommended mass (usually 100–300 mg). From Table 3.1, although for certain calibration points the recommended mass was not used, nevertheless the masses used for calibration have been shown to be appropriate, because the fluctuation of the mass used is within the uncertainty of the matrix CRM which also includes the assessment of homogeneity.

Calibration is performed by weighing different masses of a CRM; therefore, another component to uncertainty is the balance used for weighing. Depending on the mass fraction of analyte of the CRM, the balance uncertainty that is used for weighing can have a significant impact on the combined uncertainty. A high analyte fraction in the matrix CRM would imply weighing small aliquots; however, in this case, the uncertainty of weighing can account for up to 10% for masses below 0.04 mg, which is another reason why the calibration was performed with several matrix CRMs that differed in their certified Hg content.

Figure 4.1 shows the calibration curve and the regression coefficient that were obtained using matrix-matched CRM calibration. The certified analyte content in the matrix CRM was accompanied by the standard uncertainty, which was relatively large (Table 3.1), indicating that each calibration point could be within this uncertainty. Therefore, the horizontal error bars in Figure 4.1 represent the uncertainty of the Hg certified content in the matrix CRM.

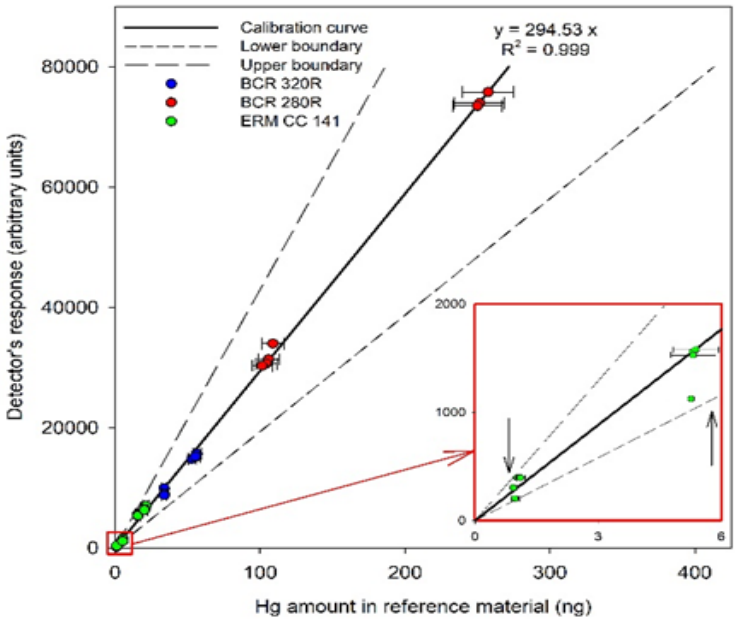

Figure 9: The calibration graph that was obtained with the matrix CRM; two black arrows show two calibration points with the highest relative standard uncertainty used to construct upper and lower boundaries of the calibration curve.

To estimate the uncertainty of the Hg amount in the matrix CRM and its influence on the calibration, the uncertainties of all CRMs were compared. However, when combining all the CRMs' uncertainties, the obtained combined standard uncertainty was enormously high and did not reflect the real variability of the experimental results (the results showed much lower variations than the estimated uncertainty). Therefore, in calculations performed, only a CRM with the highest value of standard uncertainty (ERM CC 141; 10.2% at $k = 1$) was used. To confirm that only one value could indeed cover the uncertainties of all the matrix CRMs, the estimation on both lower and upper CRM uncertainty boundaries on the calibration curve was performed (Figure 4.1). These boundaries were defined as lines connecting the origin with the minimum (maximum) value of the specific calibration points (x ± u; indicated with black arrows in Figure 4.1) having the highest relative uncertainty. All calibration points and their respective standard uncertainties (presented by whiskers in Figure 4.1) were within these boundaries, indicating that only the CRM uncertainty with the highest value should be considered when estimating the relative combined standard uncertainty.

By contrast, spiking the matrix with a standard calibration solution is a common practice when both the samples and the calibration standards are not only in the same physical form but are also affected in the same way during analysis (Cuadros-Rodríguez et al., 2001). Because the instrumentation employed in the research was selective enough, the response of the instrument was entirely due to the presence of the Hg^{2+}, which was added through the spike. Figure 4.2 presents the calibration curve obtained with this approach.

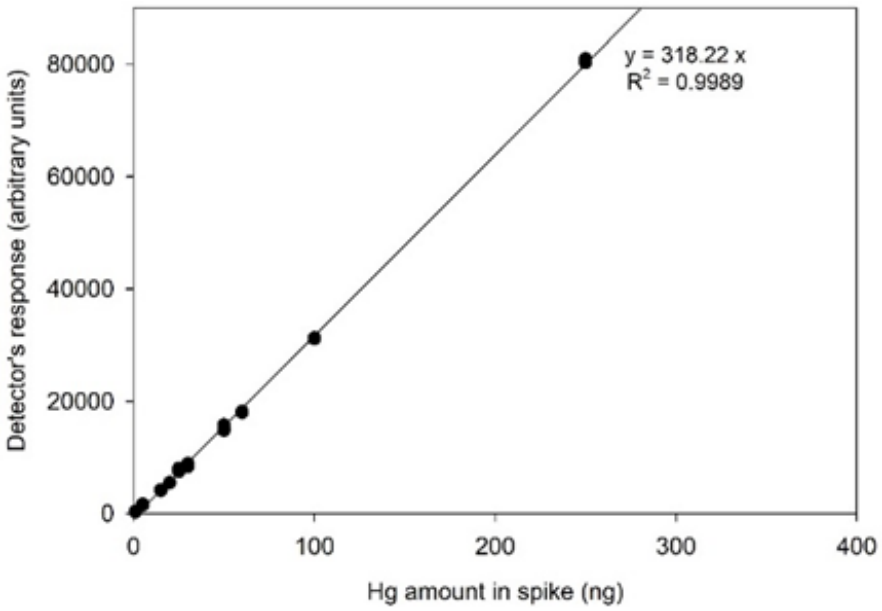

Figure 10: The calibration curve was obtained by a spiked calibration.

In comparison to the calibration by a matrix CRM, where the uncertainty of the certified Hg content was relatively large, in this approach, even after dilution of the stock standard solution (considering all sources that arise during the dilution step), the uncertainty accounted for only 3%, and it resulted from pipetting such small volumes (10 µL).

The linearity of both calibration curves was assessed by inspection of the distribution of the regression models' residuals, which were randomly distributed around zero. The working range for both calibration curves encompassed a mass from the LOQ to a 250 ng absolute mass of Hg. Obtaining a working range that is wide enough to prevent the need to extrapolate the calibration curve is a drawback of matrix CRM calibration. The possibility of extending the working range of the calibration curve that is obtained with the matrix CRM would imply utilizing other CRMs with higher Hg content, although, again, the selection of a CRM is influenced by the closeness of the matrix to the analyzed samples. The second calibration curve also encompassed the working range from the LOQ to 250 ng Hg. However, it was easy to extend it because the limitation of the amount of matrix's CRM is not present in this case. In both calibration curves, the correlation coefficient was $R > 0.999$, which is considered as satisfactory.

The conventional approach to the determination of LOD as the analyte mass or concentration that corresponds to a signal three times the standard deviation of at least 10 measurements of a blank cannot be implemented in this technique, as it is practically impossible to find such a sample that is Hg-free that could be used as blank. In this case, the standard deviation of blank value measurements would be affected primarily by the baseline noise (scatter). By applying regression coefficients, the obtained LOD is 1.7 ng of the absolute Hg mass and LOQ is 5.6 ng, and can be easily converted to the concentration by entering the sample mass (Vale et al., 2001). Although the LOD was somewhat higher compared to other methods for total Hg quantification (Clevenger et al., 1997), the obtained LOD value was suitable because raw materials used to produce cement have a low Hg content (Mlakar et al., 2010).

From Figure 4.3, it is evident that the combined uncertainty (u_c) depended on five main components: (1) sample mass determination u_s, (2) the uncertainty of the matrix CRM

that was used for calibration/the uncertainty of the standard calibration solution $u_{CRM/std}$, (3) the uncertainty resulting from the calibration curve u_{cal}, (4) intermediate precision u_{RnR} and (5) recovery u_R. The expanded uncertainty (U_{ex}) of the result was obtained by multiplication of u_c by the corresponding coverage factor ($k = 2$).

At the highest (> 200 ng), middle (50–150 ng), and lowest (< 50 ng) levels, $U_{ex,r}$ had a value of 24.7%, 24.9%, and 29.2%, respectively, for calibration with the matrix CRM. The spiked calibration approach had lower uncertainties, at 15%, 15.5%, and 21.7%, respectively. The comparison of relative contributors to the combined uncertainty using both calibration approaches is presented in Figure 4.3.

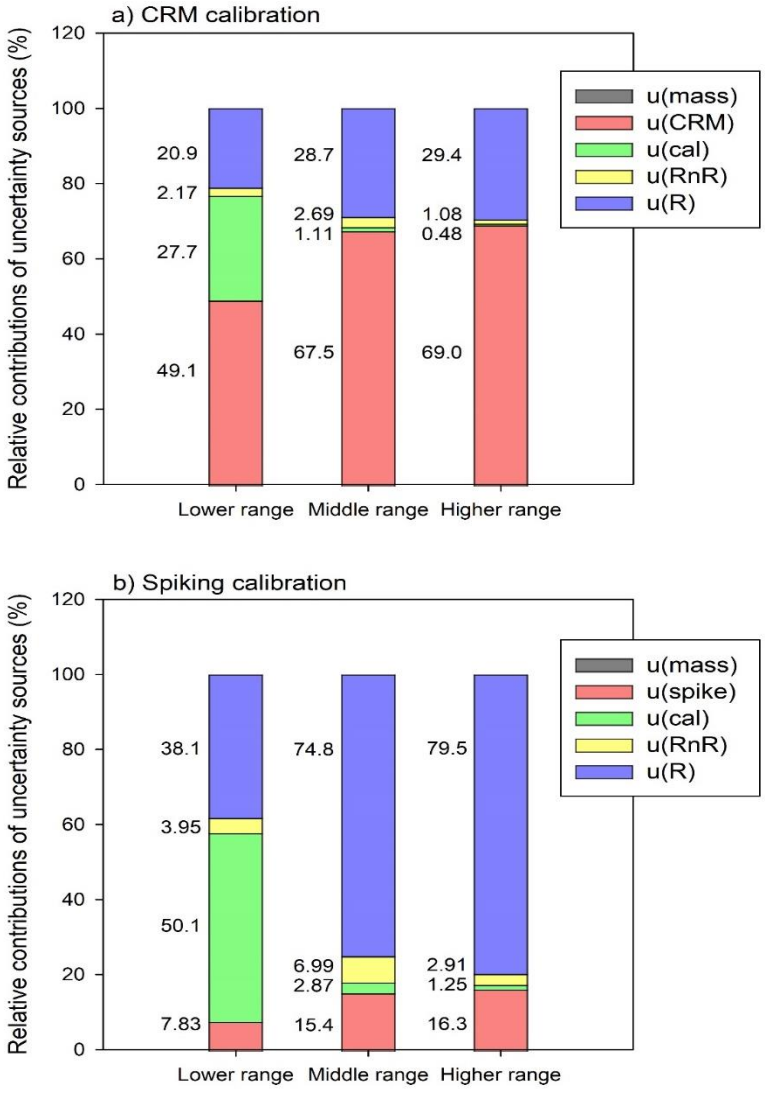

Figure 11: Relative uncertainty contribution of each source to the combined uncertainty: a) matrix CRM calibration, b) spiking calibration.

The biggest contributor to the combined uncertainty in the measurements that were performed with the matrix CRM calibration was the Hg mass fraction of the CRM itself at all concentration levels, with the uncertainty increasing with the concentration. The same was also observed in the spiked calibration approach, although the relative contribution was significantly lower. The relative standard uncertainty that resulted from the calibration curve was the same for both approaches, although its contribution was more

pronounced in the lower range of the spiked calibration. The highest contribution in the spiked calibration came from the u_{R}, which stemmed from the uncertainty of the BCR 277R itself. The contribution of u_{RnR} was relatively small and mostly dependent on the concentration level. The sample mass determination made a negligible contribution to the overall uncertainty.

The comparison of the results and the corresponding uncertainties (in logarithmic scale) of the real samples from cement production process that were obtained with the methodology that was employed in this study are presented in Figure 4.4. The results are obtained by measuring Hg content using both calibration approaches.

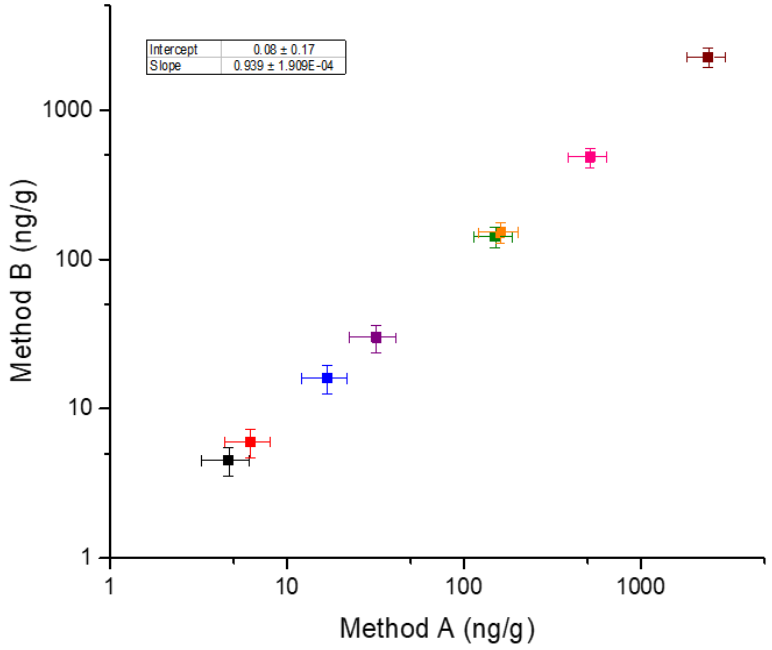

Figure 12: Comparison of the total Hg in samples that were obtained with two calibration approaches and their respective uncertainties.

Method A (x-axis) represents the results that were obtained with the matrix CRM calibration approach, while method B (y-axis) shows the results that were obtained with a spiked calibration. The whiskers represent the corresponding uncertainties of the methods. The obtained slope of 0.939 shows good agreement between the results that were obtained with both approaches; slight differences can be observed in the samples with a higher concentration. Evidently, there is a slight difference in the slopes obtained with both calibration approaches. The difference could be due to different matrix CRM used to construct the calibration curve, as in this case we have used three matrix CRM. Another issue could be attributed to the uncertainty of the matrix CRM, meaning that when the calibration curve is constructed, it is done without considering this very important information. Even though the calibration curve covers all points, the residual standard deviation (s_{xy}) of the regression in the case of matrix CRM calibration is higher (838) than in the spike calibration (723).

Metrological traceability – The purpose of a method validation is to confirm that the method employed is suitable for its intended use, and when it is correctly applied, produces reliable results, and confirms the effectiveness of the analytical method with a high degree of accuracy. Together with measurement uncertainty and metrological traceability, they present the key concepts in measurement science. The calibration of the instrumentation

used in the study was based on the specified property value that is traceable to the SI quantities which serves to link the results to the SI units.

4.2 Total Hg in Solid Samples

Table 4.1 summarizes the total Hg content in raw materials and fuels in the cement production process, along with the Hg content in the raw meal from different parts of the production process. Limestone as the principal raw material has a relatively low Hg concentration, which is comparable to that reported in other studies (Harrass et al., 2018; Kern et al., 2015; Kline & Schreiber, 2013; Paone, 2010; Zheng et al., 2012). Corrective materials such as iron-rich materials and quartz sand have a low Hg concentration, 13 ng g^{-1} and 9 ng g^{-1}, respectively. Petrol coke has a higher concentration of Hg, although the possibility of the result being overestimated exists as a portion of flue gases are routed to the petrol coke mill, and the exchange of Hg between the flue gas and petrol coke particulates can take place. Within the production process, Hg concentration changes from a relatively low content at 24 ng g^{-1} in the raw materials mixture to 65 ng g^{-1} in the raw mills. This increase in concentration reflects the fact that flue gas from the kiln is used to dry the mixture of raw materials in the raw mill. The temperature at which the raw mills operate is around 100 °C, and the exchange between Hg^0 and Hg^{2+} from the flue gas and cold particles of the raw feed is presumed to take place. The Hg content of the raw meal dosed in the kiln is 350 ng g^{-1}, reflecting the increase in Hg content due to the addition of filter dust, which is the material with the highest Hg content. As this raw meal passes through the preheater, the Hg content in the solid phase decreases due to the rise of temperature in this part of the pyro-process, which is reflected in the low Hg content of the raw meal from cyclone 5. Clinker as a final product of the production process has low Hg content (0.8 ng g^{-1}) since practically all Hg evaporates at the temperatures present in the kiln.

Apart from conventional raw materials and fuels, cement kilns offer favorable conditions for the utilization of alternative materials that could be co-processed during cement production. The introduction of these materials into the production process is primarily driven by an interest in replacing fossil fuels fostered by price increases and environmental concerns. Among alternative fuels utilized at the cement plant, waste tires, refuse-derived fuels (RDF) and small quantities of waste oils are being introduced into the process. The methodology employed for the determination of total Hg in conventional raw materials and fuels was shown to be not appropriate for alternative fuels. Determination of Hg in these samples produced inconsistent results, indicating poor repeatability (ranging from 4 to 39%), as a result of the wide range of materials and waste products that comprise this type of fuel.

Table 4.1: Average values of total Hg content in the samples of various materials and fuels used for cement production as determined by DTD AAS.

	Abbreviation	**Type of material**	**N**	**Hg content ± U ng g^{-1}, (n=3)**
Raw input materials	L	Limestone	1	9 ± 2
	RMM	Mixture of raw materials	1	24 ± 5
Solid samples from within the pyro-process	GMRM	Ground mixture in raw mill before separation	1	65 ± 14
	LPRM	Large particle raw meal	1	45 ± 10
	FRM	Ready raw meal	1	80 ± 17
	RM+FD	Raw meal with added filter dust	1	530 ± 82
	RMK	Raw meal dosed in the kiln	1	350 ± 55
	RMC5	Raw meal from cyclone 5	1	0.6 ± 1
	BPD	Bypass dust	1	38 ± 8
	C	Clinker	1	0.8 ± 0.2
	FD1	Filter dust 1	1	1840 ± 275
	FD2	Filter dust 2	1	1415 ± 210
Fuel		Petrol coke	1	295 ± 45

Results of total Hg measured in samples from other sampling campaigns are presented in Appendix A. In general, the same trend of THg is observed in all samples from different periods.

4.3 Hg Temperature Stability and Transformation Within the Cement Production Process

Determining only total Hg is not sufficient for understanding Hg migration within the cement production process. Fractionation is an approach by which the classification of an analyte or a group of analytes is performed according to either physical or chemical properties (Templeton et al., 2000). In this respect, TPD is a useful method for studying the stability of Hg in various solid samples. It is hypothesized that many Hg compounds exist in the cement production process, owing to the complexity of the production, various temperature profiles, and recirculation of the material (Paone, 2010; Senior et al., 2010;

Sikkema et al., 2011). The following results are structured according to the mass flow of solid feed inside the production process.

Limestone is the primary material used for cement production and has low Hg concentration. TPD spectra of this sample (Figure 4.5) show Hg exhibiting a broad peak from 350 to 700 °C, with a peak maximum at 582 °C. The approximate temperature of Hg release from pulverized limestone was observed in the work of Senior and Eddings (Senior & Eddings, 2006). Given the temperature at which the peak appears, it is inferred that Hg is of natural origin and is relatively strongly bound to the sample matrix. In addition, the temperature profile corresponds to the one prevailing in the preheater section, so it is assumed that Hg from limestone will be released in this part of the production process.

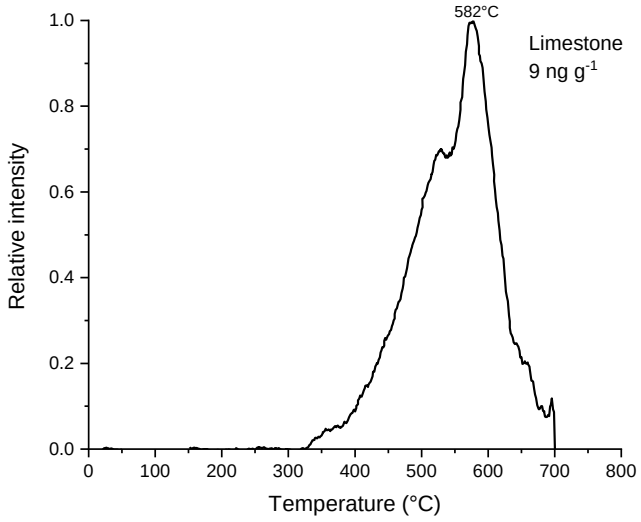

Figure 13: TPD spectra of the limestone.

The raw material mixture for cement production (Figure 4.6) consists of different components, of which limestone makes up the majority, with the rest being other natural materials from the quarry, such as clay materials, flysch, and a very small quantity (0.1%) of bottom ash. Although the total Hg of this material (Table 4.1) is not considered high, it exhibits a different desorption curve in comparison to limestone. Therefore, the thermal stability of Hg changes with the introduction of other mineral components into the raw material mixture.

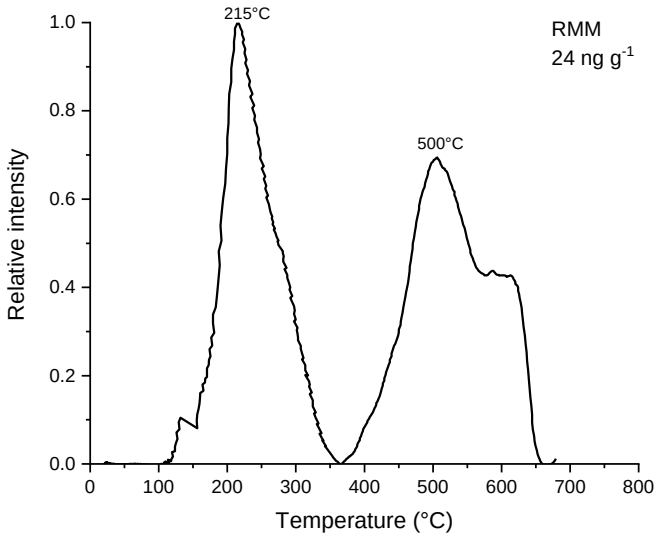

Figure 14: TPD spectra of raw materials mixture (RMM).

Figure 4.7 presents the TPD spectra of materials sampled from the raw mill, which, apart from milling the raw materials, is also used to dry this solid feed. The raw mill represents a highly dynamic part of a production process consisting of several phases. The raw meal in the mills is dried by incoming flue gas from the kiln, and the exchange of Hg^0 and Hg^{2+} between the flue gas and cold particles of the raw feed is expected to take place. This process was observed in a previous study (Mlakar et al., 2010), where the decrease of Hg^{2+} and Hg^0 content in the flue gas and the increase in Hg_p was observed in this part. Although the cement plant utilizes two raw mills for the preparation of materials, for a simplified representation of Hg temperature desorption in this part, only the results of one raw mill are presented (TPD spectra of second raw mill can be found in the Appendix). During the sampling of solid materials, raw mills were operated for 24 h. Figure 4.7 shows the Hg fractionation in the ground mixture raw meal taken before the separators, where the output of the raw meal consists of smaller and larger particles. This material then enters the larger particle separation phase, and the larger particles are returned into the mill (Figure 4.8). As the TPD spectra of this part of the process showed several peaks, the deconvolution step was performed to assist in the separation of various Hg fractions.

During the operation of the raw mill (compound mode), the potential for the adsorption of chlorine, sulfur, and alkaline compounds is higher due to the lower temperature in the raw mills and the increased load of gas flow with fresh raw material, which acts as a sorbent (Kern et al., 2015). The flue gas that comes from the kiln and is used to dry the raw meal contains Hg that can be in either the elemental or oxidized forms, and it consists of a range of various Hg compounds. Their formation depends on the operating conditions present at the site and the quenching time, both of which promote the adsorption of these compounds onto particles of raw meal (Zheng et al., 2012). Three peaks were identified in this sample (Figure 4.7), with peak maximums at 270 °C, 477 °C, and 560 °C.

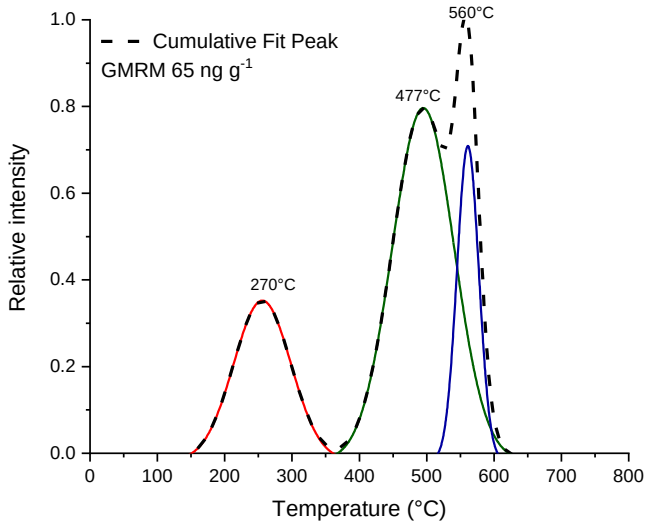

Figure 15: TPD spectra of ground mixture raw meal (before separation). Red, green, and blue lines are used to distinguish individual Hg fractions within the sample.

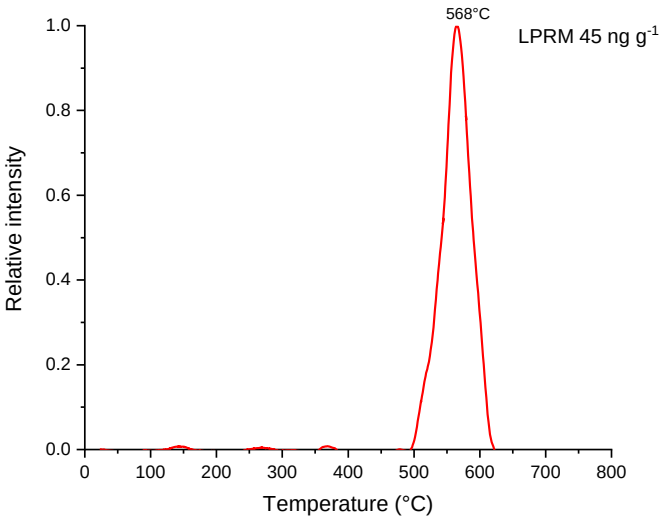

Figure 16: TPD spectra of raw meal containing large particles.

From Figure 4.8, it is evident that the raw meal containing larger particles exhibits only one peak at temperatures above 500 °C compared to the ground mixture raw meal (Figure 4.7).

Figure 4.9 represents the TPD spectra of the finished raw meal coming out of the mill, which contains only fine particles in comparison to the ground mixture raw meal (Figure 4.7). In the phase of raw materials preparation, some additional materials, such as iron-rich material, are introduced to obtain the desired chemical composition. The introduction of the above mentioned corrective materials is expected to affect the temperature stability of Hg in the finished raw mill, as demonstrated by Sedlar et al. (Sedlar et al., 2014), and the substrate affects the Hg release pattern significantly. The Hg content in this iron-rich material is 13 ng g^{-1} and while it does not contribute significantly to the total Hg in this part, it does slightly affect the TPD pattern. The change in total Hg content could also be

the consequence of the higher Hg sorption ability due to smaller particles (larger specific surface).

Compared to the spectra of the ground mixture (Figure 4.7), no major changes in terms of the number of fractions present were observed, apart from the intensity of individual fractions. The intensity of the second fraction significantly decreased, while the third became more pronounced.

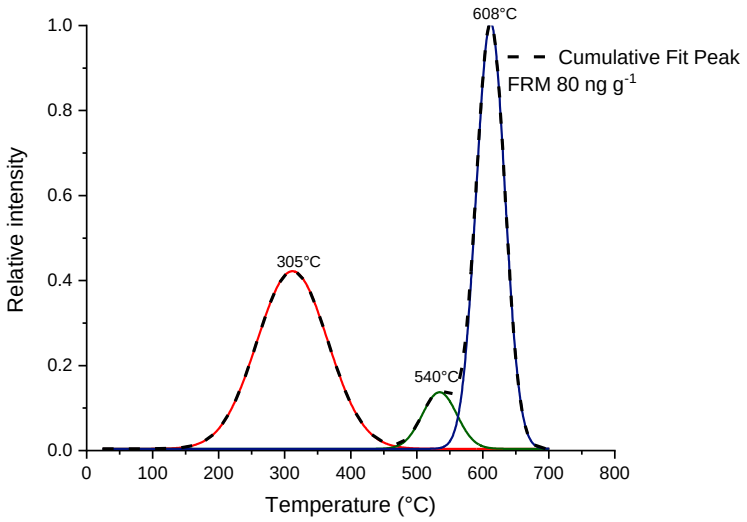

Figure 17: TPD spectra of finished raw meals in the raw mill (after separation).

The most significant change in terms of Hg fractionation occurs when dust from fabric filters (Figure 4.11) is added to the raw meal in the mills (Figure 4.10). This is a relatively common practice in cement production, as the dust accumulated on fabric filters has practically the same chemical composition as the raw meal. The dust from the fabric filters represents the material with the highest Hg content (Table 4.1), so the raw meal enriched with this dust has a higher Hg concentration compared to the other two samples from the raw mills. Even though the release pattern is, to an extent, like the previous two samples (Figure 4.7 and Figure 4.9), if we compare their TPD spectra, it is apparent that with the introduction of dust from the fabric filters, the first fraction becomes the predominant one.

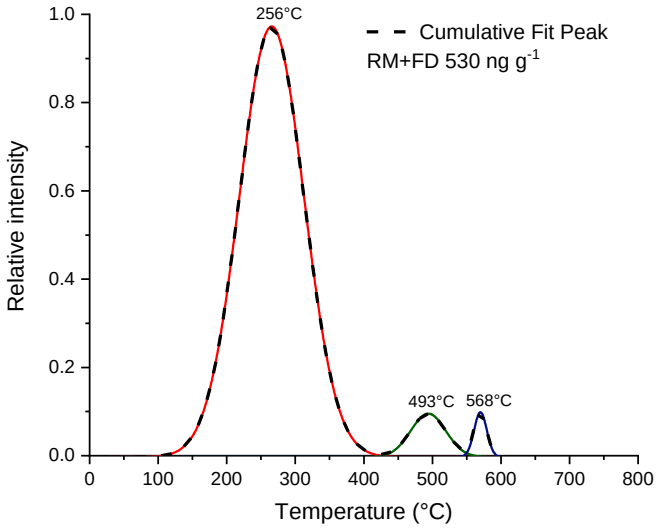

Figure 18: TPD spectra of raw meal with added filter dust.

The function of the fabric filter is to de-dust the flue gas before it reaches the stack. The fabric filters are highly efficient at particulate matter removal (> 95%), especially for fine particulate matter. The temperature at which these devices operate is around 100–130 °C, thus providing desirable conditions for Hg adsorption on particulates. The dust from filters has an unknown maximum capacity for Hg sorption. Stack emissions during regular monitoring were 0.025 mg/Nm^3 for Hg, which is below the limit of 0.05 mg/Nm^3 (N-normal conditions) included in the Industrial Emissions Directive (Directive 2010/75/EU, n.d.-b), and its subsequent decision establishing the best available techniques (BAT) on industrial emissions for the production of cement, lime and magnesium oxide (Directive 2010/75/EU, n.d.-a). Based on the TPD spectra of filter dust samples (Figure 4.11), Hg is desorbed at lower temperatures starting from 150 °C to 350 °C, with a peak maximum at 200 °C and 226 °C for the samples from FD1 and FD2, respectively. The sharp peaks point to a single compound present, but another smaller peak can be observed at 620 °C for sample FD 1, which shows the possibility of another relatively stable compound present in this type of material.

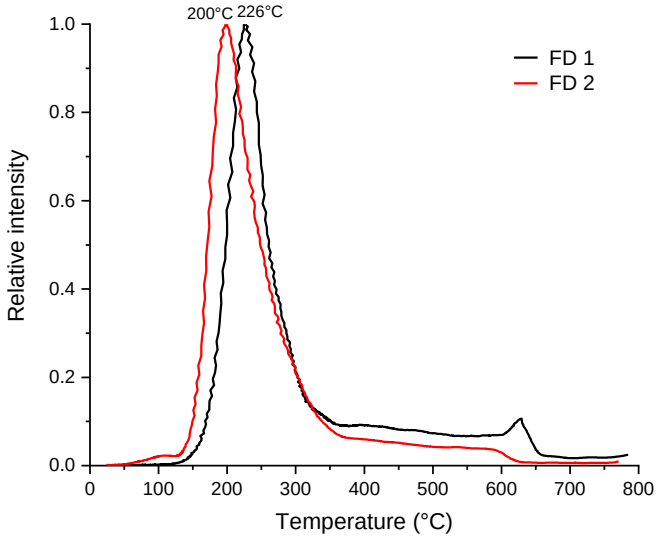

Figure 19: TPD spectra of fabric filters.

Since the QMS provides the possibility of detecting the release of other ions present in the sample during the decomposition process, desorption of chlorine compounds on a sample of filter dust was also performed (Figure 4.12).

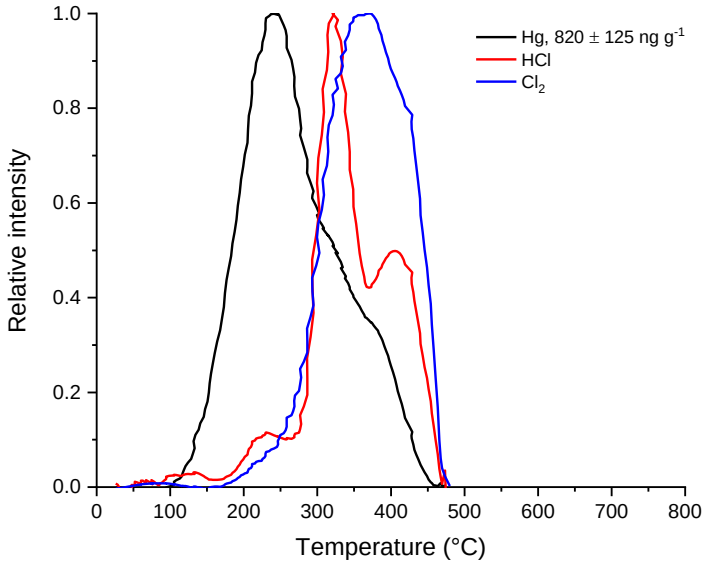

Figure 20: TPD spectra of filter dust with the desorption curves of Hg, HCl, and Cl_2.

As the desorption peaks of Hg and chlorine compounds start to overlap at the temperature range from 200 to 450 °C, one can deduce that the chlorinated Hg species are predominant in this type of material (Paone, 2010). During decomposition, Hg_2Cl_2 disproportionate to elemental Hg and $HgCl_2$ which is further decomposed to elemental Hg and chlorine (Lopez-Anton et al., 2010; Sedlar et al., 2014), and both the vapor pressures of $HgCl_2$ and Hg are similar (130 Pa at 136 °C), meaning that the two products are released at the same temperature:

$$Hg_2Cl_2 \rightleftarrows Hg^0 + HgCl_2$$
$$HgCl_2 \rightleftarrows Hg^0 + Cl_2 \quad (4.1)$$

One of the techniques for lowering Hg emissions from the cement plant is the extraction of the filter dust with high contents of Hg from the high-temperature process of cement clinker production (interruption of the recycling back in the raw meal) and leading it into a later low-temperature phase of cement grinding as a minor addition (Cement Sustainability Initiative, 2016; Mlakar et al., 2010). The TPD spectra of filter dust shows that this can be done without any further Hg emissions in cement mills that operate at temperatures of about 100 °C.

The prepared raw meal from the raw mills is then combined with the raw meal prepared in different operational regimes and with different additions of filter dust and stored in the silo, and it is dosed in the preheater. Although the presence of three Hg fractions is still observed in this material (Figure 4.13), the desorption profile is not the same as that in Figure 4.10, which is contra-intuitive. The shift of peaks toward higher temperatures was observed in this sample in comparison to Figure 4.10. The reason for this can be that the raw meal silo acts as a buffer, which causes temporal interruptions in Hg flows and cycling in the system (Mlakar et al., 2010). Once this mixture reaches the preheater, the Hg content decreases owing to the increase in temperature along with the preheater tower. In cyclone 5, where the temperature is around 750–800 °C, Hg in the raw meal is almost completely desorbed and does not show any observable fraction (Figure 4.14). The TPD spectra of this sample is not presented in the form of relative intensity, since the content of the Hg is very low (0.6 ng g^{-1}), and no reliable identification of any Hg fraction could be performed.

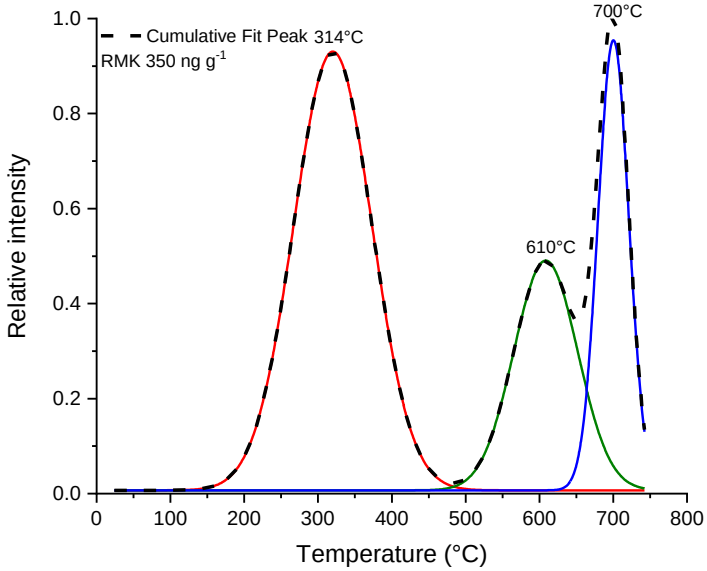

Figure 21: TPD spectra of raw meals dosed in the kiln.

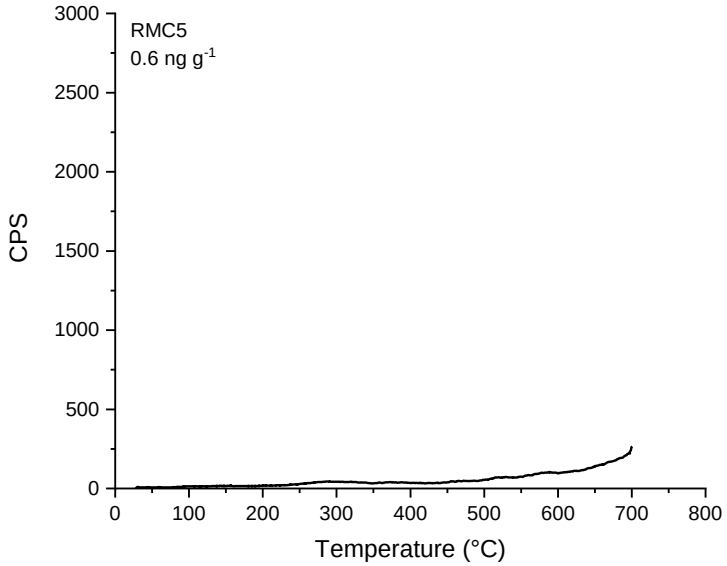

Figure 22: TPD spectra of raw meal C5.

Another feature of cement plants is the bypass system used to extract chloride from the clinker production process to prevent the material from sticking and clogging due to the formation of chlorine compounds with alkali compounds. Chlorine in cement production also originates from raw materials and fuels, either present in the crystal lattice of clay minerals or as organically bound chloride. It is primarily released as gaseous hydrochloric acid (Jons et al., 2008). The extracted chlorine gases are quenched to solidify various chlorine compounds onto the lime dust, after which the obtained dust is available for extraction using a filter (Forinton, 2013). The bypass dust consists of compounds such as KCl, K_2SO_4, NaCl, Na_2SO_4, and CaO. Based on the total Hg content (Table 1.1) of this material, through this fixture in the cement production process, Hg cannot be removed from the pyro-process to the extent that could be considered beneficial. The TPD spectra of bypass dust (Figure 4.15) exhibits two peaks, with the first being more pronounced than the second and resembling the Hg desorption pattern of filter dust. As this dust is obtained by quick quenching of the extracted gases, it is reasonable to assume that Hg in this material is superficially bound. From the TPD spectra, it is seen that Hg and HCl evolve coincidentally at a temperature range of 100–300 °C and could point out that the fraction belongs to Hg_xCl_2 (x = 1, 2). It should be noted that the content of chlorine in this material is significantly higher compared to Hg, and the desorption of HCl and Cl_2 can come from the decomposition of various chloride compounds present. The presence of a second peak with a peak maximum of 450 °C (Figure 4.15) does not resemble any of the Hg standards, and it is quite difficult to assign it to any compound, although it overlaps with decomposition patterns of both HCl and Cl_2.

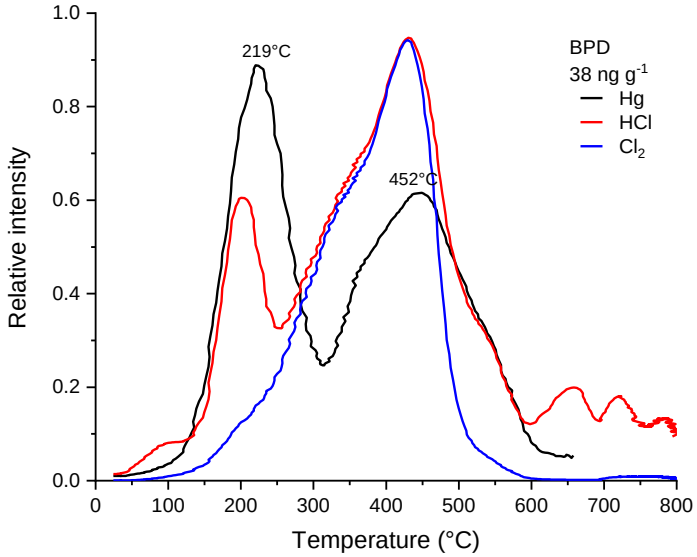

Figure 23: TPD spectra from the bypass dust.

Clinker is the final product of the sintering process taking place in the kiln. Due to the barrier of the kiln temperature, Hg in clinker is present at a very low concentration (0.8 ng g^{-1}), often posing a challenge for its reliable quantification. It is hypothesized that if Hg is present in this material, it could be in the form of Hg silicates ($HgSiO_3$ and/or $Hg_6Si_2O_7$) (Owens et al., 1995). The identification of such compounds is unlikely, even with the methodology employed in this study, because the temperature within the kiln is 1450 °C, which is a much higher one than the one used for this study. The low content of Hg measured in our case and the lack of any identifiable fraction (Figure 4.16) further confirm that Hg present in this material is very well bound to its matrix and thermally stable.

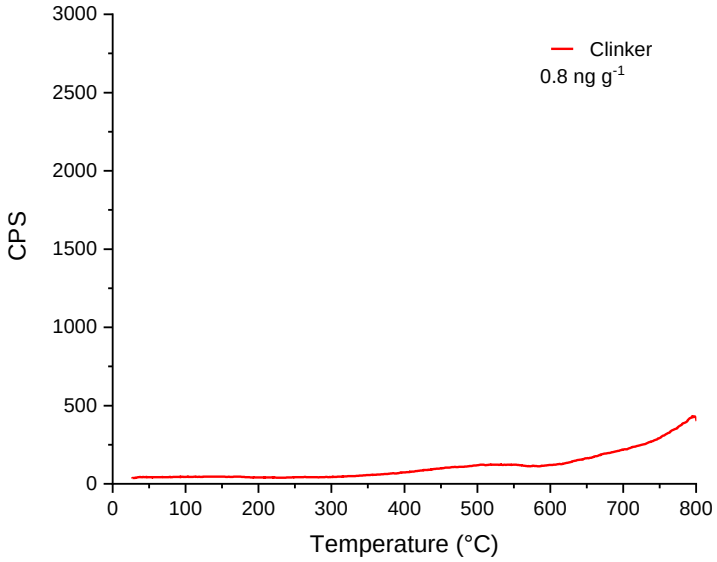

Figure 24: TPD spectra of the clinker.

Apart from raw materials, which are the major contributors of Hg to the cement production process, fuels, and in particular, petrol coke are other contributors. While the methodology employed in this study was suitable for studying Hg temperature

fractionation in solid samples, the same approach cannot be extended to studying temperature fractionation in petrol coke. Aside from other elements, Hg is only a small constituent of petrol coke, and organic matter that has a significantly higher concentration of Hg can negatively affect the instrumentation during temperature decomposition. Due to the shortcomings of the approach used in this study, the loop between gaseous Hg routed from the preheater to the petrol coke mill could not be explored.

Chapter 5

Summary and Conclusions

This doctoral dissertation represents a methodological approach to studying two aspects of Hg fate in the process of cement production. Cement production continues to be in a group of significant emitters of Hg to the atmosphere and requirements for emission limits are in place in many countries.

In this respect, a method for the determination of total Hg using direct combustion coupled to AAS was validated. Two approaches to calibration were investigated: matrix-matched calibration and "spike calibration". The drawbacks of the first calibration approach were the uncertainty of the mass fraction and the need for several CRM with differing Hg content.

The uncertainties of the matrix-matched CRM are relatively large, and the decision to use them for calibration must be based on the target measurement uncertainty of the whole method. Selection of a CRM for calibration depends on its key characteristics, such as homogeneity, stability, the chemical form of the analyte, the concentration level, matrix match, potential interference, etc. The second approach – adding standard calibration solutions to the solid matrix has proven to be convenient and was associated with lower uncertainties compared to matrix-matched calibration.

While the method is suitable for raw materials and samples of similar nature from the production process, the same cannot be said for samples of alternative fuels, concretely 2D and 3D fuel which are considered as refuse derived fuels (RDF) produced from various types of waste such as municipal, industrial or commercial waste. Such materials are not homogeneous, and repeatability and reproducibility of the results cannot be ensured.

From the results of THg in solid samples, the same trend is observed as in the previous studies. Raw input materials have relatively low content of Hg, but due to the quantities used they are the largest contributor to Hg in the process. An increase in the Hg content is observed in raw mills as it was shown in a previous study that while the system operates in compound mode (raw mill on), they act as sorbent because they operate at temperatures of approximately 100 °C, causing Hg^0 to adsorb on colder particles. Dust from fabric filters is the material with the highest Hg content. THg in clinker was at a very low concentration and some of the samples were below LOQ.

Determination of only total Hg in samples is not sufficient for understanding Hg migration within the cement production process. So, the second part of the study was devoted to studying Hg temperature fractionation using QMS, as this approach has sensitivity that allows to investigate this aspect at concentrations that are found in cement production process.

TPD spectra of solid samples show a complex process of Hg partition. Multiple fractions are observed in samples from raw mill, which could be either separate compounds or could be attributed to step decomposition of a particular compound. The most consistent results

are obtained on samples from fabric filters, majority of these samples showed peak at temperatures ranging from 200–275 °C, indicating the presence of Hg—Cl compounds. On two samples from fabric filters, another smaller peak appeared at 640–670 °C, which is difficult to assign to any compound.

In conclusion, this study has offered new insights related to the Hg challenges in cement industry:

- It was demonstrated that the method for determination of total Hg in solid samples is appropriate, with its advantages being the lack of sample pre-treatment step and rapid analysis. Calibration by spiking standard calibration solution was the best alternative in the absence of matrix matched CRM of appropriate Hg content and matrix.
- Results from temperature fractionation clearly show how the Hg undergoes transformations throughout cement production process. This information contributes to the body of knowledge of Hg behavior in cement industry in particular, but not limited to it.
- Fractionation results are plant specific, and the outlined methodology presents prospects for reiteration in the context of future research on other cement plants also, thus creating benchmark for Hg chemistry in cement kilns which can inform specific practices in mitigating Hg emissions in the cement industry.

Appendix A

Tables and Figures

A.1 Tables

Table A.1: Total mercury content (ng g^{-1}) and uncertainty with a coverage factor $k = 2$ in selected samples from cement production process analyzed by combustion coupled to the AAS.

Sample code	**Sample type**	**Total Hg** ng g^{-1} (n = 2)	**Uncertainty** $k = 2$
SA 202/18	Raw meal (DAS) June	440	68
SA 203/18	Raw meal (DAS) October	1030	155
SA 204/18	Raw meal (DAS) October	530	82
SA 205/18	Raw meal (DAS) October	415	64
SA 206/18	Raw meal (DAS) October	320	50
SA 207/18	Raw meal (DAS) November	190	41
SA 208/18	Raw meal (DAS) SOK	280	43
SA 209/18	Raw meal (WAS) April	165	35
SA 210/18	Raw meal (WAS) June	550	85
SA 211/18	Raw meal (WAS) October	645	100
SA 212/18	Raw meal (WAS) November	250	38
SA 213/18	Clinker (WAS)	1.2	0.3
SA 214/18	Clinker (WAS)	2	0.4
SA 215/18	Clinker (WAS)	1	0.2
SA 216/18	Clinker (WAS)		
SA 217/18	Clinker (ADS)	1	0.2
SA 218/18	CKD - production	100	22
SA 219/18	CKD - production	110	24
SA 220/18	CKD - production	120	26
SA 221/18	CKD + FD	1180	175
SA 222/18	CKD + FD	865	130
SA 223/18	CKD + FD	820	125
SA 224/18	CKD + FD	815	122

SA 225/18	CKD + FD	1225	185
SA 226/18	CKD + FD	745	110
SA 227/18	CKD + FD	440	68
SA 228/18	Petrol coke (AS)		
SA 229/18	2D fuel (AS)	/	/
SA 230/18	2D fuel (AS)	/	/
SA 231/18	3D fuel (AS)	/	/
SA 232/18	3D fuel (AS)	/	/
SA 233/18	Limestone Rodež	10	2.2
SA 234/18	Limestone Solkan	35	7.5

Table A.2: Total Hg content in solid samples from cement production sampled in June 2019.

Sample code	**Sample type**	**Total Hg** ng g^{-1} (n = 2)	**Uncertainty** $k = 2$
SA 123/19	Raw meal cyclone 5	0.80	0.2
SA 124/19	Clinker	0.75	0.15
SA 125/19	Raw meal (RM1)	180	39
SA 126/19	Raw meal (RM2)	45	10
SA 127/19	Raw meal HS	110	24
SA 128/19	Bypass dust	15	3.2
SA 129/19	Filter dust 1	540	84
SA 130/19	Filter dust 2	650	100
SA 131/19	Silica sand	15	3.3
SA 132/19	Iron-rich material	7	1.5
SA 133/19	Corrective material	8	1.7
SA 134/19	Raw materials mixture	25	5
SA 135/19	3D fuel	/	/
SA 136/19	2D fuel	/	/
SA 137/19	Raw meal cyclone 5	0.65	0.15
SA 138/19	Clinker	0.75	0.16
SA 139/19	Raw meal (RM1)	150	32
SA 140/19	Raw meal (RM2)	35	7.5
SA 141/19	Raw meal HS	90	20
SA 142/19	Bypass dust	20	4.3
SA 143/19	Filter dust 1	500	75
SA 144/19	Filter dust 2	610	95
SA 145/19	Silica sand	12	2.6
SA 146/19	Iron-rich material	6	1.3
SA 147/19	Corrective material	11	2.4
SA 148/19	Raw materials mixture	25	5.4
SA 149/19	3D fuel	/	/
SA 150/19	2D fuel	/	/

Table A.3: Total Hg content in solid samples from cement production sampled in December 2019.

Code of the sample	**Type of the sample**	**Total Hg** ng g^{-1} (n = 2)	**Uncertainty** $k = 2$
SA 314/19	Raw meal cyclone 5	0.70	0.15
SA 315/19	Clinker	1.4	0.3
SA 316/19	Raw meal (RM1)	80	17
SA 317/19	Raw meal (RM2)	35	8
SA 318/19	Raw meal HS	90	19
SA 319/19	Bypass dust	45	10
SA 320/19	Filter dust 1	405	63
SA 321/19	Filter dust 2	610	95
SA 322/19	Silica sand	7	1.5
SA 323/19	Iron-rich material	25	5.4
SA 324/19	Corrective material	45	10
SA 325/19	Raw materials mixture	20	4.3
SA 326/19	Petrol coke	200	43
SA 327/19	3D fuel	/	/
SA 328/19	2D fuel	/	/

Table A.4: Total Hg content in solid samples from cement production sampled in June 2020.

Code of the sample	**Type of the sample**	**Total Hg** ng g^{-1} (n = 2)	**Uncertainty** $k = 2$
SA 178/20	Raw materials mixture	15	3.2
SA 179/20	Corrective material	7	1.5
SA 180/20	Iron-rich material	75	16
SA 181/20	Silica sand	5	1
SA 182/20	Filter dust 1	400	62
SA 183/20	Filter dust 2	705	110
SA 184/20	Bypass dust	50	11
SA 185/20	2D fuel	/	/
SA 186/20	3D fuel	/	/
SA 187/20	Petrol coke	180	40
SA 188/20	Raw meal (RM1)	125	27
SA 189/20	Raw meal HS	120	26
SA 190/20	Raw meal cyclone 5	3	0.65
SA 191/20	Clinker	0.1	0.02

A.2 Figures

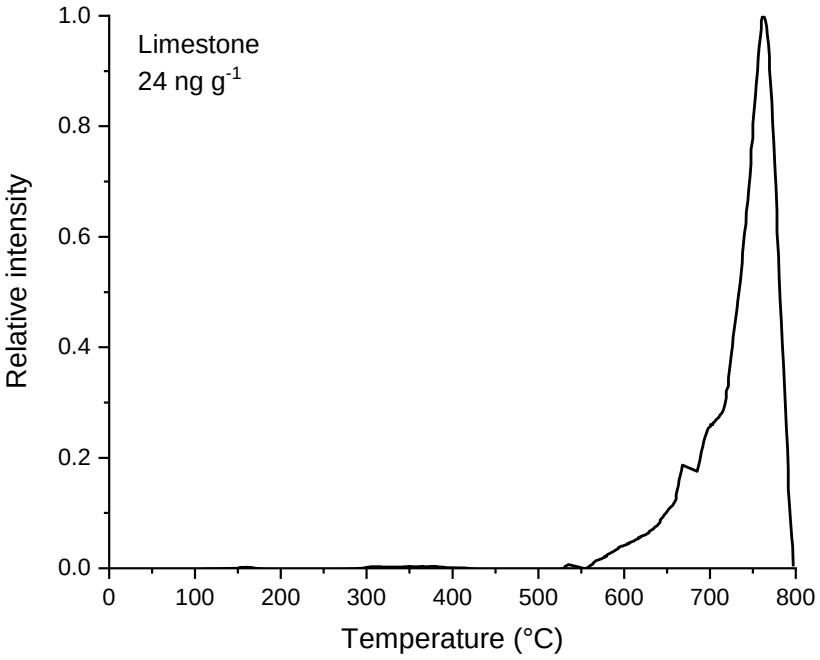

Figure A.1: TDP spectra of limestone Perunk.

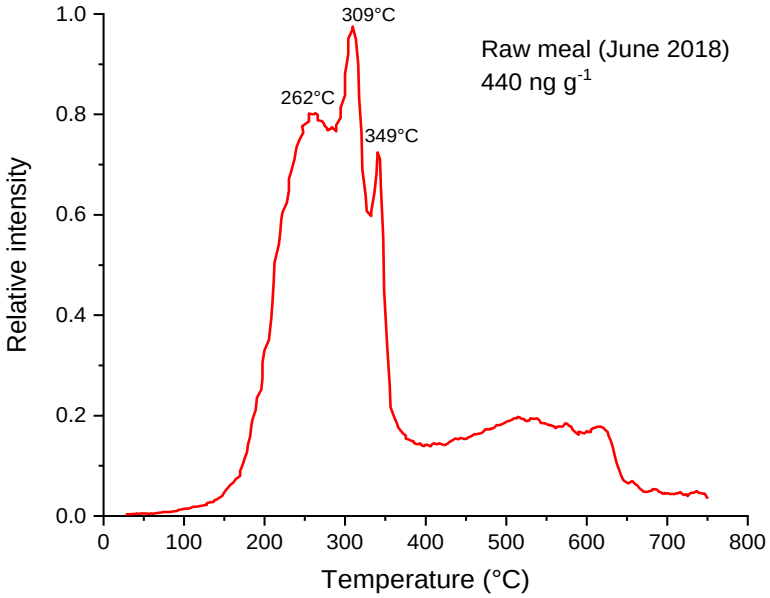

Figure A.2: TPD spectra of raw meals and cement kiln dust, sampled in June 2018 during cement production.

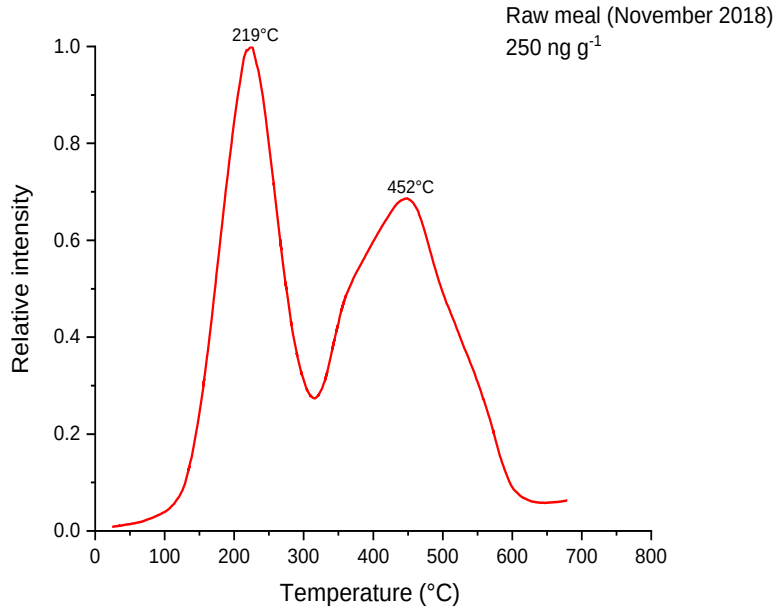

Figure A.3: TPD spectra of raw meals and cement kiln dust, sampled in November 2018 during cement production.

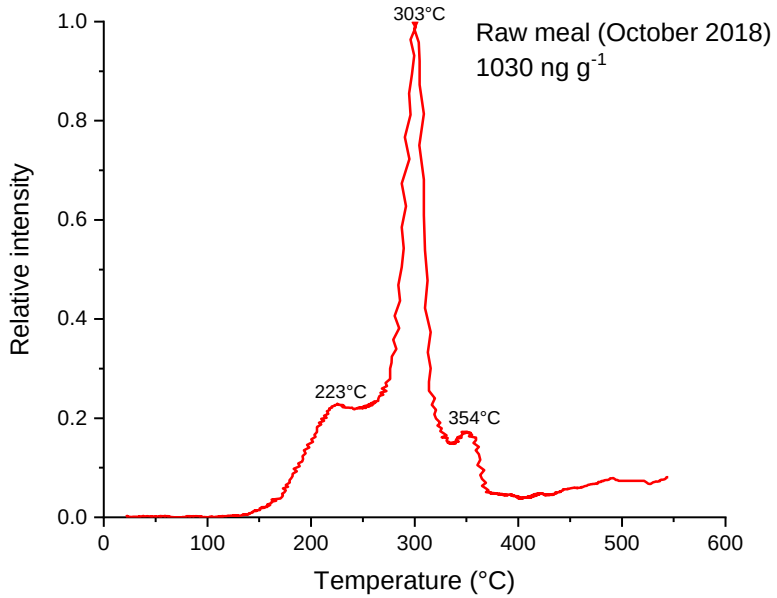

Figure A.4: TPD spectra of raw meals and cement kiln dust, sampled in October 2018 during cement production.

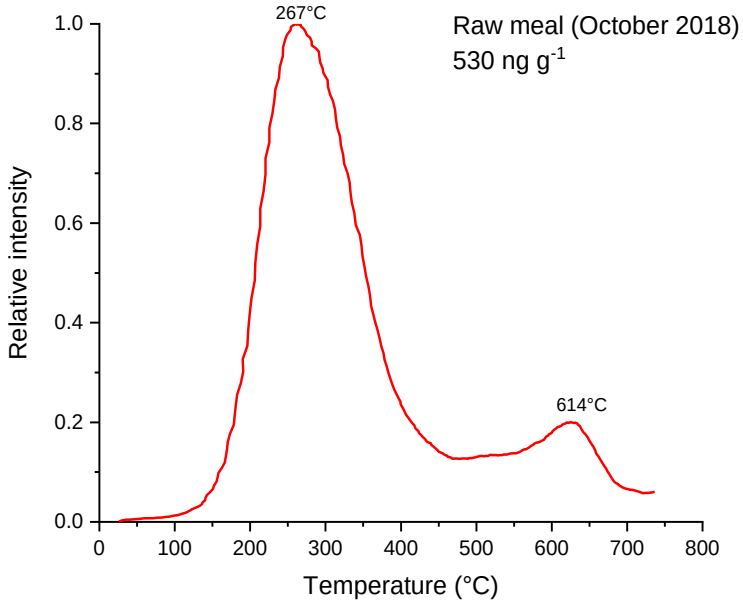

Figure A.5: TPD spectra of raw meals and cement kiln dust, sampled in October 2018 during cement production.

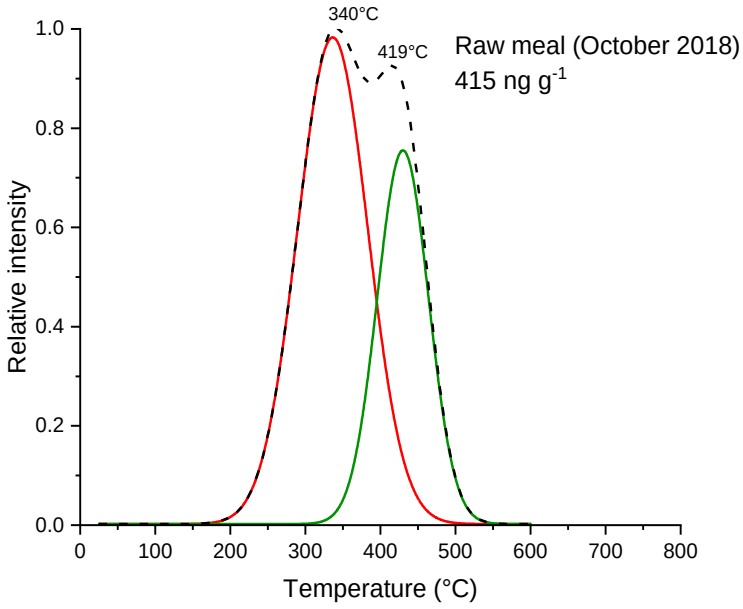

Figure A.6: TPD spectra of raw meals and cement kiln dust, sampled in October 2018 during cement production.

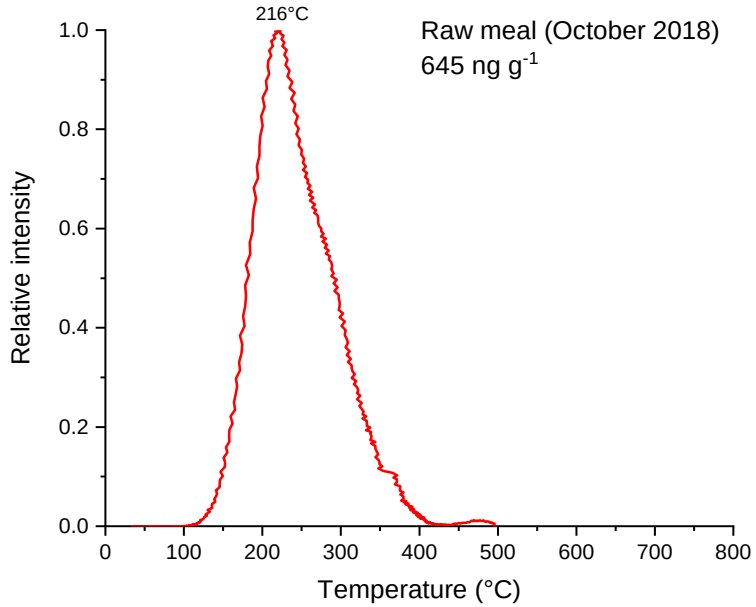

Figure A.7: TPD spectra of raw meals and cement kiln dust, sampled in October 2018 during cement production.

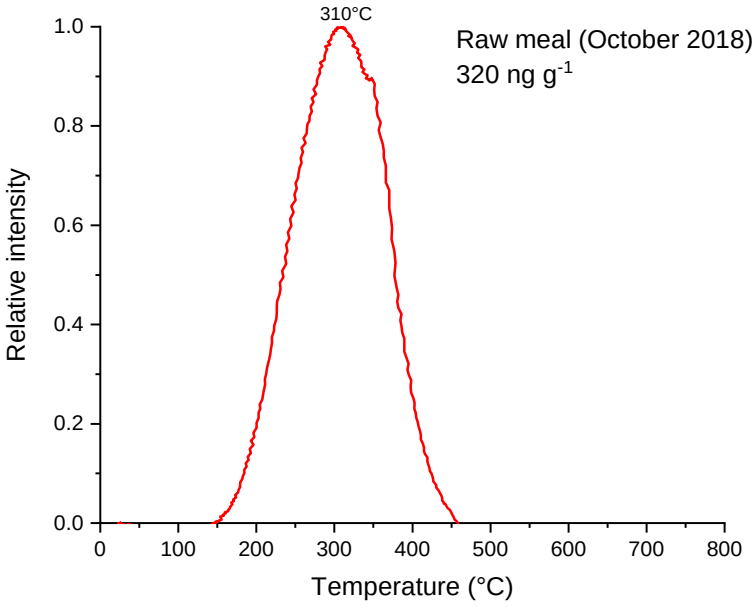

Figure A.8: TPD spectra of raw meals and cement kiln dust, sampled in October 2018 during cement production.

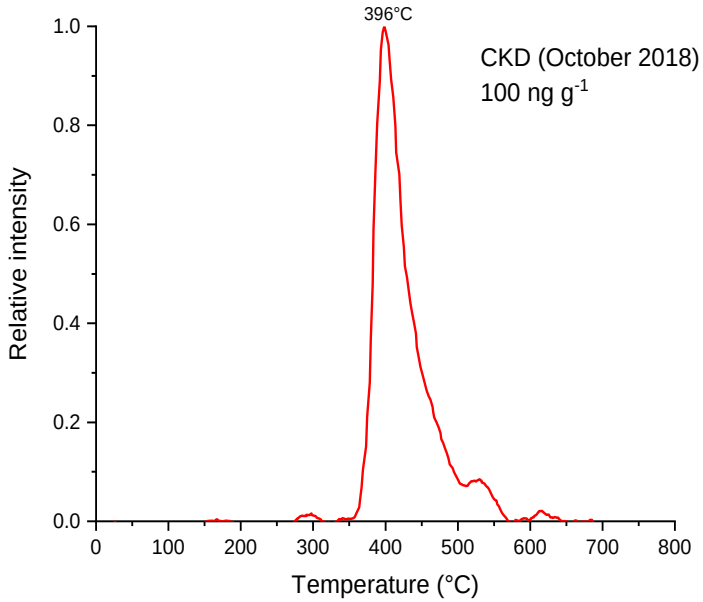

Figure A.9: TPD spectra of raw meals and cement kiln dust, sampled in October 2018 during cement production.

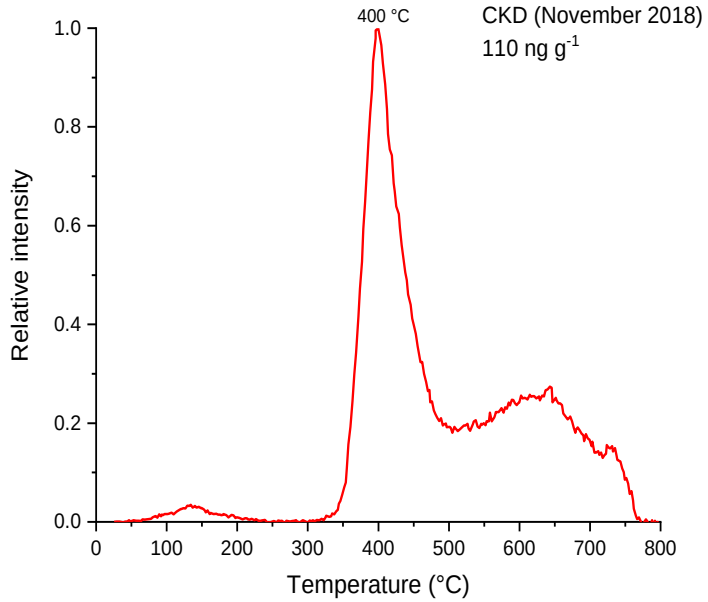

Figure A.10: TPD spectra of raw meals and cement kiln dust, sampled in October 2018 during cement production.

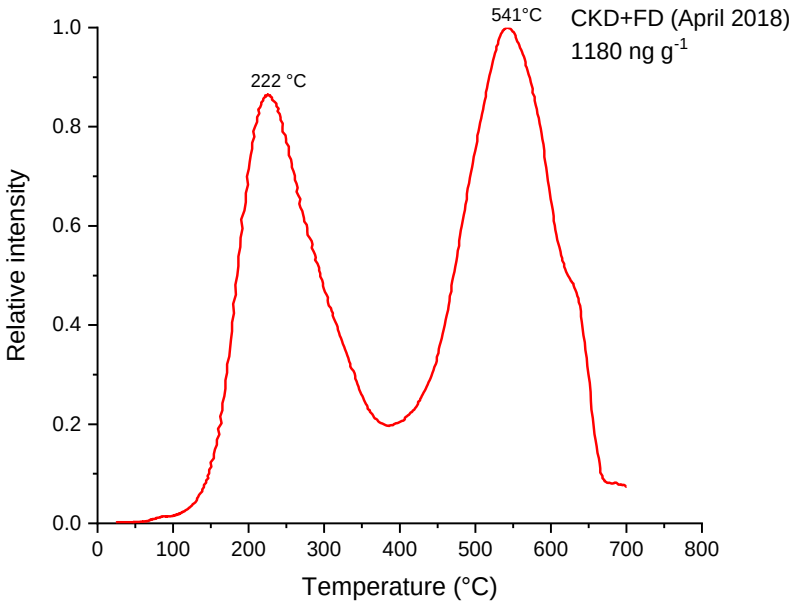

Figure A.11: TPD spectra of cement kiln dust and filter dust, sampled in April 2018 during cement production.

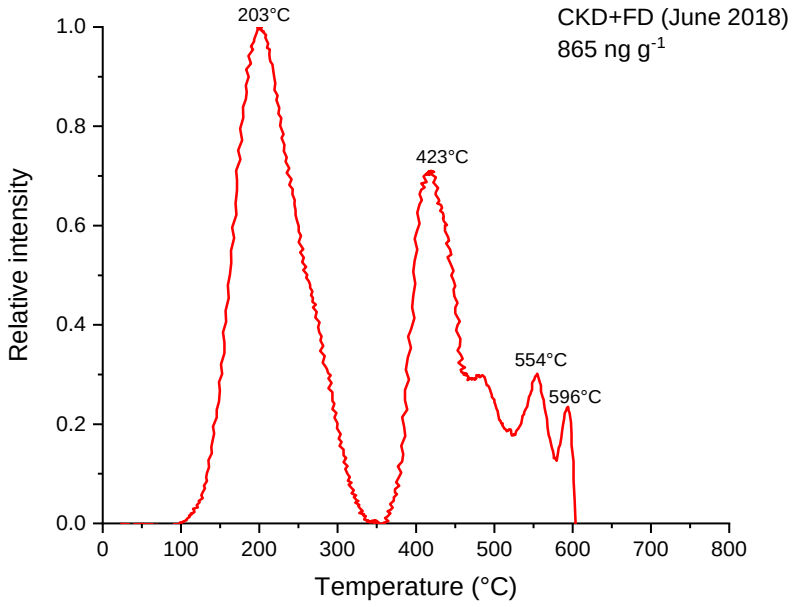

Figure A.12: TPD spectra of cement kiln dust and filter dust, sampled in June 2018 during cement production.

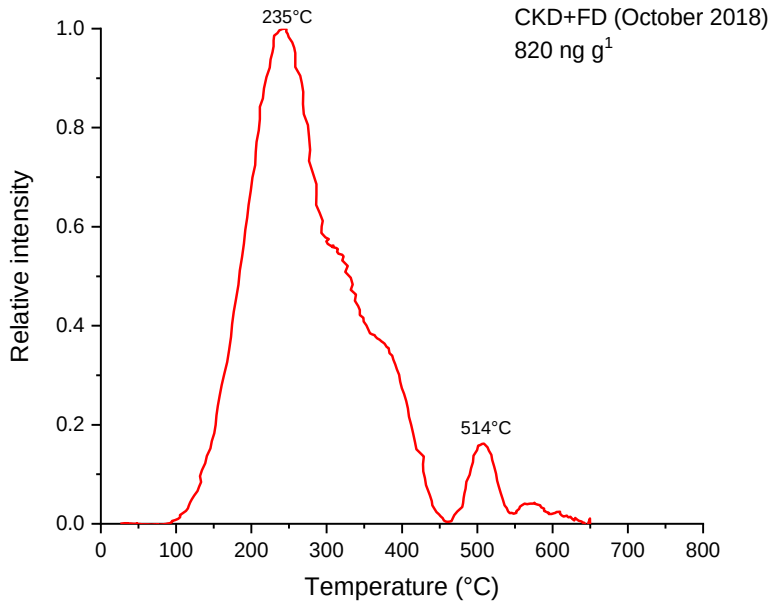

Figure A.13: TPD spectra of cement kiln dust and filter dust, sampled in October 2018 during cement production.

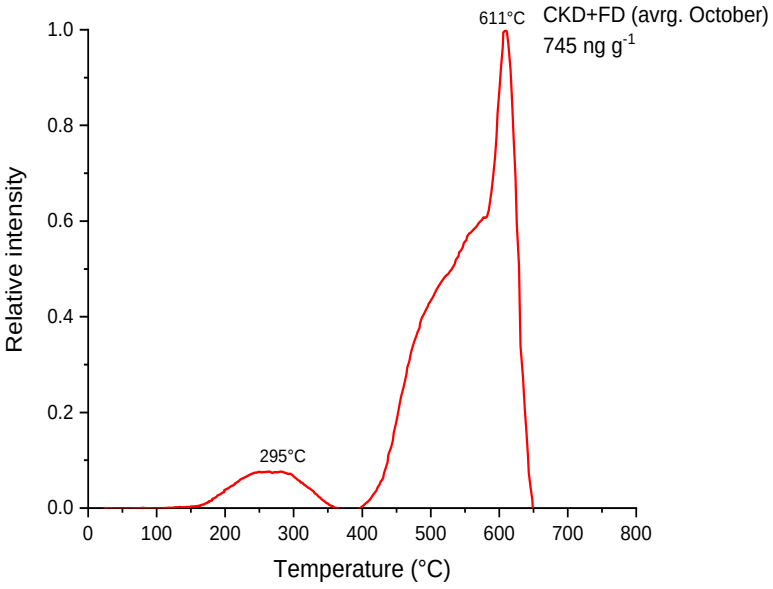

Figure A.14: TPD spectra of cement kiln dust and filter dust, sampled in October 2018 during cement production.

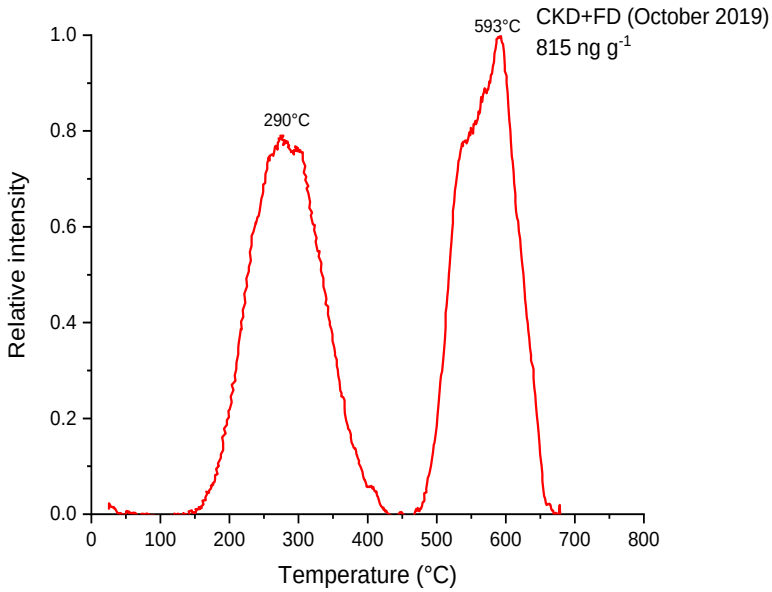

Figure A.15: TPD spectra of cement kiln dust and filter dust, sampled in October 2019 during cement production.

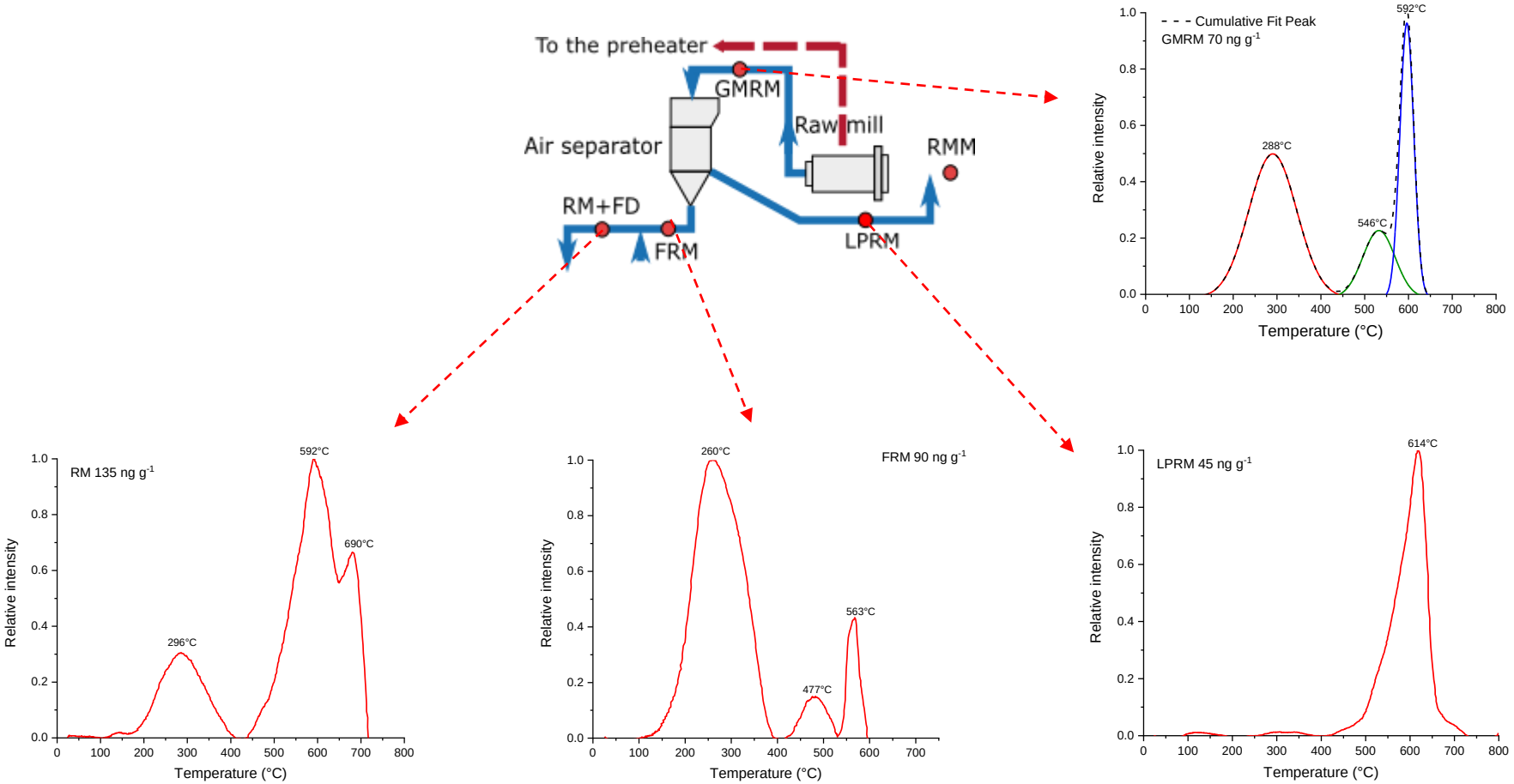

Figure A.16: TPD spectra of samples from raw mill 2 sampled during the sampling campaign in December 2018.

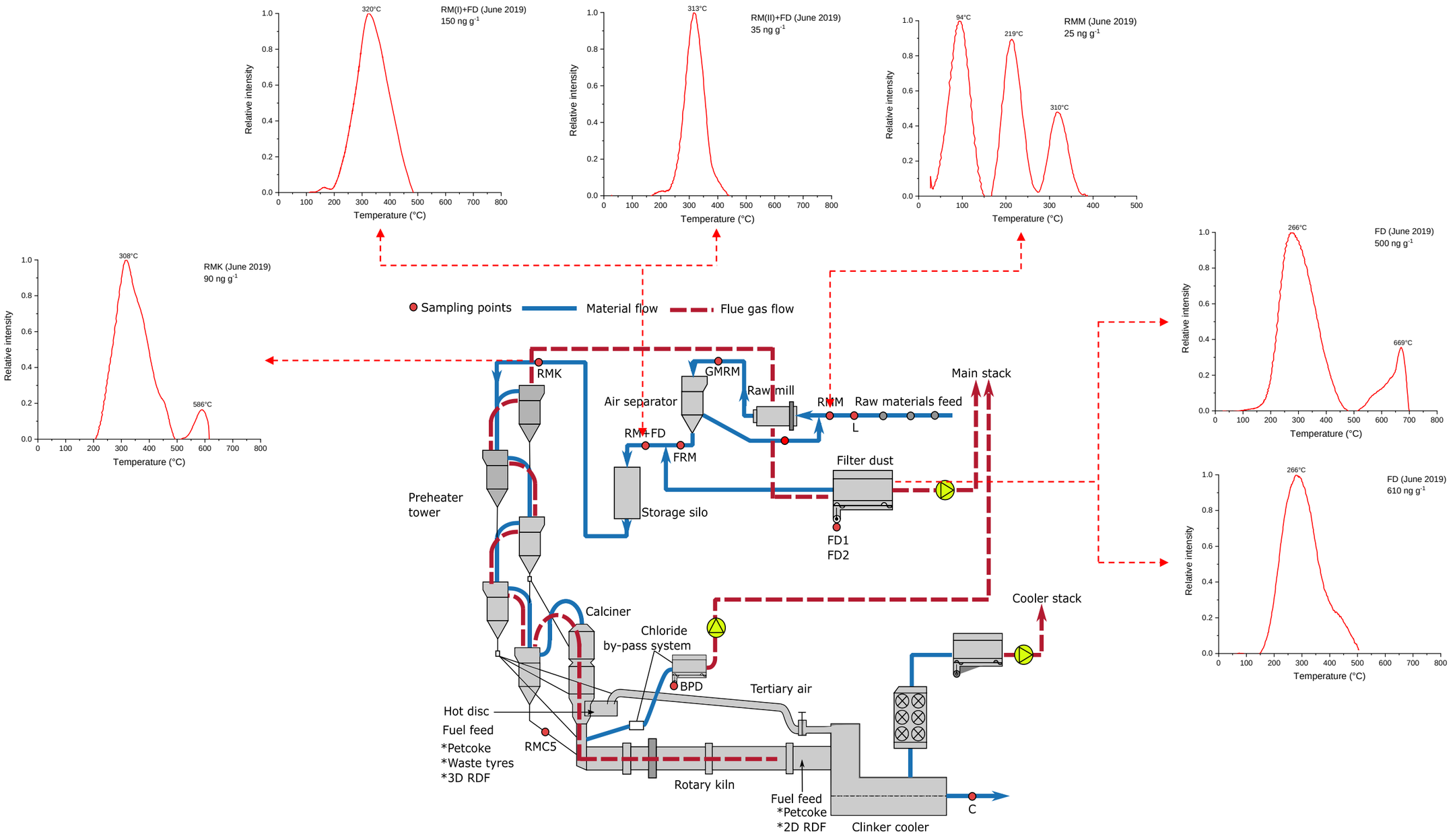

Figure A.17: TPD spectra of samples sampled in June 2019.

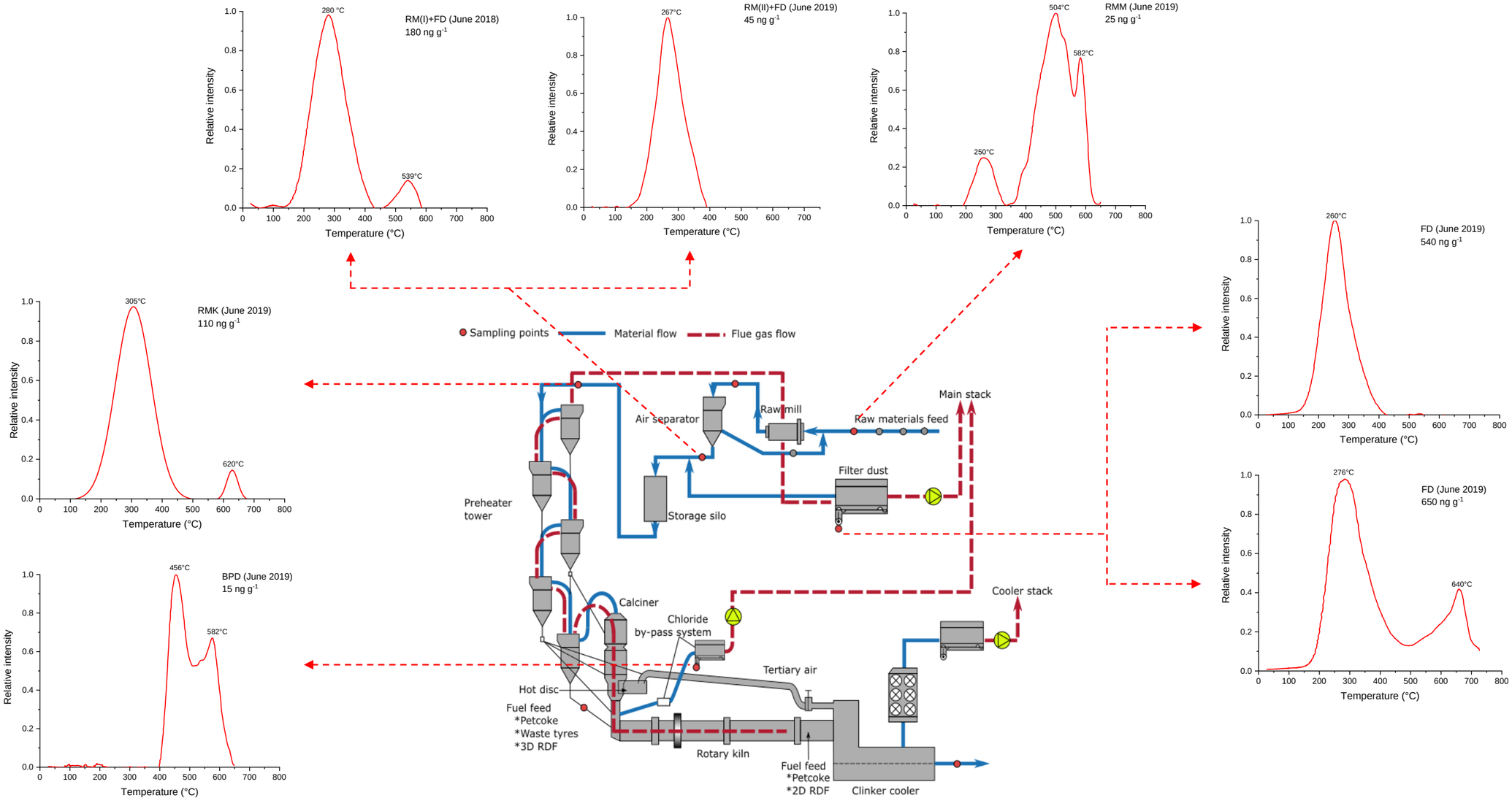

Figure A.18: TPD spectra of samples sampled in June 2019.

References

Aastrup, M., Johnson, J., Bringmark, E., Bringmark, I., & Iverfeldt, Å. (1991). Occurence and transport of mercury within a small catchment area. *Water Air & Soil Pollution*, *56*(1), 155–167. https://doi.org/10.1007/BF00342269

Abu-Daabes, M. A., & Pinto, N. G. (2005). Synthesis and characterization of a nano-structured sorbent for the direct removal of mercury vapor from flue gases by chelation. *Chemical Engineering Science*, *60*(7), 1901–1910. https://doi.org/10.1016/j.ces.2004.11.028

Adaska, P.E., W. S., & Taubert, D. H. (2008). Beneficial Uses of Cement Kiln Dust. *2008 IEEE Cement Industry Technical Conference Record*, 210–228. https://doi.org/10.1109/CITCON.2008.24

AMAP/UN Environment. (2019). *Technical background report for the global mercury assessment 2018. Arctic Monitoring and Assessment Programme, Oslo, Norway/UN Environment Programme, Chemical and Health Branch, Geneva, Switzerland.* (p. 426). AMAP/UNEP. https://wedocs.unep.org/bitstream/handle/20.500.11822/29831/gma_tech.pdf?sequence=1&isAllowed=y

Amos, H. M., Jacob, D. J., Holmes, C. D., Fisher, J. A., Wang, Q., Yantosca, R. M., Corbitt, E. S., Galarneau, E., Rutter, A. P., Gustin, M. S., Steffen, A., Schauer, J. J., Graydon, J. A., Louis, V. L. St., Talbot, R. W., Edgerton, E. S., Zhang, Y., & Sunderland, E. M. (2012). Gas-particle partitioning of atmospheric Hg(II) and its effect on global mercury deposition. *Atmospheric Chemistry and Physics*, *12*(1), 591–603. https://doi.org/10.5194/acp-12-591-2012

Amos, H. M., Jacob, D. J., Kocman, D., Horowitz, H. M., Zhang, Y., Dutkiewicz, S., Horvat, M., Corbitt, E. S., Krabbenhoft, D. P., & Sunderland, E. M. (2014). Global Biogeochemical Implications of Mercury Discharges from Rivers and Sediment Burial. *Environmental Science & Technology*, *48*(16), 9514–9522. https://doi.org/10.1021/es502134t

Amos, H. M., Jacob, D. J., Streets, D. G., & Sunderland, E. M. (2013). Legacy impacts of all-time anthropogenic emissions on the global mercury cycle: GLOBAL IMPACTS OF LEGACY MERCURY. *Global Biogeochemical Cycles*, *27*(2), 410–421. https://doi.org/10.1002/gbc.20040

Ariya, P. A., Amyot, M., Dastoor, A., Deeds, D., Feinberg, A., Kos, G., Poulain, A., Ryjkov, A., Semeniuk, K., Subir, M., & Toyota, K. (2015). Mercury Physicochemical and Biogeochemical Transformation in the Atmosphere and at Atmospheric Interfaces: A Review and Future Directions. *Chemical Reviews*, *115*(10), 3760–3802. https://doi.org/10.1021/cr500667e

ASTM. (2009). *ASTM C150/C150M: Standard Specification for Portland Cement. West Conshohocken, PA: American Society for Testing and Materials, 2009. C150/C150M.*

Bagnato, E., Tamburello, G., Avard, G., Martinez-Cruz, M., Enrico, M., Fu, X., Sprovieri, M., & Sonke, J. E. (2015). Mercury fluxes from volcanic and geothermal sources: An

update. *Geological Society, London, Special Publications*, *410*(1), 263–285. https://doi.org/10.1144/SP410.2

Balcom, P. H., Hammerschmidt, C. R., Fitzgerald, W. F., Lamborg, C. H., & O'Connor, J. S. (2008). Seasonal distributions and cycling of mercury and methylmercury in the waters of New York/New Jersey Harbor Estuary. *Marine Chemistry*, *109*(1–2), 1–17. https://doi.org/10.1016/j.marchem.2007.09.005

Bank, M. S. (Ed.). (2012). *Mercury in the environment: Pattern and process* (1st ed). University of California Press.

Barbalace, K. (1995). Periodic Table of Elements. *Environmental Chemistry*. https://environmentalchemistry.com/yogi/periodic/Hg.html

Barwick, V. (2003). *Preparation of Calibration Curves. A Guide to Best Practice* (LGC/VAM/2003/032). LGC Limited. https://biosearch-cdn.azureedge.net/assetsv6/Calibration-curve-guide.pdf

Benoit, J. M., Gilmour, C. C., Heyes, A., Mason, R. P., & Miller, C. L. (2002). Geochemical and Biological Controls over Methylmercury Production and Degradation in Aquatic Ecosystems. In *Biogeochemistry of Environmentally Important Trace Elements*. American Chemical Society.

Bhatty, J. I., Miller, F. M. G., & Kosmatka, S. H. (2004). *Innovations in Portland Cement Manufacturing*. Portland Cement Association. https://books.google.at/books?id=4uJSPwAACAAJ

Biester, H., & Scholz, C. (1997). Determination of Mercury Binding Forms in Contaminated Soils: Mercury Pyrolysis versus Sequential Extractions. *Environmental Science & Technology*, *31*(1), 233–239. https://doi.org/10.1021/es960369h

Black, F. J., Conway, C. H., & Flegal, A. R. (2012). Mercury in the Marine Environment. In *Mercury in the Environment. Pattern and Process* (First). University of California Press.

Bombach, G., Bombach, K., & Klemm, W. (1994). Speciation of mercury in soils and sediments by thermal evaporation and cold vapor atomic absorption. *Fresenius' Journal of Analytical Chemistry*, *350*(1–2), 18–20. https://doi.org/10.1007/BF00326246

Brooks, W. E. (2012). Industrial Use of Mercury in the Ancient World. In *Mercury in the Environment. Pattern and Process* (First). University of California Press.

Bye, G. C. (1999). Portland cement: Composition, production and properties / G. C. Bye. In *Portland cement: Composition, production and properties* (Second edition). Thomas Telford.

Calvert, J., & Lindberg, S. (2005). Mechanisms of mercury removal by O and OH in the atmosphere. *Atmospheric Environment*, *39*(18), 3355–3367. https://doi.org/10.1016/j.atmosenv.2005.01.055

Cao, Y., Gao, Z., Zhu, J., Wang, Q., Huang, Y., Chiu, C., Parker, B., Chu, P., & Pan, W. (2008). Impacts of Halogen Additions on Mercury Oxidation, in A Slipstream Selective Catalyst Reduction (SCR), Reactor When Burning Sub-Bituminous Coal. *Environmental Science & Technology*, *42*(1), 256–261. https://doi.org/10.1021/es071281e

Cement Sustainability Initiative. (2016). *Guidance for reducing and controlling emissions of mercury compounds in the cement industry*. WBCSD. http://docs.wbcsd.org/2016/07/CSI_Guidance_Cement_Industry.pdf

Clevenger, W. L., Smith, B. W., & Winefordner, J. D. (1997). Trace Determination of Mercury: A Review. *Critical Reviews in Analytical Chemistry*, *27*(1), 1–26. https://doi.org/10.1080/10408349708050578

Cortes, J., Peralta, J., & Díaz-Navarro, R. (2018). Acute respiratory syndrome following accidental inhalation of mercury vapor. *Clinical Case Reports*, *6*(8), 1535–1537. https://doi.org/10.1002/ccr3.1656

Cossa, D., Martin, J.-M., & Sanjuan, J. (1994). Dimethylmercury formation in the Alboran Sea. *Marine Pollution Bulletin*, *28*(6), 381–384. https://doi.org/10.1016/0025-326X(94)90276-3

Cossa, D., Martin, J.-M., Takayanagi, K., & Sanjuan, J. (1997). The distribution and cycling of mercury species in the western Mediterranean. *Deep Sea Research Part II: Topical Studies in Oceanography*, *44*(3–4), 721–740. https://doi.org/10.1016/S0967-0645(96)00097-5

Cremer, D., Kraka, E., & Filatov, M. (2008). Bonding in Mercury Molecules Described by the Normalized Elimination of the Small Component and Coupled Cluster Theory. *ChemPhysChem*, *9*(17), 2510–2521. https://doi.org/10.1002/cphc.200800510

Cuadros-Rodríguez, L., Gámiz-Gracia, L., Almansa-López, E. M., & Bosque-Sendra, J. M. (2001). Calibration in chemical measurement processes. II. A methodological approach. *TrAC Trends in Analytical Chemistry*, *20*(11), 620–636. https://doi.org/10.1016/S0165-9936(01)00111-X

Dekov, V. M. (2007). Native Hgliq in the metalliferous sediments of the East Pacific Rise (21°S). *Marine Geology*, *238*(1–4), 107–113. https://doi.org/10.1016/j.margeo.2007.01.001

Diamantopoulou, Ir., Skodras, G., & Sakellaropoulos, G. P. (2010). Sorption of mercury by activated carbon in the presence of flue gas components. *Fuel Processing Technology*, *91*(2), 158–163. https://doi.org/10.1016/j.fuproc.2009.09.005

Dibble, T. S., & Schwid, A. C. (2016). Thermodynamics limits the reactivity of BrHg radical with volatile organic compounds. *Chemical Physics Letters*, *659*, 289–294. https://doi.org/10.1016/j.cplett.2016.07.065

Dibble, T. S., Zelie, M. J., & Mao, H. (2012). Thermodynamics of reactions of ClHg and BrHg radicals with atmospherically abundant free radicals. *Atmospheric Chemistry and Physics*, *12*(21), 10271–10279. https://doi.org/10.5194/acp-12-10271-2012

Directive 2010/75/EU. (n.d.-a). *Commission Implementing Decision of 26 March 2013 establishing the best available techniques (BAT) conclusions under Directive 2010/75/EU of the European Parliament and of the Council on industrial emissions for the production of cement, lime and magnesium oxide (2013) OJ L100.* https://eur-lex.europa.eu/

Directive 2010/75/EU. (n.d.-b). *Directive 2010/75/EU of the European Parliamend and of the Council of 24 November 2010 on industrial emissions (integrated pollution prevention and control) (OJ L 334, 17.12.2010, p. 17).* https://eur-lex.europa.eu/

Dyrssen, D., & Wedborg, M. (1991). The sulphur-mercury(II) system in natural waters. *Water Air & Soil Pollution*, *56*(1), 507–519. https://doi.org/10.1007/BF00342295

Eckley, C. S., & Hintelmann, H. (2006). Determination of mercury methylation potentials in the water column of lakes across Canada. *Science of The Total Environment*, *368*(1), 111–125. https://doi.org/10.1016/j.scitotenv.2005.09.042

Eckley, C. S., Watras, C. J., Hintelmann, H., Morrison, K., Kent, A. D., & Regnell, O. (2005). Mercury methylation in the hypolimnetic waters of lakes with and without connection to wetlands in northern Wisconsin. *Canadian Journal of Fisheries and Aquatic Sciences*, *62*(2), 400–411. https://doi.org/10.1139/f04-205

Eto, K. (1997). Review Article: Pathology of Minamata Disease. *Toxicologic Pathology*, *25*(6), 614–623. https://doi.org/10.1177/019262339702500612

Evers, D. C., Han, Y.-J., Driscoll, C. T., Kamman, N. C., Goodale, M. W., Lambert, K. F., Holsen, T. M., Chen, C. Y., Clair, T. A., & Butler, T. (2007). Biological Mercury

Hotspots in the Northeastern United States and Southeastern Canada. *BioScience*, *57*(1), 29–43. https://doi.org/10.1641/B570107

Faganeli, J., Horvat, M., Covelli, S., Fajon, V., Logar, M., Lipej, L., & Cermelj, B. (2003). Mercury and methylmercury in the Gulf of Trieste (northern Adriatic Sea). *Science of The Total Environment*, *304*(1–3), 315–326. https://doi.org/10.1016/S0048-9697(02)00578-8

Ferrari, C., Gauchard, P., Aspmo, K., Dommergue, A., Magand, O., Bahlmann, E., Nagorski, S., Temme, C., Ebinghaus, R., & Steffen, A. (2005). Snow-to-air exchanges of mercury in an Arctic seasonal snow pack in Ny-Ålesund, Svalbard. *Atmospheric Environment*, *39*(39), 7633–7645. https://doi.org/10.1016/j.atmosenv.2005.06.058

Forinton, J. (2013). Recycling kiln bypass dust into valuable materials. *2013 IEEE-IAS/PCA Cement Industry Technical Conference*, 1–6. https://doi.org/10.1109/CITCON.2013.6525279

Frescholtz, T. F., & Sexauer Gustin, M. (2004). Soil and Foliar Mercury Emission as a Function of Soil Concentration. *Water, Air, & Soil Pollution*, *155*(1–4), 223–237. https://doi.org/10.1023/B:WATE.0000026530.85954.3f

Fritsche, J., Obrist, D., & Alewell, C. (2008). Evidence of microbial control of Hg ^{0} emissions from uncontaminated terrestrial soils. *Journal of Plant Nutrition and Soil Science*, *171*(2), 200–209. https://doi.org/10.1002/jpln.200625211

Furtado Da Silva, A., Grandis Lepri, F., Gallindo Borges, D. L., Welz, B., Curtius, A. J., & Heitmann, U. (2006). Determination of mercury in biological samples using solid sampling high-resolution continuum source electrothermal atomization atomic absorption spectrometry with calibration against aqueous standards. *Journal of Analytical Atomic Spectrometry*, *21*(11), 1321. https://doi.org/10.1039/b607256a

Gabriel, M. C., & Williamson, D. G. (2004). Principal Biogeochemical Factors Affecting the Speciation And Transport of Mercury through the terrestrial environment. *Environmental Geochemistry and Health*, *26*(3–4), 421–434. https://doi.org/10.1007/s10653-004-1308-0

Gilmour, C. C., & Riedel, G. S. (1995). Measurement of Hg methylation in sediments using high specific-activity203Hg and ambient incubation. *Water, Air, & Soil Pollution*, *80*(1–4), 747–756. https://doi.org/10.1007/BF01189726

Gilmour, C. C., Riedel, G. S., Ederington, M. C., Bell, J. T., Gill, G. A., & Stordal, M. C. (1998). Methylmercury concentration and production rates across a trophic gradient in the northern Everglades. *Biogeochemistry*, *40*(2/3), 327–345. https://doi.org/10.1023/A:1005972708616

Glew, D. N., & Hames, D. A. (1971). Aqueous Nonelectrolyte Solutions. Part X. Mercury Solubility in Water. *Canadian Journal of Chemistry*, *49*(19), 3114–3118. https://doi.org/10.1139/v71-520

Goodsite, M. E., Plane, J. M. C., & Skov, H. (2004). A Theoretical Study of the Oxidation of Hg ^{0} to HgBr $_{2}$ in the Troposphere. *Environmental Science & Technology*, *38*(6), 1772–1776. https://doi.org/10.1021/es034680s

Grigal, D. F. (2003). Mercury Sequestration in Forests and Peatlands: A Review. *Journal of Environmental Quality*, *32*(2), 393–405. https://doi.org/10.2134/jeq2003.3930

Gustin, M. S., Biester, H., & Kim, C. S. (2002). Investigation of the light-enhanced emission of mercury from naturally enriched substrates. *Atmospheric Environment*, *36*(20), 3241–3254. https://doi.org/10.1016/S1352-2310(02)00329-1

Hall, G. E. M., & Pelchat, P. (1997). Evaluation of a Direct Solid Sampling Atomic Absorption Spectrometer for the Trace Determination of Mercury in Geological Samples. *The Analyst*, *122*(9), 921–924. https://doi.org/10.1039/a700194k

Han, S., & Gill, G. A. (2005). Determination of Mercury Complexation in Coastal and Estuarine Waters Using Competitive Ligand Exchange Method. *Environmental Science & Technology*, *39*(17), 6607–6615. https://doi.org/10.1021/es048667z

Harada, M. (1978). Congenital Minamata disease: Intrauterine methylmercury poisoning. *Teratology*, *18*(2), 285–288. https://doi.org/10.1002/tera.1420180216

Harada, M. (1995). Minamata Disease: Methylmercury Poisoning in Japan Caused by Environmental Pollution. *Critical Reviews in Toxicology*, *25*(1), 1–24. https://doi.org/10.3109/10408449509089885

Harrass, R., Schaefer, S., & Hoenig, V. (2018). Mercury in the German cement industry—A balance. *Cement International*, *16*.

Harris, R. C., Rudd, J. W. M., Amyot, M., Babiarz, C. L., Beaty, K. G., Blanchfield, P. J., Bodaly, R. A., Branfireun, B. A., Gilmour, C. C., Graydon, J. A., Heyes, A., Hintelmann, H., Hurley, J. P., Kelly, C. A., Krabbenhoft, D. P., Lindberg, S. E., Mason, R. P., Paterson, M. J., Podemski, C. L., … Tate, M. T. (2007). Whole-ecosystem study shows rapid fish-mercury response to changes in mercury deposition. *Proceedings of the National Academy of Sciences*, *104*(42), 16586–16591. https://doi.org/10.1073/pnas.0704186104

Hazen, R. M., Golden, J., Downs, R. T., Hystad, G., Grew, E. S., Azzolini, D., & Sverjensky, D. A. (2012). Mercury (Hg) mineral evolution: A mineralogical record of supercontinent assembly, changing ocean geochemistry, and the emerging terrestrial biosphere. *American Mineralogist*, *97*(7), 1013–1042. https://doi.org/10.2138/am.2012.3922

Hintelmann, H., Harris, R., Heyes, A., Hurley, J. P., Kelly, C. A., Krabbenhoft, D. P., Lindberg, S., Rudd, J. W. M., Scott, K. J., & St.Louis, V. L. (2002). Reactivity and Mobility of New and Old Mercury Deposition in a Boreal Forest Ecosystem during the First Year of the METAALICUS Study. *Environmental Science & Technology*, *36*(23), 5034–5040. https://doi.org/10.1021/es025572t

Holmes, C. D., Jacob, D. J., Corbitt, E. S., Mao, J., Yang, X., Talbot, R., & Slemr, F. (2010). Global atmospheric model for mercury including oxidation by bromine atoms. *Atmospheric Chemistry and Physics*, *10*(24), 12037–12057. https://doi.org/10.5194/acp-10-12037-2010

Horowitz, H. M., Jacob, D. J., Zhang, Y., Dibble, T. S., Slemr, F., Amos, H. M., Schmidt, J. A., Corbitt, E. S., Marais, E. A., & Sunderland, E. M. (2017). A new mechanism for atmospheric mercury redox chemistry: Implications for the global mercury budget. *Atmospheric Chemistry and Physics*, *17*(10), 6353–6371. https://doi.org/10.5194/acp-17-6353-2017

Horvat, M., Kotnik, J., Logar, M., Fajon, V., Zvonarić, T., & Pirrone, N. (2003). Speciation of mercury in surface and deep-sea waters in the Mediterranean Sea. *Atmospheric Environment*, *37*, 93–108. https://doi.org/10.1016/S1352-2310(03)00249-8

Issaro, N., Abi-Ghanem, C., & Bermond, A. (2009). Fractionation studies of mercury in soils and sediments: A review of the chemical reagents used for mercury extraction. *Analytica Chimica Acta*, *631*(1), 1–12. https://doi.org/10.1016/j.aca.2008.10.020

Jasinski, S. M. (1995). The materials flow of mercury in the United States. *Resources, Conservation and Recycling*, *15*(3–4), 145–179. https://doi.org/10.1016/0921-3449(95)00032-1

Jiao, Y., & Dibble, T. S. (2017). First kinetic study of the atmospherically important reactions $BrHg^{\cdot}$ + NO_2 and $BrHg^{\cdot}$ + HOO. *Physical Chemistry Chemical Physics*, *19*(3), 1826–1838. https://doi.org/10.1039/C6CP06276H

Jiskra, M., Sonke, J. E., Obrist, D., Bieser, J., Ebinghaus, R., Myhre, C. L., Pfaffhuber, K. A., Wängberg, I., Kyllönen, K., Worthy, D., Martin, L. G., Labuschagne, C.,

Mkololo, T., Ramonet, M., Magand, O., & Dommergue, A. (2018). A vegetation control on seasonal variations in global atmospheric mercury concentrations. *Nature Geoscience*, *11*(4), 244–250. https://doi.org/10.1038/s41561-018-0078-8

Jochum, K., & Enzweiler, J. (2014). Reference Materials in Geochemical and Environmental Research. In *Treatise on Geochemistry* (pp. 43–70). Elsevier.

Johansen, V. C., & Hawkins, G. J. (2003). *Mercury emissions and speciation from portland cement kilns, R&D serial No. 2567a*. Portland Cement Association.

Jons, E., Hundebol, S., & Clausen, K. (2008). New Reasons for Installing a Chloride By-Pass. Interaction Between Chloride and Sulphur. *2008 IEEE Cement Industry Technical Conference Record*, 195–209. https://doi.org/10.1109/CITCON.2008.23

Kelly, J. G., Han, F. X., Su, Y., Xia, Y., Philips, V., Shi, Z., Monts, D. L., Pichardo, S. T., & Xia, K. (2012). Rapid Determination of Mercury in Contaminated Soil and Plant Samples Using Portable Mercury Direct Analyzer without Sample Preparation, a Comparative Study. *Water, Air, & Soil Pollution*, *223*(5), 2361–2371. https://doi.org/10.1007/s11270-011-1030-3

Kerin, E. J., Gilmour, C. C., Roden, E., Suzuki, M. T., Coates, J. D., & Mason, R. P. (2006). Mercury Methylation by Dissimilatory Iron-Reducing Bacteria. *Applied and Environmental Microbiology*, *72*(12), 7919–7921. https://doi.org/10.1128/AEM.01602-06

Kern, S., Salzer, F., & Reinhold, H. (2015). *Breaking the mercury cycle for emission abatement with the "ExMercury—Splitted preheater system." 68*, 38–44. https://www.zkg.de/en/artikel/zkg_Breaking_the_mercury_cycle_for_emission_abatement_with_the_ExMercury_2411467.html

Kim, C. S., Brown, G. E., & Rytuba, J. J. (2000). Characterization and speciation of mercury-bearing mine wastes using X-ray absorption spectroscopy. *The Science of The Total Environment*, *261*(1–3), 157–168. https://doi.org/10.1016/S0048-9697(00)00640-9

Kirkup, L., & Mulholland, M. (2004). Comparison of linear and non-linear equations for univariate calibration. *Journal of Chromatography A*, *1029*(1–2), 1–11. https://doi.org/10.1016/j.chroma.2003.12.013

Kline, J., & Schreiber, R. (2013). Mercury balances in modern cement plants. *2013 IEEE-IAS/PCA Cement Industry Technical Conference*, 1–16. https://doi.org/10.1109/CITCON.2013.6525269

Kozin, L. F., & Hansen, S. C. (2013). *Mercury Handbook: Chemistry, Applications and Environmental Impact*. Royal Society of Chemistry. https://doi.org/10.1039/9781849735155

Kozin, L. F., Hansen, S. C., Zakharchenko, N. F., & Gray, J. (2013). CHAPTER 12. Environmental Aspects of the Industrial Application of Mercury. In *Mercury Handbook* (pp. 209–227). Royal Society of Chemistry. https://doi.org/10.1039/9781849735155-00209

Kurfürst, U. (1998). General Aspects of the Graphite Furnace Solid Sampling Method. In U. Kurfürst (Ed.), *Solid Sample Analysis* (pp. 21–127). Springer Berlin Heidelberg. https://doi.org/10.1007/978-3-662-03716-4_2

Lalonde, J. D., Amyot, M., Orvoine, J., Morel, F. M. M., Auclair, J.-C., & Ariya, P. A. (2004). Photoinduced Oxidation of Hg^0 (aq) in the Waters from the St. Lawrence Estuary. *Environmental Science & Technology*, *38*(2), 508–514. https://doi.org/10.1021/es034394g

Lalonde, J. D., Poulain, A. J., & Amyot, M. (2002). The Role of Mercury Redox Reactions in Snow on Snow-to-Air Mercury Transfer. *Environmental Science & Technology*, *36*(2), 174–178. https://doi.org/10.1021/es010786g

Lamborg, C. H., Fitzgerald, W. F., O'Donnell, J., & Torgersen, T. (2002). A non-steady-state compartmental model of global-scale mercury biogeochemistry with interhemispheric atmospheric gradients. *Geochimica et Cosmochimica Acta*, *66*(7), 1105–1118. https://doi.org/10.1016/S0016-7037(01)00841-9

Lamborg, C. H., Fitzgerald, W. F., Skoog, A., & Visscher, P. T. (2004). The abundance and source of mercury-binding organic ligands in Long Island Sound. *Marine Chemistry*, *90*(1–4), 151–163. https://doi.org/10.1016/j.marchem.2004.03.014

Lasorsa, B. K., Gill, G. A., & Horvat, M. (2012). Analytical Methods for Measuring Mercury in Water, Sediment, and Biota. In *Mercury in the Environment: Pattern and Process* (1 st ed.). University of California Press.

Laurier, F. J. G., Cossa, D., Gonzalez, J. L., Breviere, E., & Sarazin, G. (2003). Mercury transformations and exchanges in a high turbidity estuary: *Geochimica et Cosmochimica Acta*, *67*(18), 3329–3345. https://doi.org/10.1016/S0016-7037(03)00081-4

Lea, F. M., & Hewlett, P. C. (2004). *Lea's chemistry of cement and concrete* (4th edition). Elsevier-Butterworth-Heinemann.

Lecomte, T., de la Fuente, J. F. F., Neuwahl, F., Canova, M., Pinasseau, A., Jankov, I., Brinkman, T., Roudler, S., & Delgado Sancho, L. (2017). *Best Available Techniques (BAT) Reference Document for Large Combustion Plants; EUR 28836 EN*. Publications Office. https://data.europa.eu/doi/10.2760/949

Lee, C. W., Srivastava, R. K., Ghorishi, S. B., Karwowski, J., Hastings, T. W., & Hirschi, J. C. (2006). Pilot-Scale Study of the Effect of Selective Catalytic Reduction Catalyst on Mercury Speciation in Illinois and Powder River Basin Coal Combustion Flue Gases. *Journal of the Air & Waste Management Association*, *56*(5), 643–649. https://doi.org/10.1080/10473289.2006.10464475

Lee, J.-Y., Ju, Y., Keener, T. C., & Varma, R. S. (2006). Development of Cost-Effective Noncarbon Sorbents for Hg ^{0} Removal from Coal-Fired Power Plants. *Environmental Science & Technology*, *40*(8), 2714–2720. https://doi.org/10.1021/es0519511

Lee, Y. H., Bishop, K. H., Munthe, J., Iverfeldt, Å., Verta, M., Parkman, H., & Hultberg, H. (1998). An examination of current Hg deposition and export in Fenno-Scandian catchments. *Biogeochemistry*, *40*(2/3), 125–135. https://doi.org/10.1023/A:1005926321337

Leermakers, M., Galletti, S., De Galan, S., Brion, N., & Baeyens, W. (2001). Mercury in the Southern North Sea and Scheldt estuary. *Marine Chemistry*, *75*(3), 229–248. https://doi.org/10.1016/S0304-4203(01)00039-1

Li, Y., Daukoru, M., Suriyawong, A., & Biswas, P. (2009). Mercury Emissions Control in Coal Combustion Systems Using Potassium Iodide: Bench-Scale and Pilot-Scale Studies. *Energy & Fuels*, *23*(1), 236–243. https://doi.org/10.1021/ef800656v

Lide, D. R. (2009). CRC Handbook of Chemistry and Physics, 2009−2010, 90th ed. *Journal of the American Chemical Society*, *131*(35), 12862–12862. https://doi.org/10.1021/ja906434c

Lin, C.-J., & Pehkonen, S. O. (1999). The chemistry of atmospheric mercury: A review. *Atmospheric Environment*, *33*(13), 2067–2079. https://doi.org/10.1016/S1352-2310(98)00387-2

Lindberg, S. E., Kim, K.-Hyun., Meyers, T. P., & Owens, J. G. (1995). Micrometeorological Gradient Approach for Quantifying Air/Surface Exchange of Mercury Vapor: Tests Over Contaminated Soils. *Environmental Science & Technology*, *29*(1), 126–135. https://doi.org/10.1021/es00001a016

Lopez-Anton, M. A., Yuan, Y., Perry, R., & Maroto-Valer, M. M. (2010). Analysis of mercury species present during coal combustion by thermal desorption. *Fuel*, *89*(3), 629–634. https://doi.org/10.1016/j.fuel.2009.08.034

MacLeod, M., McKone, T. E., & Mackay, D. (2005). Mass Balance for Mercury in the San Francisco Bay Area. *Environmental Science & Technology*, *39*(17), 6721–6729. https://doi.org/10.1021/es050112w

Malcolm, E. G., Ford, A. C., Redding, T. A., Richardson, M. C., Strain, B. M., & Tetzner, S. W. (2009). Experimental investigation of the scavenging of gaseous mercury by sea salt aerosol. *Journal of Atmospheric Chemistry*, *63*(3), 221–234. https://doi.org/10.1007/s10874-010-9165-y

Mandjukov, P., Orani, A. M., Han, E., & Vassileva, E. (2015). Determination of total mercury for marine environmental monitoring studies by solid sampling continuum source high resolution atomic absorption spectrometry. *Spectrochimica Acta Part B: Atomic Spectroscopy*, *103–104*, 24–33. https://doi.org/10.1016/j.sab.2014.11.006

Mason, R. P., & Fitzgerald, W. F. (1993). The distribution and biogeochemical cycling of mercury in the equatorial Pacific Ocean. *Deep Sea Research Part I: Oceanographic Research Papers*, *40*(9), 1897–1924. https://doi.org/10.1016/0967-0637(93)90037-4

Mason, R. P., Lawson, N. M., Lawrence, A. L., Leaner, J. J., Lee, J. G., & Sheu, G.-R. (1999). Mercury in the Chesapeake Bay. *Marine Chemistry*, *65*(1–2), 77–96. https://doi.org/10.1016/S0304-4203(99)00012-2

Mason, R. P., Lawson, N. M., & Sheu, G.-R. (2001). Mercury in the Atlantic Ocean: Factors controlling air–sea exchange of mercury and its distribution in the upper waters. *Deep Sea Research Part II: Topical Studies in Oceanography*, *48*(13), 2829–2853. https://doi.org/10.1016/S0967-0645(01)00020-0

Mason, R. P., & Sheu, G. R. (2002). Role of the ocean in the global mercury cycle: *Global Biogeochemical Cycles*, *16*(4), 40-1-40–14. https://doi.org/10.1029/2001GB001440

Meierfrankenfeld, D., Bury, A., & Thoennessen, M. (2011). Discovery of scandium, titanium, mercury, and einsteinium isotopes. *Atomic Data and Nuclear Data Tables*, *97*(2), 134–151. https://doi.org/10.1016/j.adt.2010.11.001

Miller, E. K., Vanarsdale, A., Keeler, G. J., Chalmers, A., Poissant, L., Kamman, N. C., & Brulotte, R. (2005). Estimation and Mapping of Wet and Dry Mercury Deposition Across Northeastern North America. *Ecotoxicology*, *14*(1–2), 53–70. https://doi.org/10.1007/s10646-004-6259-9

Mlakar, T. L., Horvat, M., Vuk, T., Stergaršek, A., Kotnik, J., Tratnik, J., & Fajon, V. (2010). Mercury species, mass flows and processes in a cement plant. *Fuel*, *89*(8), 1936–1945. https://doi.org/10.1016/j.fuel.2010.01.009

Moore, T. R., Bubier, J. L., Heyes, A., & Flett, R. J. (1995). Methyl and Total Mercury in Boreal Wetland Plants, Experimental Lakes Area, Northwestern Ontario. *Journal of Environmental Quality*, *24*(5), 845–850. https://doi.org/10.2134/jeq1995.00472425002400050007x

Murakami, A., Uddin, Md. A., Ochiai, R., Sasaoka, E., & Wu, S. (2010). Study of the Mercury Sorption Mechanism on Activated Carbon in Coal Combustion Flue Gas by the Temperature-Programmed Decomposition Desorption Technique. *Energy & Fuels*, *24*(8), 4241–4249. https://doi.org/10.1021/ef100288f

Obrist, D., Kirk, J. L., Zhang, L., Sunderland, E. M., Jiskra, M., & Selin, N. E. (2018). A review of global environmental mercury processes in response to human and natural perturbations: Changes of emissions, climate, and land use. *Ambio*, *47*(2), 116–140. https://doi.org/10.1007/s13280-017-1004-9

Obrist, D., Tas, E., Peleg, M., Matveev, V., Faïn, X., Asaf, D., & Luria, M. (2011). Bromine-induced oxidation of mercury in the mid-latitude atmosphere. *Nature Geoscience*, *4*(1), 22–26. https://doi.org/10.1038/ngeo1018

OriginPro 2018 (Version 2018). (n.d.). [Computer software]. OriginLab Corporation.

Owens, T. M., Wu, C.-Y., & Biswas, P. (1995). An equilibrium analysis for reaction of metal compounds with sorbents in high temperature systems. *Chemical Engineering Communications*, *133*(1), 31–52. https://doi.org/10.1080/00986449508936310

Panichev, N. A., & Panicheva, S. E. (2015). Determination of total mercury in fish and sea products by direct thermal decomposition atomic absorption spectrometry. *Food Chemistry*, *166*, 432–441. https://doi.org/10.1016/j.foodchem.2014.06.032

Paone, P. (2010). Mercury controls for the cement industry. *2010 IEEE-IAS/PCA 52nd Cement Industry Technical Conference*, 1–12. https://doi.org/10.1109/CITCON.2010.5470076

Park, C. H., Eom, Y., Lee, L. J.-E., & Lee, T. G. (2013). Simple and accessible analytical methods for the determination of mercury in soil and coal samples. *Chemosphere*, *93*(1), 9–13. https://doi.org/10.1016/j.chemosphere.2013.04.044

Pavlin, M. (2018). *Mass spectrometric approach for identificatio of mercury compounds in solid samples* [PhD]. Jožef Stefan international Postgraduate School.

Pavlish, J. H., Sondreal, E. A., Mann, M. D., Olson, E. S., Galbreath, K. C., Laudal, D. L., & Benson, S. A. (2003). Status review of mercury control options for coal-fired power plants. *Fuel Processing Technology*, *82*(2–3), 89–165. https://doi.org/10.1016/S0378-3820(03)00059-6

Pirrone, N., Cinnirella, S., Feng, X., Finkelman, R. B., Friedli, H. R., Leaner, J., Mason, R., Mukherjee, A. B., Stracher, G., Streets, D. G., & Telmer, K. (2009). Global Mercury Emissions to the Atmosphere from Natural and Anthropogenic Sources. In R. Mason & N. Pirrone (Eds.), *Mercury Fate and Transport in the Global Atmosphere* (pp. 1–47). Springer US. https://doi.org/10.1007/978-0-387-93958-2_1

Pontes, F. V. M., Carneiro, M. C., Vaitsman, D. S., Monteiro, M. I. C., Neto, A. A., Tristão, M. L. B., & Guerrante, M. D. F. (2013). Comparative study of sample decomposition methods for the determination of total Hg in crude oil and related products. *Fuel Processing Technology*, *106*, 122–126. https://doi.org/10.1016/j.fuproc.2012.07.011

Poulain, A. J., Garcia, E., Amyot, M., Campbell, P. G. C., Raofie, F., & Ariya, P. A. (2007). Biological and Chemical Redox Transformations of Mercury in Fresh and Salt Waters of the High Arctic during Spring and Summer. *Environmental Science & Technology*, *41*(6), 1883–1888. https://doi.org/10.1021/es061980b

Rezende, P. S., Silva, N. C., Moura, W. D., & Windmöller, C. C. (2018). Quantification and speciation of mercury in streams and rivers sediment samples from Paracatu, MG, Brazil, using a direct mercury analyzer®. *Microchemical Journal*, *140*, 199–206. https://doi.org/10.1016/j.microc.2018.04.006

Rolfhus, K. R., & Fitzgerald, W. F. (2001). The evasion and spatial/temporal distribution of mercury species in Long Island Sound, CT-NY. *Geochimica et Cosmochimica Acta*, *65*(3), 407–418. https://doi.org/10.1016/S0016-7037(00)00519-6

Rolfhus, K. R., & Fitzgerald, W. F. (2004). Mechanisms and temporal variability of dissolved gaseous mercury production in coastal seawater. *Marine Chemistry*, *90*(1–4), 125–136. https://doi.org/10.1016/j.marchem.2004.03.012

Rubio, R., & Rauret, G. (1996). Validation of the methods for heavy metal speciation in soils and sediments. *Journal of Radioanalytical and Nuclear Chemistry Articles*, *208*(2), 529–540. https://doi.org/10.1007/BF02040070

Rumayor, M., Diaz-Somoano, M., Lopez-Anton, M. A., & Martinez-Tarazona, M. R. (2015). Application of thermal desorption for the identification of mercury species in solids derived from coal utilization. *Chemosphere*, *119*, 459–465. https://doi.org/10.1016/j.chemosphere.2014.07.010

Rumayor, M., Lopez-Anton, M. A., Díaz-Somoano, M., & Martínez-Tarazona, M. R. (2015). A new approach to mercury speciation in solids using a thermal desorption technique. *Fuel*, *160*, 525–530. https://doi.org/10.1016/j.fuel.2015.08.028

Saiz-Lopez, A., Sitkiewicz, S. P., Roca-Sanjuán, D., Oliva-Enrich, J. M., Dávalos, J. Z., Notario, R., Jiskra, M., Xu, Y., Wang, F., Thackray, C. P., Sunderland, E. M., Jacob, D. J., Travnikov, O., Cuevas, C. A., Acuña, A. U., Rivero, D., Plane, J. M. C., Kinnison, D. E., & Sonke, J. E. (2018). Photoreduction of gaseous oxidized mercury changes global atmospheric mercury speciation, transport and deposition. *Nature Communications*, *9*(1), 4796. https://doi.org/10.1038/s41467-018-07075-3

Sakamoto, M., Tatsuta, N., Izumo, K., Phan, P., Vu, L., Yamamoto, M., Nakamura, M., Nakai, K., & Murata, K. (2018). Health Impacts and Biomarkers of Prenatal Exposure to Methylmercury: Lessons from Minamata, Japan. *Toxics*, *6*(3), 45. https://doi.org/10.3390/toxics6030045

Schoenberger, H. (2015). *Personal communications.*

Schreiber, R. J., Hasan, S., Yonley, C., & Kellet, C. D. (2015). Mercury Emissions Control for the Cement Manufacturing Industry. In *Mercury Control: For Coal-Derived Gas Streams*. Wiley-VCH Verlag GmbH & Co. KGaA.

Schreiber, R. J., & Kellet, C. D. (2009). *Compilation of Mercury Emissions Data,* (PCA R&D Serial No. 3091). Portland Cement Association.

Schreiber, R. J., Kellet, C. D., & Joshi, N. (2005). *Inherent Mercury Montrols Within the Portland Cement Kiln System* (PCA R&D Serial No. 2841). Portland Cement Association.

Schreiber, R. J., Kellett, C. D., & Streitman, F. (2009). Development of a Quantitative, Predictive Mercury Model for a Cement Kiln. *2009 IEEE Cement Industry Technical Conference Record*, 1–4. https://doi.org/10.1109/CITCON.2009.5116169

Schroeder, W. H., & Munthe, J. (1998). Atmospheric mercury—An overview. *Atmospheric Environment*, *32*(5), 809–822. https://doi.org/10.1016/S1352-2310(97)00293-8

Sedlar, M., Pavlin, M., Popovič, A., & Horvat, M. (2014). Temperature stability of mercury compounds in solid substrates. *Open Chemistry*, *13*(1). https://doi.org/10.1515/chem-2015-0051

Selin, N. E. (2009). Global Biogeochemical Cycling of Mercury: A Review. *Annual Review of Environment and Resources*, *34*(1), 43–63. https://doi.org/10.1146/annurev.environ.051308.084314

Selin, N. E., Jacob, D. J., Yantosca, R. M., Strode, S., Jaeglé, L., & Sunderland, E. M. (2008). Global 3-D land-ocean-atmosphere model for mercury: Present-day versus preindustrial cycles and anthropogenic enrichment factors for deposition: GLOBAL 3-D LAND-OCEAN-ATMOSPHERE MODEL FOR MERCURY. *Global Biogeochemical Cycles*, *22*(2), n/a-n/a. https://doi.org/10.1029/2007GB003040

Senior, C., & Eddings, E. (2006). *Evolution of Mercury from Limestone* (R&D 2949). Portland Cement Association.

Senior, C., Montgomery, C. J., & Sarofim, A. (2010). Transient Model for Behavior of Mercury in Portland Cement Kilns †. *Industrial & Engineering Chemistry Research*, *49*(3), 1436–1443. https://doi.org/10.1021/ie901344b

Shanley, J. B., & Bishop, K. (2012). Mercury Cycling in Terrestrial Watersheds. In *Mercury in the Environment. Pattern and Process* (First). University of California Press.

Sholupov, S., Pogarev, S., Ryzhov, V., Mashyanov, N., & Stroganov, A. (2004). Zeeman atomic absorption spectrometer RA-915+ for direct determination of mercury in air and complex matrix samples. *Fuel Processing Technology*, *85*(6–7), 473–485. https://doi.org/10.1016/j.fuproc.2003.11.003

Shuvaeva, O. V., Gustaytis, M. A., & Anoshin, G. N. (2008). Mercury speciation in environmental solid samples using thermal release technique with atomic absorption detection. *Analytica Chimica Acta*, *621*(2), 148–154. https://doi.org/10.1016/j.aca.2008.05.034

Sikkema, J. K., Alleman, J. E., Kee Ong, S., & Wheelock, T. D. (2011). Mercury regulation, fate, transport, transformation, and abatement within cement manufacturing facilities: Review. *Science of The Total Environment*, *409*(20), 4167–4178. https://doi.org/10.1016/j.scitotenv.2011.05.064

Slemr, F., Brunke, E.-G., Ebinghaus, R., & Kuss, J. (2011). Worldwide trend of atmospheric mercury since 1995. *Atmospheric Chemistry and Physics*, *11*(10), 4779–4787. https://doi.org/10.5194/acp-11-4779-2011

Sloss, L. (2015). International Legislation and Trends. In *Mercury Control: For Coal-Dervied Gas Streams* (First Edition). Wiley-VCH Verlag GmbH & Co. KGaA.

Sprovieri, F., Pirrone, N., Bencardino, M., D'Amore, F., Carbone, F., Cinnirella, S., Mannarino, V., Landis, M., Ebinghaus, R., Weigelt, A., Brunke, E.-G., Labuschagne, C., Martin, L., Munthe, J., Wängberg, I., Artaxo, P., Morais, F., Barbosa, H. de M. J., Brito, J., … Norstrom, C. (2016). Atmospheric mercury concentrations observed at ground-based monitoring sites globally distributed in the framework of the GMOS network. *Atmospheric Chemistry and Physics*, *16*(18), 11915–11935. https://doi.org/10.5194/acp-16-11915-2016

Stoffers, P., Hannington, M., Wright, I., Herzig, P., & De Ronde, C. (1999). Elemental mercury at submarine hydrothermal vents in the Bay of Plenty, Taupo volcanic zone, New Zealand. *Geology*, *27*(10), 931. https://doi.org/10.1130/0091-7613(1999)027<0931:EMASHV>2.3.CO;2

Sunderland, E. M., & Mason, R. P. (2007). Human impacts on open ocean mercury concentrations. *Global Biogeochemical Cycles*, *21*(4), n/a-n/a. https://doi.org/10.1029/2006GB002876

Tariq, S. A., & Hill, J. O. (1981). Thermal analysis of mercury(I) sulfate and mercury(II) sulfate. *Journal of Thermal Analysis*, *21*(2), 277–281. https://doi.org/10.1007/BF01914211

Templeton, D. M., Ariese, F., Cornelis, R., Danielsson, L.-G., Muntau, H., van Leeuwen, H. P., & Lobinski, R. (2000). Guidelines for terms related to chemical speciation and fractionation of elements. Definitions, structural aspects, and methodological approaches (IUPAC Recommendations 2000). *Pure and Applied Chemistry*, *72*(8), 1453–1470. https://doi.org/10.1351/pac200072081453

UN Environment. (2019). *Global Mercury Assessment 2018*. UN Environment Programme, Chemicals and Health Branch Geneva, Switzerland.

UNEP. (2019). *Guidance on best available techniques and best environmental practices. Secretariat of the Minamata Convention on Mercury. Chemicals and Health Branch. International Environment House. 11-13, Chemin des Anemones. CH-1219 Chatelaine Geneva, Switzerland.*

Vale, M. G. R., Silva, M. M., Welz, B., & Lima, É. C. (2001). Determination of cadmium, copper and lead in mineral coal using solid sampling graphite furnace atomic absorption spectrometry. *Spectrochimica Acta Part B: Atomic Spectroscopy*, *56*(10), 1859–1873. https://doi.org/10.1016/S0584-8547(01)00336-6

Vincent L. St.Louis,*, Hintelmann, H., Graydon, J. A., Kirk, J. L., Barker, J., Dimock, B., Sharp, M. J., & Lehnherr, I. (2007). Methylated Mercury Species in Canadian High Arctic Marine Surface Waters and Snowpacks. *Environmental Science & Technology*, *41*(18), 6433–6441. https://doi.org/10.1021/es070692s

Waldron, H. A. (1983). Did the Mad Hatter have mercury poisoning? *BMJ*, *287*(6409), 1961–1961. https://doi.org/10.1136/bmj.287.6409.1961

Wang, F., Wang, S., Zhang, L., Yang, H., Wu, Q., & Hao, J. (2016). Characteristics of mercury cycling in the cement production process. *Journal of Hazardous Materials*, *302*, 27–35. https://doi.org/10.1016/j.jhazmat.2015.09.042

Watling, R. J., Davis, G. R., & Meyer, W. J. (1972). *Trace identification of mercury compounds as a guide to sulphide mineralization at Keel, Erie.* 59–69.

Weisspenzias, P., Jaffe, D., Swartzendruber, P., Hafner, W., Chand, D., & Prestbo, E. (2007). Quantifying Asian and biomass burning sources of mercury using the Hg/CO ratio in pollution plumes observed at the Mount Bachelor observatory. *Atmospheric Environment*, *41*(21), 4366–4379. https://doi.org/10.1016/j.atmosenv.2007.01.058

Whalin, L., Kim, E.-H., & Mason, R. (2007). Factors influencing the oxidation, reduction, methylation and demethylation of mercury species in coastal waters. *Marine Chemistry*, *107*(3), 278–294. https://doi.org/10.1016/j.marchem.2007.04.002

Windmöller, C. C., Wilken, R.-D., & Jardim, W. D. F. (1996). Mercury speciation in contaminated soils by thermal release analysis. *Water, Air, and Soil Pollution*, *89*(3–4), 399–416. https://doi.org/10.1007/BF00171644

Wocken, C. (2004). *Evaluation of enviroscrub's multipollutant PahlmanTM process for mercury removal at facility burning subbituminous coal. Final plant report* (05-EERC-04–04).

Žagar, D., Petkovšek, G., Rajar, R., Sirnik, N., Horvat, M., Voudouri, A., Kallos, G., & Četina, M. (2007). Modelling of mercury transport and transformations in the water compartment of the Mediterranean Sea. *Marine Chemistry*, *107*(1), 64–88. https://doi.org/10.1016/j.marchem.2007.02.007

Zheng, Y., Jensen, A. D., Windelin, C., & Jensen, F. (2012). Review of technologies for mercury removal from flue gas from cement production processes. *Progress in Energy and Combustion Science*, *38*(5), 599–629. https://doi.org/10.1016/j.pecs.2012.05.001

Bibliography

Publications Related to the Thesis

Journal Articles

Berisha, S., Živković, I., Kotnik, J., Mlakar, T.L., Horvat, M., Quantification of total mercury in samples from cement production processing with thermal decomposition coupled with AAS, Accred. Qual. Assur. (2020), https://doi.org/10.1007/s00769-020-01432-w. [COBISS.SI-ID 13446915]

Berisha, S., Živković, I., Kotnik, J., Mlakar, T.L., Horvat, M., Temperature fractionation of mercury in the cement production process using quadrupole mass spectrometry, Cem. Concr. Res. (2022), https://doi.org/10.1016/j.cemconres.2022.106970

Conference contribution

Berisha, S., Mlakar, T.L., Pavlin, M., Horvat, M., Thermo-desorption approach to mercury stability study in samples from cement production. V: *Abstract volume*. 14th International Conference on Mercury as a Global Pollutant, ICMGP 2019, 8-13 September 2019, Krakow, Poland. [S. l.: s. n.], 2019. https://mercury2019krakow.com/public/files/ICMGP2019-abstract-volume.pdf. [COBISS.SI-ID 32752167]

Berisha, S., Kotnik, J., Mlakar, T.L., Horvat, M., Total Hg in samples from cement production using pyrolysis coupled to AAA - method validation. V: *Abstract volume*. 14th International Conference on Mercury as a Global Pollutant, ICMGP 2019, 8-13 September 2019, Krakow, Poland. [S. l.: s. n.], 2019. Str. 220. https://mercury2019krakow.com/public/files/ICMGP2019-abstract-volume.pdf. [COBISS.SI-ID 32928039

Other Publications

Živković, I., Berisha, S., Kotnik, J., Gačnik, J., Horvat, M., Traceable determination of gaseous elemental mercury using impregnated activated coal as an efficient trapping sorbent. V: *Abstract volume*. 14th International Conference on Mercury as a Global Pollutant, ICMGP 2019, 8-13 September 2019, Krakow, Poland. [S. l.: s. n.], 2019. Str. 219. https://mercury2019krakow.com/public/files/ICMGP2019-abstract-volume.pdf. [COBISS.SI-ID 32684839]

Chouhan, R.S., Fajon, V., Živković, I., Pavlin, M., Berisha, S., Horvat, M., A unique interactive nanostructure knitting based passive sampler adsorbent at the

microscale for trace level monitoring H2+ in water. V: *Abstract volume*. 14th International Conference on Mercury as a Global Pollutant, ICMGP 2019, 8-13 September 2019, Krakow, Poland. [S. l.: s. n.], 2019. Str. 221-222. https://mercury2019krakow.com/public/files/ICMGP2019-abstract-volume.pdf. [COBISS.SI-ID 32685607]

Chouhan, R.S., Žitko, G., Fajon, V., Živković, I., Pavlin, M., Berisha, S., Jerman, I., Vesel, A., Horvat, M., A unique interactive nanostructure knitting based passive sampler adsorbent for monitoring of Hg^{2+} in water. *Sensors*. 2019, vol. 19, no. 15, str. 3432-1-3432-14. ISSN 1424-8220. DOI: 10.3390/s19153432. [COBISS.SI-ID 32549159]

Gačnik, J., Živković, I., Ribeiro Guevara, S., Kotnik, J., Berisha, S., Vijayakumaran Nair, S., Jurov, A., Cvelbar, U., Horvat, M., Calibration approach for gaseous oxidized mercury based on nonthermal plasma oxidation of elemental mercury, Analytical Chemistry. 2022, Vol. 94, iss. 23. DOI; 10.1021/acs.analchem.2c00260. [COBISS.SI-ID 110172419]

Biography

Sabina Berisha obtained her bachelor's degree in Chemistry and Physics from University of Prishtina, Faculty of Education. She enrolled in Master studies in International Postgraduate School Jožef Stefan, and obtained her Master's degree in the field of Ecotechnologies and successfully defended the master thesis entitled "Mosses as bioindicators of trace elements and nitrogen in Ljubljana forests". At the same educational institution, she continued her Doctoral studies. During her studies, she published two articles as a first author, and many others as a contributing author. She has also gained a comprehensive knowledge and experience on various research methods and techniques in determination of mercury in solid samples primarily.